ANALYSIS OF THE HUMAN ANTIBODY RESPONSE TO OLD WORLD ALPHAVIRUS INFECTION

By

Laura A. Powell

Dissertation

Submitted to the Faculty of the

Graduate School of Vanderbilt University

in partial fulfillment of the requirements

for the degree of

DOCTOR OF PHILOSOPHY

in

Microbiology and Immunology

May 8, 2020

Nashville, Tennessee

Approved:

Mark R. Denison, M.D.

Kathryn M. Edwards, M.D.

Amy S. Major, Ph.D.

Kristen M. Ogden, Ph.D.

James E. Crowe, Jr., M.D.

ACKNOWLEDGEMENTS

I would like to first thank my mentor, James Crowe, for his support and inspiration, and for allowing me to pursue this project. I am grateful for his trust in me and for allowing me the freedom to explore and learn what I am most passionate about. He has encouraged and inspired me with his leadership, dedication to science, and desire to help people and leave the world a better place.

I am also very grateful to my committee, Mark Denison (chair), Kristen Ogden, Amy Major, and Kathy Edwards, for providing scientific guidance and direction throughout my graduate studies. I have greatly appreciated their support and suggestions throughout my time working on this project.

This body of work was greatly enhanced by the contribution of a talented team of collaborators. I would like to thank Julie Fox in Michael Diamond's group for performing all mouse studies and for offering guidance on protocols and providing key reagents and viruses. I am also grateful to two other members of the Diamond group, James Earnest and Arthur Kim, for providing me with Mxra8-Fc fusion protein and mouse Mayaro-specific antibodies for use in competition ELISA studies. Thomas Morrison at University of Colorado provided me with several viruses, including clinical isolate strains of Ross River virus as well as a mutant RRV. Finally, I would like to thank Richard Kuhn's group at Purdue University, and specifically Andy Miller, for their contribution of three cryo-EM structures.

I am grateful to so many members of the Crowe Lab, both current and former, for their friendship and scientific mentorship. Specifically, I would like to thank Nurgun Kose for training me in the hybridoma process and for imparting to me her deep knowledge of cell culture. Pavlo and Iuliia Gilchuk, Matt Vogt, and Seth Zost provided invaluable scientific mentorship and project guidance during my time in the lab. I also thank Rob Carnahan and his iCore team for

their help with antibody purification and transfections, and Robin Bombardi and team for providing me with antibody sequences. The Vanderbilt Flow Cytometry Core staff, and in particular Dave Flaherty and Brittany Matlock, guided and trained me on flow cytometry assays, and provided crucial support for hybridoma cell sorting, for which I am very grateful.

My family and friends have been a constant support and have encouraged me in innumerable ways throughout my graduate studies. I am particularly thankful to both of my parents, who have always placed an importance on education and have encouraged and made it possible for me to pursue advanced academic work. I thank my sister for being the best roommate and friend I could ask for, and to Grandma for all the ways she has constantly served and supported me. I'm thankful to my dance and music friends for helping me continue to pursue my artistic passions, and keeping me sane on many long days in lab. Finally, I would like to thank my church family for keeping me grounded and encouraging me in my faith. Soli Deo gloria.

TABLE OF CONTENTS

LIST OF FIGURES

LIST OF TABLES

LIST OF ABBREVIATIONS

ADCC	Antibody-dependent cellular cytotoxicity
ADE	Antibody-dependent enhancement
CDC	Complement-dependent cytotoxicity
CHIKV	chikungunya virus
cryo-EM	cryo-electron microscopy
EC_{50}	50% maximum-binding concentration
EEEV	Eastern equine encephalitis virus
GETV	Getah virus
IC_{50}	50% maximum-inhibitory concentration
mAb	monoclonal antibody
ONNV	O'nyong'nyong virus
SAGV	Sagiyama virus
SFV	Semliki Forest virus
SINV	Sindbis virus
VEEV	Venezuelan equine encephalitis virus
WEEV	Western equine encephalitis virus

CHAPTER I

INTRODUCTION

Thesis overview

This document represents the culmination of my work characterizing the antibody response against alphaviruses causing musculoskeletal disease. I have divided my work into five chapters. In chapter I, I provide an overview of alphaviruses, including structural information, replication cycle, and pathogenesis. I also highlight the epidemiology of some of the most clinically relevant alphaviruses and provide information on the innate and adaptive immune responses, with a focus on the role antibodies play. Finally, I survey progress on current vaccines and antibody therapies.

In Chapter II, I describe my work characterizing a panel of human monoclonal antibodies (mAbs) specific for RRV from two donors who experienced natural infection. I elaborate on how these mAbs elucidate antigenic regions and reveal mechanisms by which Ross River virus (RRV) is neutralized. Additionally, I present *in vivo* data demonstrating that these mAbs reduce musculoskeletal disease, viral burden, and death in several mouse challenge models. This work provides insight into the antibody response during natural infection with RRV, and suggests that therapeutic administration of mAbs could mitigate disease burden.

In Chapter III, I describe human mAbs that bind to and neutralize multiple distantly-related alphaviruses. I show that these mAbs compete for an antigenic site and prevent attachment to the recently discovered Mxra8 alphavirus receptor. I also provide three cryo-electron microscopy (cryo-EM) structures of Fab of one antibody in complex with RRV, Mayaro (MAYV), or chikungunya (CHIKV) viruses which reveal a conserved footprint of the mAb RRV-12 in a region of the E2 glycoprotein B domain. My work shows that this mAb neutralizes virus *in vitro* by preventing virus attachment, entry, and spread. In addition, RRV-12 was protective *in vivo* in

mouse models of infection. My work suggests that RRV-12 has potential for use as a therapeutic agent, and knowledge of its epitope may advance the design of a vaccine against multiple emerging arthritogenic alphavirus infections.

In chapter IV, I briefly describe a panel of mAbs isolated from a MAYV-immune individual. I demonstrate that some of these mAbs are potently neutralizing and bind to both recombinant E2 protein and virus. In addition, I show how these mAbs recognize both known antigenic sites as well as potentially new sites on the virus. Finally, I provide preliminary mechanistic data, including evidence that these mAbs block binding of MAYV to Mxra8 receptor.

Chapter V summarizes my findings and provides directions for future work. This body of work impacts the alphavirus field by providing new insight into the antibody response against both established and emerging viruses, and will advance the design of rational vaccines and therapeutic candidates.

Introduction to alphaviruses

Alphaviruses are positive-sense single-stranded RNA viruses that belong to the *Togoviridae* family and are mosquito-transmitted. They cause outbreaks worldwide, and are divided into two main groups: Old World alphaviruses that cause arthritis-like symptoms, and New World alphaviruses that cause encephalitis (Garmashova et al., 2007; Leung et al., 2011; Paredes et al., 2005). Common to all arthritogenic alphavirus infections are clinical manifestations that include rash, fever, fatigue, arthralgia, and muscle pain that typically appear 3-10 days after infection (Lwande et al., 2015; Mostafavi et al., 2019). Although arthritis and inflammation typically resolve a few weeks after infection, joint pain may persist for months or years and is quite debilitating (Hawman et al., 2013). In contrast to arthritis-causing alphaviruses, encephalitic alphaviruses have a higher rate of mortality, with typical symptoms ranging from mild neurological illness to severe encephalitis leading to death. The most lethal virus, Eastern equine encephalitis virus (EEEV), causes mortality in 50-75% of human cases and 70-90% of

equine cases, but is also rare, typically causing less than 10 cases per year (Franklin et al., 2002; Zacks and Paessler, 2010). Outbreaks of arthritogenic alphaviruses are more prevalent and may result in millions of cases worldwide, as occurred during the widespread chikungunya epidemic from 2004 to 2011(Johansson, 2015; Morrison et al., 2016).

Alphaviruses have traditionally been divided into seven antigenic complexes based on cross-reactivity tests, where members of a complex have greater cross-reactivity with each other than with members of another complex (**Figure 1**) (Powers et al., 2001). Members of the same clade generally share similar clinical disease characteristics, with the exception of the WEE complex, which contains both encephalitic and arthritogenic viruses (Powers et al., 2001). The Semliki Forest complex contains the majority of arthritis-causing alphaviruses, while the VEE and EEE complexes contain the encephalitis-causing viruses.

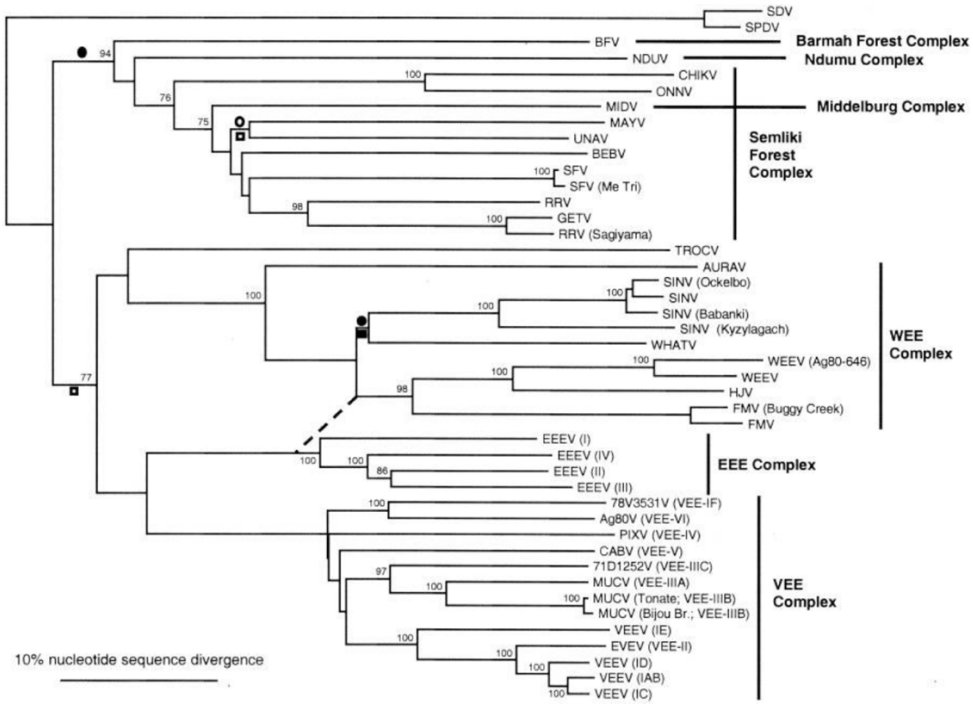

Figure 1. **Phylogenetic relationships among New and Old World alphaviruses**. Several antigenic complexes exist based on cross-reactivity tests. Members of the same complex typically share disease symptoms. From (Powers et al., 2001).

Epidemiology of arthritis-causing alphaviruses

Because my work has focused on alphaviruses that cause musculoskeletal disease and arthritis-like symptoms, I will highlight the epidemiology of the most prominent and clinically relevant viruses belonging to that group in this section. However, I would like to briefly mention that the main encephalitic alphaviruses are Venezuelan equine encephalitis virus (VEEV), Western equine encephalitis virus (WEEV) and Eastern equine encephalitis virus (EEEV), which are distributed throughout North, Central, and South America (Zacks and Paessler, 2010). WEEV has caused sporadic outbreaks throughout the United States, with cases spanning 21 states, from the Midwest to the West Coast and extending up into Canada (Phelps et al., 2017). Cases of EEEV typically concentrate along the Gulf and Atlantic coasts, with the occasional patient reported in the Midwest and Canada (Davis et al., 2008). In contrast to WEEV and EEEV, VEEV is widely distributed in Central and South America (Aguilar et al., 2011).

Ross River virus (RRV) is endemic to Australia, Papua New Guinea, and the Pacific Islands, and infects approximately 5,000 individuals every year (Harley et al., 2001). RRV first was isolated from human serum in 1972, but was not connected with symptoms until large epidemics in the South Pacific islands in 1979-1980, in which up to 500,000 people were infected (Aaskov et al., 1981; Doherty et al., 1972; Harley et al., 2001). RRV is transmitted by a wide range of mosquito vectors, including *Culex*, *Aedes*, *Anopheles*, *Coquillettidia*, and *Mansonia* species, and reservoirs for the virus are thought to be species endemic to Australia, such as wallabies and kangaroos. However, recent evidence indicates that other mammalian species such as rodents, rabbits, and flying foxes can act as reservoirs for the virus and contribute to its spread (Lau et al., 2017; Stephenson et al., 2018). Traditionally, reservoirs of RRV were thought to be marsupials endemic to Australia, including kangaroos and wallabies (Claflin and Webb, 2015; Stephenson et al., 2018). This finding suggests that RRV may have the potential to spread to

regions outside of Australia and the Pacific Islands and raises concerns about future epidemic transmission.

Chikungunya virus (CHIKV) was first isolated in 1952 in Tanzania, though epidemics had previously been reported as early as 1870 in Africa (Lwande et al., 2015; Mason and Haddow, 1957). The name chikungunya means “that which bends up” in reference to the debilitating arthritis and joint pain induced by the virus (Mason and Haddow, 1957). Acute symptoms of CHIKV disease, such as rash and fever, resemble dengue virus (DENV) infection, but CHIKV is set apart from DENV by arthralgia and debilitating joint pain that can persist anywhere from months to years (Krutikov and Manson, 2016). CHIKV is transmitted primarily by the *Aedes* species of mosquito (Wong et al., 2016). An outbreak of CHIKV in Kenya in 2004 subsequently led to a worldwide pandemic with an estimated 6 million cases (Wahid et al., 2017; Zeller et al., 2016), and in 2013-2014, CHIKV spread into islands of the Caribbean, as well as North and South America, areas which had not previously been exposed (Fischer et al., 2014; Nasci, 2014). This increased range was caused in part by an alanine-to-valine mutation in the E1 glycoprotein that allowed enhanced transmission in the *Aedes albopictus* vector (Arias-Goeta et al., 2013; Silva et al., 2014).

MAYV was first isolated in 1954 from the blood of symptomatic individuals in Trinidad and Tobago (Acosta-Ampudia et al., 2018). The *Haemagogus* species of mosquito is the main vector for MAYV transmission, and primary reservoirs include monkeys and possibly birds (Izurieta et al., 2011). Several outbreaks of MAYV have occurred in South America, including one in Brazil in 1978, and antibodies against MAYV have been isolated from humans in Panama, Bolivia, Colombia, Brazil, Venezuela, Peru, Trinidad and Tobago, French Guiana, Suriname, and Mexico (**Figure 2**) (Izurieta et al., 2011; Levi and Vignuzzi, 2019). In addition, cases of MAYV have been exported to North America and Europe, including the countries of Germany, France, Switzerland, Netherlands, and the United States (Acosta-Ampudia et al., 2018; Hassing et al., 2010). However, cases of MAYV disease are thought to be underreported

due to the difficulty of distinguishing symptoms of infection from those of DENV (Smith et al., 2018).

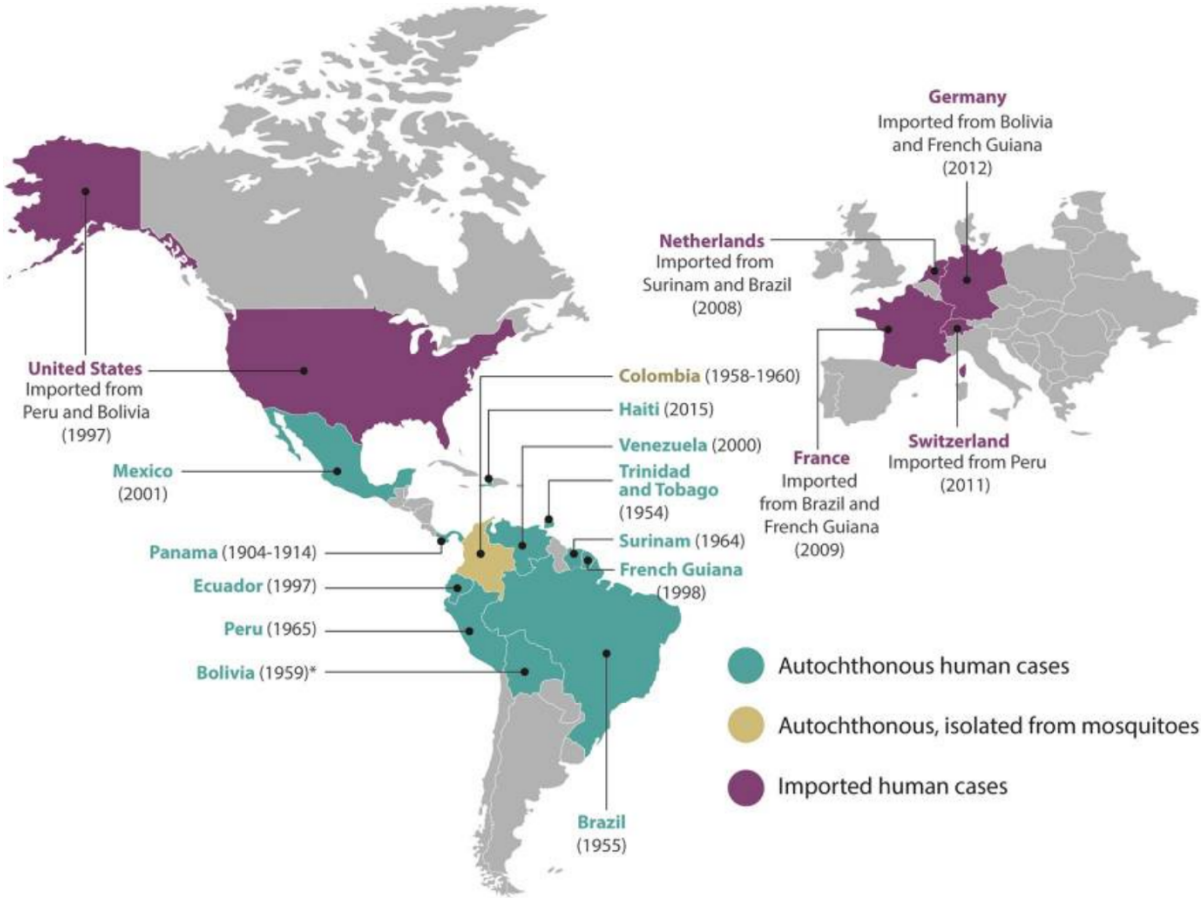

Figure 2. Epidemiological spread of MAYV globally. Both autochthonous (locally acquired) and imported cases are shown. From (Acosta-Ampudia et al., 2018).

O'nyong'nyong (ONNV) was first identified in Uganda in 1959 (Rezza et al., 2017; Williams et al., 1965). An outbreak in Africa from 1959-1962 affected greater than 2 million people, and other outbreaks as recently as 2012 have been reported in Liberia, Cameroon, Uganda, Kenya, and Chad (**Figure 3**) (Rezza et al., 2017). Two mosquito species are known to transmit ONNV:

Anopheles funestus and *Anopheles gambiae* (Nanfack Minkeu and Vernick, 2018; Valentine et al., 2019). Although reservoirs for the virus are unknown, serological studies have indicated that both humans and animals have antibodies against ONNV (Rezza et al., 2017; Woodruff et al., 1978). During extended periods between outbreaks, serological data has indicated that continued transmission and exposure most likely occur, suggesting that perhaps the virus has a low rate of symptomatic infection (Rezza et al., 2017).

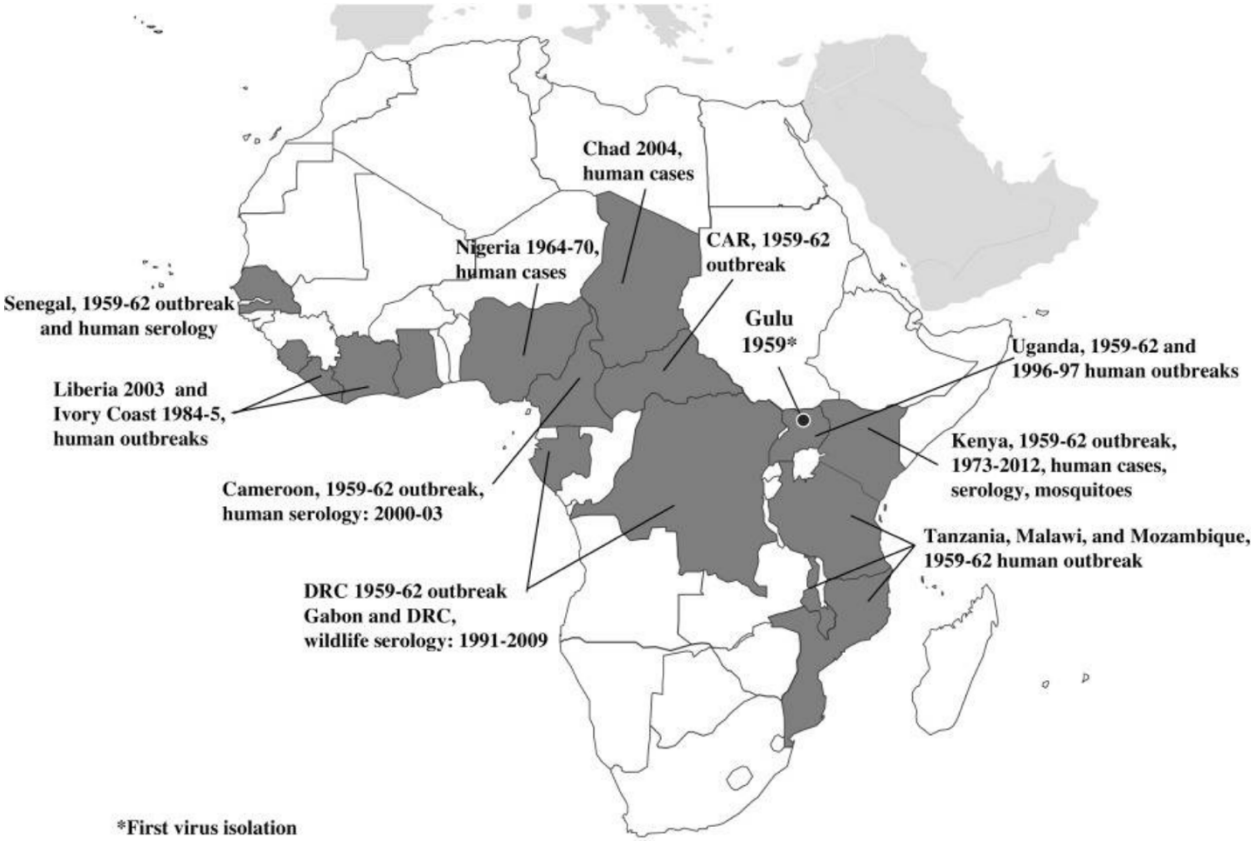

Figure 3. Spread of ONNV in Africa. Outbreaks since the isolation of ONNV in 1959 are shown, with affected countries colored in gray. From (Rezza et al., 2017).

Sindbis virus (SINV) also originated in Africa and was isolated from *Culex* mosquitos in Cairo, Egypt in 1952. From 1963-1974, a large number of SINV outbreaks regularly occurred in South Africa and Northern Europe, including the countries of Finland and Sweden (Jöst et al., 2010; Ling et al., 2019). The largest reported outbreak occurred in Finland in 1995, with more than 1,000 infected individuals (Brummer-Korvenkontio et al., 2002). Additionally, human cases have been reported outside of Europe and Africa, in portions of China, Australia, and the Middle East (Ling et al., 2019). Outbreaks have been reported to follow a seasonal pattern, with the majority of cases peaking from July to October in Sweden and Finland, and March to April in South Africa (Lundström et al., 2019). Genetic factors are thought to determine susceptibility to symptomatic infection, including a higher prevalence of the HLA allele DRB1*01 among infected people, and especially those experiencing persistent joint pain (Sane et al., 2012).

Sagiyama virus (SAGV) was isolated in 1956 from mosquitoes in Japan, and the closely related Getah virus (GETV) was isolated in in 1955 in Malaysia (Lu et al., 2019; Shirako and Yamaguchi, 2000). While SAGV and GETV viruses are not pathogenic in humans, they are known to cause disease in horses and pigs in Asia and Australia (Shirako and Yamaguchi, 2000). Clinical symptoms of infection in horses include fever, edema of the hind legs, and lymph node enlargement (Kumanomido et al., 1988). Although neutralizing antibodies against SAGV and GETV have been found in humans, infection appears to be asymptomatic (Shirako and Yamaguchi, 2000).

Alphavirus structural features

Alphaviruses are enveloped, positive-sense, single-stranded RNA viruses of approximately 65-70 nm in diameter (Jose et al., 2009; Shin et al., 2012). Their 11.5 kb genome is composed of four nonstructural proteins, nsp1-4, and five structural proteins, namely the capsid, E3, E2, 6K, and E1 proteins (Jose et al., 2009). The glycoprotein is formed from the association of E1 and E2 as a heterodimer, which is expressed as a trimeric spike on the virus surface. The viral

envelope is composed of a total of 240 monomers, or 80 trimers, of the E1/E2 glycoprotein (Cheng et al., 1995; Roussel et al., 2006). The main role of the E2 protein is to mediate cellular attachment, while the E1 protein contains the fusion loop and functions primarily in directing viral fusion with the endosomal membrane (Schnierle, 2019; Weger-Lucarelli et al., 2015).

Current alphavirus structures

In recent years, much progress has been made in understanding alphavirus structure through the aid of crystallographic and cryo-EM studies. To date, several cryo-EM structures of alphaviruses have been determined, including a 3.5 Å resolution structure of SINV and a 25 Å resolution structure of RRV for the Old World alphaviruses, and a 4.4 Å resolution structure of VEEV, a 9 Å resolution structure of encephalitic Semliki Forest virus (SFV), a 17 Å resolution structure of Aura virus, and a 13 Å resolution structure of WEEV for the New World alphaviruses (Chen et al., 2014; Lee et al., 1996; Mancini et al., 2000; Sherman and Weaver, 2010; Zhang et al., 2002a). These structures showed that alphaviruses have icosahedral T=4 symmetry with 20 trimeric spikes located on the 3-fold axes and 60 quasi-3-fold spikes at general positions (Lee et al., 1996; Sun et al., 2013; Yap et al., 2017). A lipid membrane encapsulates the capsid shell, which is associated with the RNA genome. These cryo-EM structures have also revealed minor structural differences for New and Old World alphaviruses, including a more ordered nucleocapsid for Old World alphaviruses as well as an opposite rotation of the pentameric and hexameric capsomers of the nucleocapsid (Sherman and Weaver, 2010).

More recently, X-ray crystallographic studies have revealed atomic resolution structures for the CHIKV and SINV E1/E2 glycoprotein and the SFV E1 protein (Li et al., 2010; Voss et al., 2010). These structures have illuminated many previously unknown aspects of the alphavirus life cycle, including details of the low-pH-mediated fusion process, and have revealed the presence of three distinct domains on the E2 protein: domain A, which is located at the N-terminus and is thought to contain the putative receptor binding site, domain B in the middle,

and domain C at the C-terminus (**Figure 4**). Domain B covers the fusion loop on the E1 protein, which is positioned between domains A and B of the E2 protein, and a flexible linker connects domain B of E2 to domain A (Kielian, 2010) (Voss et al., 2010). Crystallization of SINV at an acidic pH revealed a disordered B domain, indicating that the B domain likely dissociates to uncover the fusion loop during the endosomal fusion step (Zhang et al., 2002b). Further details of this process will be discussed in the alphavirus replication cycle section.

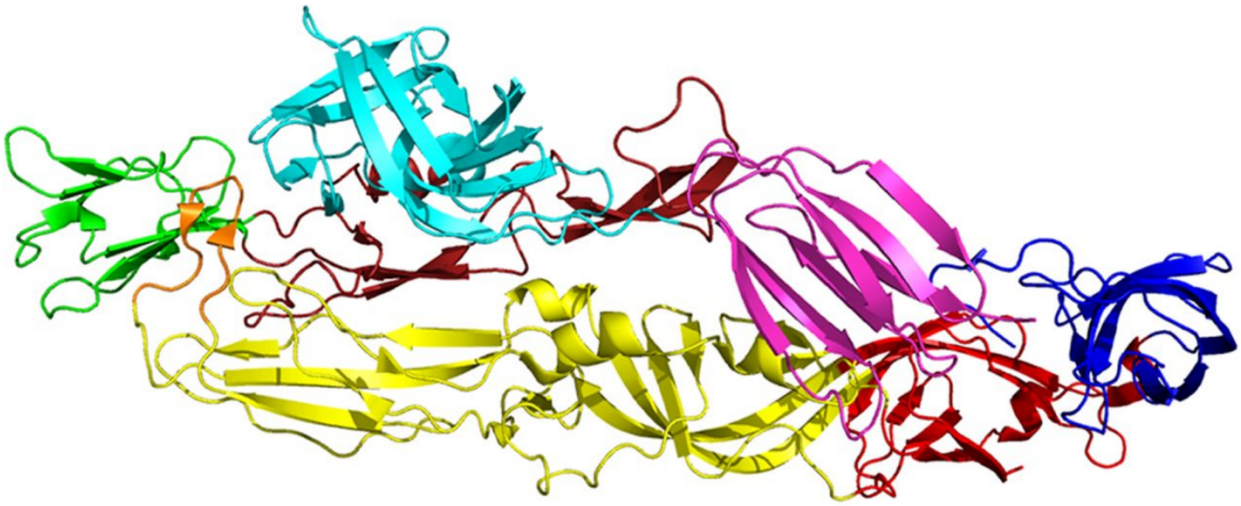

Figure 4. Structure of the E1/E2 heterodimer for CHIKV. Shown in red, yellow, and blue are E1 domains I, II, and III, respectively, and domains A, B, and C of E2 are shown in cyan, green, and magenta. The E1 fusion loop is shown in orange. Structure is from PDB 3N42. Modified from (Porta et al., 2014).

In addition to structures of virus alone, several structures of alphaviruses in complex with neutralizing antibodies have been determined. In particular, a combination of cryo-EM and crystallography was used to reveal chikungunya virus-like particles (VLPs) in complex with neutralizing chikungunya antibodies at a resolution of 5.3 Å (Porta et al., 2016; Sun et al., 2013). A mouse mAb, CHK-152, was found to block viral fusion by binding to the B domain and

preventing uncovering of the fusion loop, while three other mAbs, CHK-9, m10, and m242, inhibited cellular attachment through binding near a putative receptor-binding site on the A domain of E2 (Sun et al., 2013).

Alphavirus replication cycle

Attachment

Alphaviruses can infect cells from a wide variety of species, including mammals, birds, and insects. This breadth of infection is most likely due to the presence of multiple attachment factors or receptors, including the high-affinity laminin receptor, class I major histocompatibility antigen, α1ß1 integrin, DC-SIGN and L-SIGN, and heparan sulfate (HS) (Heil et al., 2001; Klimstra et al., 1998; 2003). However, binding to HS is seen only for tissue-culture adapted, attenuated virus, indicating that HS may not be an *in vivo* receptor (Heil et al., 2001). Additionally, virus passaged on mosquito cells has shown increased binding to DC-SIGN and L-SIGN lectins due to large amounts of mannose produced in mosquitoes (Klimstra et al., 2003). However, while evidence exists that these attachment factors aid in binding of alphaviruses to cells, until recently no alphavirus receptor had been confirmed. Cryo-EM and X-ray crystallography studies have determined that Mxra8 is a shared receptor for arthritogenic alphaviruses, and contacts both the A and B domains of the E2 protein (Basore et al., 2019; Zhang et al., 2018). Mxra8 binds in a cleft created by two adjacent E1/E2 spikes, and also contacts a neighboring spike. The footprint of Mxra8 includes residues 18, 26–29, 71–72, 74–76, 119–121, 123, 178–182, 189, 191, 193, 212–214, and 221–223 on the E2 A and B domains as well as residues 5–6, 62, 64, 144, 150, 157–160, 263–265, and 267 on the intraspike heterodimer (Basore et al., 2019).

Entry and fusion

After binding to cells, alphaviruses are internalized via the clathrin-mediated endocytic pathway (Kielian et al., 2010; Leung et al., 2011). Once inside the endosome, the clathrin coat is removed before the E1 and E2 glycoproteins initiate fusion with the endosomal membrane. The E1 protein contains three fusion loops that initiate fusion through contact with the cell membrane (Sánchez-San Martín et al., 2008). An acidic pH is necessary to trigger fusion, and the first step involves a conformational change where the E2 protein is removed in order to expose E1, possibly through protonation of histidine residues (Gibbons et al., 2004) (Li et al., 2010). E1 then inserts into the host membrane, forming a trimer that pulls the host cell and viral membrane together, before the E1 protein folds back to create a hairpin-like structure (**Figure 5**) (Kielian, 2010).

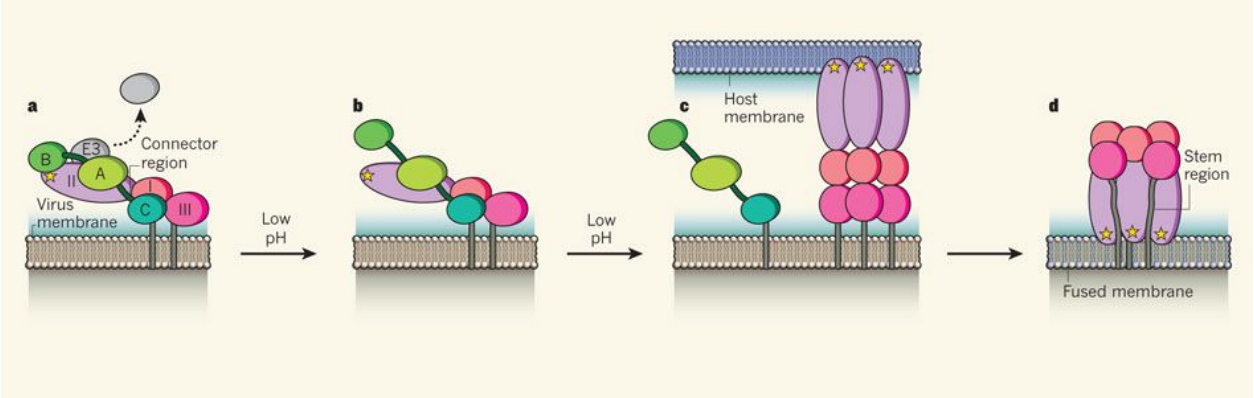

Figure 5. Steps in alphavirus fusion. (**a**) The three domains of the E2 protein (A-C) and the E1 protein (I-III) are shown, with the viral fusion loop represented with a star and the dissociation of E3 indicated. (**b**) Under low pH conditions, the B domain shifts to reveal the fusion loop on E1. (**c**) E1 then dissociates from E2 and inserts into the host membrane, forming a trimer. (**d**) The final fused membrane is shown, resulting from the refolding of E1 into a hairpin-like structure. From (Fields and Kielian, 2013).

Translation

After viral fusion with the endosome, the nucleocapsid is released into the cytoplasm, and the nonstructural proteins (nsp1-4) are translated directly from the genomic RNA (Abu Bakar and Ng, 2018). Through the use of a second reading frame, subgenomic RNA is produced and translated into a polyprotein of the structural proteins, consisting of capsid (C), precursor to E2 (pE2), 6K, E1 and the transframe (Firth et al., 2008). The capsid is first cleaved off autoproteolytically, and functions in assembling the gRNA with the nucleocapsid (Jose et al., 2009). The other proteins are then individually cleaved with the aid of signal sequences and transmembrane domains before transport to the ER (Jose et al., 2009). In order to prevent early conformational change at low pH, E1 is protected through association with p62 (Leung et al., 2011). With the exception of SFV and VEEV, E3 is cleaved off of p62 by furin in the late secretory pathway, producing the mature E2 protein (Simizu et al, 1984).

Budding

After trafficking to the plasma membrane, the gRNA and structural proteins assemble to form the mature virion. Interactions between the nucleocapsid and E1/E2 glycoprotein are known to be important for alphavirus budding (Brown et al., 2018). For SFV, budding has been shown to be dependent on residues located in the E2 cytoplasmic tail region, and mutations in residues 399, 400, and 402 in particular result in a budding defect (Owen and Kuhn, 1997) (Zhao and Garoff, 1992). The formation of stable E1/E2 heterodimers is essential for budding, and mutations that destabilize the complex may result in budding defects (Duffus et al., 1995). The accumulation of actin in the cytoplasm of the host cell is thought to promote trafficking of the glycoprotein to the budding location at the plasma membrane (Radoshitzky et al., 2016). In contrast to other enveloped viruses, alphavirus budding is independent of the ESCRT (endosomal sorting complexes required for transport) pathway, and factors that contribute to

release of virus from the plasma membrane are currently unknown (Taylor et al., 2007). A summary of the replication cycle is shown in **Figure 6.**

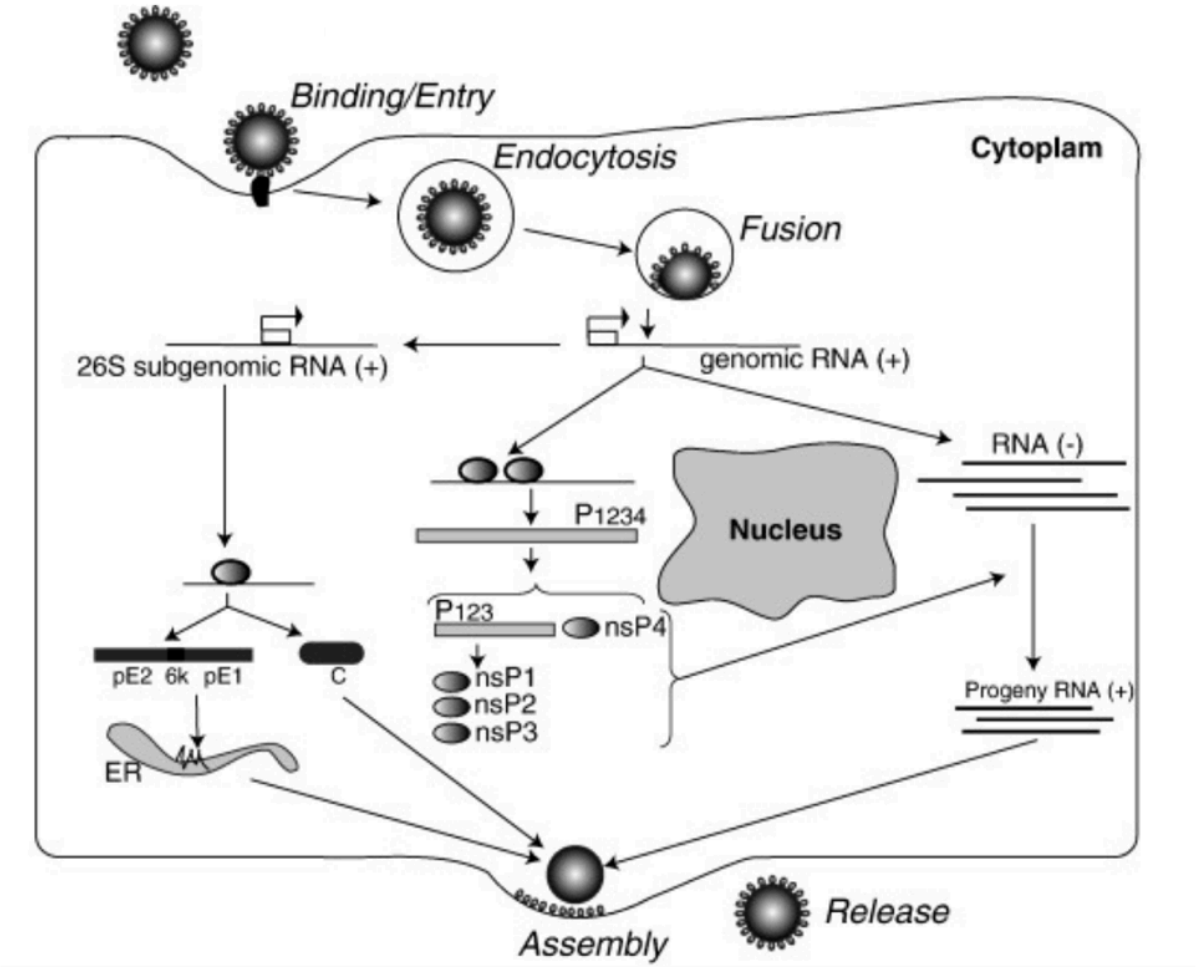

Figure 6. Summary of alphavirus replication cycle. Alphaviruses enter cells by binding to a variety of attachment factors and the recently discovered Mxra8 receptor. Entry then occurs through receptor-mediated endocytosis, and the virion undergoes low pH-mediated fusion with the plasma membrane, releasing the nucleocapsid (NC) into the cytoplasm. After translation of non-structural and structural proteins from genomic RNA and sub-genomic RNA, respectively, stable E1/E2 heterodimer complexes are trafficked to the membrane, where budding occurs. Modified from (Solignat et al., 2009).

Cell-to-cell spread

During alphavirus cell-cell transmission, both short <2–7 μm and long <10 μm extensions protruding from the surface of infected cells are formed (Brown et al., 2018; Martinez et al., 2014). The short extensions contain actin and their formation is thought to be mediated by the nsp1 protein (Laakkonen et al., 1998). They function in localizing virus away from the plasma membrane, thus protecting from inhibitory membrane-associated proteins and preventing superinfection of the same cell (Brown et al., 2018). Longer extensions have been observed for several alphaviruses, including SINV, SFV, CHIKV, VEEV, and are composed of both actin and tubulin (Brown et al., 2018; Martinez and Kielian, 2016). These structures do not fuse with the neighboring cell, but instead end in a flattened edge in close proximity to the cell membrane, thus promoting infection by creating a high concentration of viral particles near the cell surface and offering protection from neutralizing antibodies (Martinez and Kielian, 2016).

Alphavirus pathogenesis

Innate immune response

After the bite of a mosquito, alphaviruses enter the bloodstream and are first disseminated by dendritic cells (DCs) and Langerhans cells to the lymph nodes and spleen, where they replicate before spreading to muscles, bone, and cartilage (Assunção-Miranda et al., 2013). The acute inflammatory immune response is then activated by pattern recognition receptors (PRRs) on cell membranes responding to pathogen associated molecular patterns (PAMPs) on the virus (Akhrymuk et al., 2016; Carpentier and Morrison, 2018). This in turn leads to infiltration of monocytes, macrophages, neutrophils, natural killer (NK) cells, and lymphocytes into the synovium surrounding the joints, resulting in swelling and joint pain that simulates arthritis-like symptoms (Hazelton et al., 1985; Her et al., 2010; Poo et al., 2014). A type I Interferon (IFN) response predominates, although other proinflammatory cytokines and chemokines, such as L-

1, IL-6, IL-8, IL-16, CCL2, CCL4 and CXCL10, are also produced (Carpentier and Morrison, 2018; Mostafavi et al., 2019). It is thought that chronic arthritis may be due to persistent infection and replication of virus in macrophages (Assunção-Miranda et al., 2010; Way et al., 2002). Some studies have suggested that a more robust cytokine response early after initial infection may aid in clearing virus more rapidly, thus preventing chronic arthritis resulting from viral persistence in immune cells (Mostafavi et al., 2019). The acute phase of infection for alphaviruses typically extends to day 7 after initial infection, during which time the virus can be isolated and viral RNA detected via RT-PCR (Edwards et al., 2017; Silva and Dermody, 2017; Tanabe et al., 2018). IgG and IgM antibodies are produced starting 2 and 4 days after infection, respectively, and while the IgM response wanes after 4 months, IgG can persist for years after infection (Jain et al., 2017; Tanabe et al., 2018).

Adaptive immune response

The adaptive immune response, including T and B cells, plays an important role during alphavirus infection. Both CD4+ and CD8+ T lymphocytes have been observed in synovial fluid infiltrate (Assunção-Miranda et al., 2013; Mostafavi et al., 2019). For CHIKV infection, Th1, Th2, and Th17 responses predominate, while regulatory T cells (Tregs) are more prevalent during MAYV infections (Danillo and Benedito, 2018; Mostafavi et al., 2019). Presence of CD8+ T cells are predictive of rate of virus clearance, and patients not experiencing persistent joint pain were found to have higher levels of CD8+ T cells and recovered more quickly (Burrack et al., 2015; Miner et al., 2015).

Several studies using CHIKV animal models of infection have shown that antibody is an essential component of the immune response and also functions in clearing virus from infected cells. CHIKV-infected mice lacking mature B cells typically exhibit virus persistence in their joints (Hawman et al., 2013). In addition, prophylactic antibody administration of CHIKV mAbs in mice lacking both B and T cells prevented viral persistence, and both prophylactic and therapeutic

administration of mAb in IFNAR-/- mice prevented mortality and reduced CHIKV infection (Hawman et al., 2013; Pal et al., 2013). When anti-CHIKV mAbs were administered to rhesus macaques 1-3 days after infection, inflammation and viral spread to joint and muscle tissues was also reduced (Broeckel et al., 2017).

Antibodies against alphaviruses

RRV antibodies

A handful of mouse antibodies have previously been generated against RRV. Additionally, three mouse monoclonal antibodies were isolated against RRV, and limited characterization work has been performed (Davies et al., 2000; Kerr et al., 1992; Vrati et al., 1988). Neutralization escape mutants revealed that the binding sites for these mAbs are at residues 216, 234, and 246 on the RRV E2 glycoprotein, which are within the B domain and flanking region (Davies et al., 2000; Vrati et al., 1988). However, little is known about these antibodies, such as their mechanism of neutralization and whether they protect in animal models.

MAYV antibodies

In a recent study examining serum samples collected from individuals infected with MAYV, VEEV, or CHIKV in South America, a protein microarray analysis was used to determine the specificity of the antibody response against nine New and Old World alphaviruses (Smith et al., 2018). The analysis found that E2 was an antibody binding site targeted by all alphaviruses, while E1 was the target of antibodies in serum taken from only MAYV-infected individuals (Smith et al., 2018). This finding is also supported by a recent study conducted by Earnest et al. in which 18 neutralizing mouse mAbs were generated against MAYV (Earnest et al., 2019). The antibodies with the greatest neutralization potency were found to map to both the fusion peptide of the E1 protein and domain B of the E2 protein (Earnest et al., 2019). Surprisingly, the most

neutralizing mAbs were not necessarily protective against disease and viral spread when tested in a mouse model. Instead, Fc effector functions, including phagocytosis, were the most important predictors of efficacy *in vivo* (Earnest et al., 2019).

CHIKV antibodies

A number of mAbs, both human and mouse, have been generated against CHIKV, and most of these are well-characterized with both binding epitope and mechanism of neutralization available. Several human mAbs were generated from a CHIKV-immune donor, and these mAbs exhibit potent *in vitro* neutralization activity, with half maximal inhibitory (IC_{50}) values below 10 ng/mL (Smith et al., 2015). CHIKV mAbs have been found to block infection at the attachment, entry, fusion, and release steps with epitopes on both the A and B domains of the E2 protein (Fox et al., 2015; Jin and Simmons, 2019; Pal et al., 2013; Quiroz et al., 2019; Smith et al., 2015). Cryo-EM reconstructions of two human mAbs, C9 and IM-CKV063, revealed that it is possible for an alphavirus mAb epitope to span two heterodimers on the same trimeric spike, specifically the A domain of one E2 and the B domain of a neighboring E2, in such a way that the B domain is stabilized and fusion is prevented at acidic pH (Jin et al., 2015). Another human mAb, 5F10, also inhibits low-pH mediated fusion, but accomplishes this through binding solely to the B domain without any crosslinking activity (Porta et al., 2016). For inhibition of virus release from the cell membrane, bivalent mAb binding is essential, since Fab fragments from several CHIKV mAbs are less effective at inhibiting the budding step (Jin et al., 2015).

Alphavirus vaccines and therapeutic strategies

Vaccines

While no vaccine yet exists for any alphavirus, multiple clinical trials are in progress for CHIKV vaccines (Goyal et al., 2018). Promising candidates include live-attenuated, inactivated,

VLP, measles-virus-vectored, and mRNA-based strategies. I would like to highlight two of the relatively new platforms here. In the VLP vaccine strategy, HEK-293 cells are transfected with vectors encoding the CHIKV structural genes. The resulting particle undergoes only a single round of infection, but has been show to induce high titers of neutralizing antibodies and protects nonhuman primates from infection (Akahata et al., 2010; Goyal et al., 2018). In a phase I clinical trial, the VLP vaccine was safe, well-tolerated, and highly immunogenic after three intramuscular doses (Chang et al., 2014). While this vaccine seems promising, drawbacks include low-yield production as well as the necessity for multiple doses to elicit high titers of neutralizing antibodies (Goyal et al., 2018). However, these problems are being addressed as several candidates move forward into phase II trials (Goyal et al., 2018).

Another promising approach uses a recombinant measles virus in which the structural proteins of an attenuated strain of measles are replaced with those of CHIKV. In a Phase I trial in healthy individuals, neutralizing antibodies were generated after one vaccine dose, and 100% seroconversion was observed after the second dose (Ramsauer et al., 2015). Although some mild-to-moderate adverse effects were noted, no serious events occurred (Ramsauer et al., 2015). Several Phase II trials are ongoing, and this vaccine is advantageous due to low manufacturing costs combined with few doses required for efficacy, although pre-existing immunity to measles must be considered (Goyal et al., 2018).

mRNA delivery of antibodies

Recently, technological advances have enabled the delivery of antibodies in an mRNA instead of protein format, which reduces costs associated with manufacturing and development. mRNA therapy technology involves systemic or local delivery of naked mRNA or mRNA complexed with a particle RNA, which is then taken up by cells and translated by cellular machinery in the cytoplasm (Van Hoecke and Roose, 2019). Use of RNA rather than DNA has several advantages for nucleic acid therapeutics, including the induction of protein expression in

the cytoplasm and decreased risks of mutagenesis (Van Hoecke and Roose, 2019). Several preclinical and clinical trials are ongoing for mRNA therapy across several disciplines, including infectious diseases, antitoxins, and oncology (Bahl et al., 2017; Thran et al., 2017; Van Lint et al., 2012). Delivery of an ultra-potent CHIKV antibody as an mRNA encapsulated in a lipid nanoparticle was shown to protect mice from arthritis and musculoskeletal disease (Kose et al., 2019). In addition, high levels of mAb expression that protected against lethal virus challenge were achieved in both mice and macaques, and virus was reduced to undetectable levels (Kose et al., 2019). This mAb has been selected for further studies in humans, and could be used either prophylactically or therapeutically.

Antibody-dependent enhancement

Antibody-dependent enhancement (ADE) is a phenomenon that has been observed for some viruses, particularly flaviviruses, whereby antibodies produced in a prior infection lead to a more severe subsequent infection. Antibodies against the initial virus serotype are often non-neutralizing towards virus of a different serotype, and instead facilitate increased uptake of virus by monocytes and macrophages via Fcγ receptors (Smatti et al., 2018). For RRV, antibody-dependent enhancement (ADE) has been demonstrated in a few *in vitro* studies in the presence of subneutralizing concentrations of antibody, and the mechanism is thought to involve specific inhibition of antiviral gene transcription after entry of the virus into macrophages (Lidbury and Mahalingam, 2000; Linn et al., 1996). However, during RRV vaccine trials, ADE was not observed in mice passive transfer studies, and neutralizing antibodies in the serum of vaccinated individuals conferred protection in mice (Holzer et al., 2011). It is thus unlikely that ADE occurs during alphavirus infections *in vivo*.

Antibody Fc effector functions

Even though neutralizing antibodies are traditionally considered to be the gold standard for conferring protection, non-neutralizing antibodies have recently been shown to provide protection for a number of viruses, including HIV, influenza, Sindbis, yellow fever, and Marburg (Ackerman et al., 2016; Boere et al., 1985; Gould et al., 1986; Jegaskanda et al., 2016; Kajihara et al., 2012; Mendoza et al., 1988). While the Fv portion of the antibody mediates neutralization, the Fc region can mediate viral clearance through effector functions such as antibody-dependent cellular cytotoxicity (ADCC), complement-dependent cytotoxicity (CDC), cytokine production, or FcγR-mediated phagocytosis. These functions are increasingly being recognized as important for *in vivo* protection and viral clearance. Antibody-dependent cellular phagocytosis (ADCP) is mediated through binding of the Fc region to Fcγ receptors on monocytes, and promotes uptake and clearance of viral antigen (Tay et al., 2019). Another important effector function is ADCC, the result of antibody Fc interaction with Fcγ receptors on effector immune cells, typically NK cells (van Erp et al., 2019). Receptor binding causes the release of granzyme and perforin, triggering lysis of infected cells. Additionally, complement-dependent cytotoxicity (CDC) can occur when antibodies bind to viral antigen presented on the cell surface, which subsequently activates complement to form a membrane attack complex that may lead to cell lysis (Yamashita et al., 2016). For several alphaviruses, including MAYV and CHIKV, effector functions have also been shown to be important for mAb protection *in vivo* through mediating virus clearance of infected cells (Earnest et al., 2019; Fox et al., 2019).

Goals of thesis work

In the following chapters, I describe work addressing significant unanswered questions in the field of alphavirus biology. Although the human antibody response to natural infection with CHIKV has been characterized, the virus-specific antibody response to natural infection with emerging viruses MAYV and RRV has not been studied. In addition, whether cross-reactive

human antibodies can be elicited during a natural infection is not well understood, and the putative epitope(s) targeted by broadly neutralizing human antibodies remains unknown. In the context of these outstanding questions in the field, the overall goals of the work presented here are to 1) understand how antibodies contribute to protection during RRV and MAYV natural infection and 2) to determine whether antibodies that are broadly neutralizing against several alphavirus species can be elicited during a natural infection, and if so, to elucidate the binding footprint of such broadly neutralizing mAbs. Knowledge of the molecular determinants and mechanism of antibody cross-neutralization against multiple alphaviruses will inform rational vaccine design, and better insight into the virus-specific human antibody response to emerging alphaviruses will reveal protective epitopes and advance potential therapeutic candidates.

CHAPTER II

HUMAN MONOCLONAL ANTIBODIES AGAINST ROSS RIVER VIRUS TARGET EPITOPES WITHIN THE E2 PROTEIN AND PROTECT AGAINST DISEASE

Introduction

In a previous clinical trial of an experimental inactivated RRV vaccine, immunized individuals produced neutralizing antibodies in serum that conferred protection in mice during subsequent passive transfer studies (Aichinger et al., 2011; Holzer et al., 2011; Wressnigg et al., 2015). However, we know little about the humoral immune response to RRV, and human monoclonal antibodies (mAbs) specific for RRV have not been reported. Several murine mAbs that bind to RRV exist, although functional characterization is limited (Davies et al., 2000; Fox et al., 2015; Kerr et al., 1992; Vrati et al., 1988). Neutralization escape mutants of mouse anti-RRV mAbs have identified residues in the B domain and the flanking region within the E2 glycoprotein that may be important for antibody engagement (Davies et al., 2000; Fox et al., 2015; Vrati et al., 1988). In comparison, the A and B domains on the E2 glycoprotein and domain II of the E1 glycoprotein of the related alphavirus chikungunya virus (CHIKV) are important targets of neutralizing antibodies (Chua et al., 2014; Pal et al., 2013; Smith et al., 2015).

In this chapter, I describe human mAbs isolated from individuals who were naturally infected with RRV. These mAbs neutralize RRV infectivity in cell culture, protect mice from clinical disease when administered therapeutically, and reduce viral burden in multiple tissues. Furthermore, these mAbs bind to multiple domains on the E2 protein, as determined by alanine scanning mutagenesis, and roughly fall into two competition-binding groups, revealing that the A and B domains are the major antigenic targets for the human neutralizing antibody response. Additionally, I These mAbs blocked infection by preventing viral attachment and entry to the cell

and also blocked at a later step in the virus life cyle associated with viral fusion. Notably, nearly all of the neutralizing mAbs blocked attachment of RRV to Mxra8, a recently discovered entry receptor for RRV, CHIKV, and other arthritogenic alphaviruses (Zhang et al., 2018).

I would like to acknowledge Julie Fox in Michael Diamond's group at Washington University in St. Louis for performing all mouse experiments, Thomas Morrison at the University of Colorado for providing clinical isolate strains of RRV, and Chris Slaughter at Vanderbilt University for performing logistical curve analyses for neutralization data.

Isolation of RRV-reactive human mAbs

I isolated a panel of mAbs from two subjects, one with a previous laboratory-confirmed case of RRV that was acquired in Australia in 1987, and the other with a history of childhood infection in Australia in the 1990s. We obtained blood samples after written informed consent with approval from the Vanderbilt University Medical Center Institutional Review Board from the first donor in 2016 and from the second donor in 2017, and peripheral blood mononuclear cells (PBMCs) were isolated. I transformed B cells with Epstein-Barr virus (EBV) before screening for RRV-reactive antibodies in cell supernatants through direct virus binding ELISA. I then established stable hybridoma cell lines from B cells secreting antibody reactive with the virus, and purified 21 mAbs after cloning cell lines by single-cell flow cytometric sorting. All but one of the mAbs isolated were of IgG1 subclass, and the antibody clonotypes identified by the recombined antibody variable genes were distinct. Two antibodies, designated RRV-130 and RRV-135, had identical variable (V) gene region sequences, but used a different joining (J) gene in the heavy chain (**Table 1**).

Table 1. Antibody variable gene region sequence features for RRV antibodies. mRNA was isolated from clonal hybridoma cells, and cDNA was synthesized for Sanger automated DNA sequence analysis. The specific gene, allele, CDR length, and V-D and D-J junctions were determined through use of the IMGT program.

Name	V-GENE/allele	J-GENE/allele	D-GENE/allele	CDR-IMGT lengths	AA JUNCTION
RRV 6-HC	*IGHV3-23*04 F*, or *IGHV3-23D*02 F*	*IGHJ5*01 F*, or *IGHJ5*02 F*	*IGHD6-13*01 F*	8.8.11	CANLYISSWYLYW
RRV 6-LC	*IGKV3-15*01 F*	*IGKJ1*01 F*		6.3.11	CQQYNDWPPGGTF
RRV 12-HC	*IGHV4-31*03 F*	*IGHJ3*02 F*	*IGHD5-24*01 ORF*	10.7.15	CARVGGDGNNRDAFDIW
RRV 12-LC	*IGLV3-1*01 F*	*IGLJ3*02 F*		6.3.9	CQAWDSTTGVF
RRV 19-HC	*IGHV3-21*01 F*	*IGHJ6*02 F*	*IGHD2-15*01 F*	8.8.18	CARDDCSGSSCYYYYGMDVW
RRV 19-LC	*IGKV2-28*01 F*, or *IGKV2D-28*01 F*	*IGKJ3*01 F*		10.3.11	CMQALQTPRSFTF
RRV 34-HC	*IGHV3-7*01 F*	*IGHJ4*02 F*	*IGHD6-19*01 F*	8.8.13	CARDFDSSGWFPAYW
RRV 34-LC	*IGLV8-61*01 F*	*IGLJ3*02 F*		9.3.X	CLLYMISVLS#VF
RRV 49-HC	*IGHV4-61*01 F*	*IGHJ4*02 F*	*IGHD3-22*01 F*	10.7.14	CARGTRGYPQGYPDSW
RRV 49-LC	*IGLV3-10*01 F*	*IGLJ3*02 F*		6.3.10	CYSTDSSGTPLF
RRV 86-HC	*IGHV2-70*01 F*	*IGHJ4*02 F*	*IGHD6-13*01 F*	10.7.11	CTGGSSWYVPDYW
RRV 86-LC	*IGLV1-44*01 F*	*IGLJ2*01 F*, or *IGLJ3*01 F*		8.3.12	CAVWDNSLNGRVVF
RRV 92-HC	*IGHV3-15*01 F*	*IGHJ4*02 F*	*IGHD3-10*01 F*	8.10.19	CVNEAYYYGSGSYWEYYFDYW
RRV 92-LC	*IGLV3-19*01 F*	*IGLJ2*01 F*, or *IGLJ3*01 F*		6.3.10	CNSRDTSGNHLF
RRV 130-HC	*IGHV1-24*01 F*	*IGHJ2*01 F*	*IGHD3-10*01 F*	8.8.21	CTTGSYYHGWGSYSGRNWYFDLW
RRV 130-LC	*IGLV3-19*01 F*	*IGLJ2*01 F*, or *IGLJ3*01 F*		6.3.6	CNSRDSGF
RRV 133-HC	*IGHV3-30*03 F*, or *IGHV3-30*18 F* or *IGHV3-30-5*01 F*	*IGHJ6*02 F*	*IGHD3-3*02 F*	8.8.23	CARDQGLEVAFSQWSHYDYYGMDVW
RRV 133-LC	*IGLV2-14*01 F*	*IGLJ2*01 F*, or *IGLJ3*01 F*		9.3.11	CSSYTSISTSVLF
RRV 135-HC	*IGHV1-24*01 F*	*IGHJ4*02 F*	*IGHD3-10*01 F*	8.8.19	CATVAHYHGSDSYYNFYFDFW
RRV 135-LC	*IGLV3-19*01 F*	*IGLJ2*01 F*, or *IGLJ3*01 F*		6.3.12	CTSRDSSSSDLVIF
RRV 136-HC	*IGHV3-15*01 F*	*IGHJ5*02 F*	*IGHD2-8*01 F*	8.10.10	CMTESDMTFDPW
RRV 136-LC	*IGKV2-28*01 F*, or *IGKV2D-28*01 F*	*IGKJ3*01 F*		11.3.9	CMQALQTPYTF
RRV 139-HC	*IGHV3-23*04 F*	*IGHJ6*02 F*	*IGHD4-17*01 F*	8.8.16	CATATTVTYYYYYGMDVW
RRV 139-LC	*IGKV2-28*01 F*, or *IGKV2D-28*01 F*	*IGKJ3*01 F*		11.3.10	CMQALQPPRFTF
RRV-191 HC	*IGHV4-38-2*01 F*	*IGHJ6*02 F*	*IGHD2-21*02 F*	9.7.15	CVRERVGVTSYFGMDVW
RRV-191 LC	*IGKV-39*01 F* or *IGKV1D-39*01 F*	*IGKJ4*01 F*		6.8.8	CHQSYTGNTF
RRV-196 HC	*IGHV3-15*01 F*	*IGHJ1*01 F*	*IGHD3-3*01 F*	8.8.22	CTTISYYDFWSGHYMGREEYFQHW
RRV-196 LC	*IGLV3-19*01 F*	*IGLJ2*01 F* or *IGLJ3*01 F*		6.3.12	CNSRDSSGDPHVVF
RRV-199 HC	*IGHV3-33*01 F*, or *IGHV3-33*05* or *IGHV3-33*06 F*	*IGHJ6*202 F*	*IGHD6-19*01*		

RRV-199 LC	*IGLV2-8*01 F*	*IGLJ2*01 F,* or *IGLJ3*01 F*		9.3.11	CSSYADNNNFVVF
RRV-200 HC	*IGHV3-21*01 F,* or *IGHV3-21*02 F*	*IGHJ6*02 F*	*IGHD3-22*01 F*	8.8.28	CAREIVSYGDYGDSSGTSKY FYYYYGVDVW
RRV-200 LC	*IGKV1-12*01 F,* or *IGKV1-12*02,* or *IGKV1D-12*02 F*	*IGKJ3*01 F*		6.3.11	CQQANSFPPGFTF
RRV-201 HC	*IGHV3-33*01 F,* or *IGHV3-33*05 F,* or *IGHV3-33*06 F*	*IGHJ6*02*	*IGHD6-19*01 F*	8.8.18	CARDQGQWLVRPGWYGMD VW
RRV-201 LC	*IGLV2-8*01 F*	*IGLJ2*01 F,* or *IGLJ3*01 F*		9.3.11	CSSYADNNNFVVF
RRV-205 HC	*IGHV3-73*02 F*	*IGHJ6*02*	*IGHD5-12*01 F*	8.10.16	CLGNSGYDPEYFYGMDVW
RRV-205 LC	*IGLV6-57*01 F,* or *IGLV6-57*02 F*	*IGLJ2*01 F,* or *IGLJ3*01 F*		8.3.9	CQSYDRSNVVF
RRV-207 HC	*IGHV4-34*01 F*	*IGHJ4*02 F*	*IGHD6-13*01 F*	8.7.13	CARYVLGSSWPFDYW
RRV-207 LC	*IGKV1-39*01 F,* or *IGKV1D-39*01*	*IGKJ4*01 F*		6.3.9	CQQSSSTPLTF
RRV-210 HC	*IGHV3-11*01F*	*IGHJ5*02 F*	*IGHD1-26*01 F*	8.8.16	CARSVMGGTTMGEWFDPW
RRV 210 LC	*IGLV1-40*01 F*	*IGLJ2*01 F,* or *IGLJ3*01 F*		9.3.12	CQSYDSSLSGSVVF
RRV-221 HC	*IGHV1-18*01 F*	*IGHJ6*02 F*	*IGHD3-10*01 F*	8.8.22	CAREEGITLVRGTSNYYYYG MDVW
RRV-221 LC	*IGKV2-28*01 F,* or *IGKV2D-28*01 F*	*IGKJ2*01 F*		11.3.9	CMQALQTPHTF

Assessment of mAb binding and neutralization activity

I determined that 21 RRV-reactive mAbs bound to infectious RRV virions in a direct ELISA. Fifteen of these mAbs had half maximal effective concentration (EC_{50}) values for binding to RRV of less than 100 ng/mL (**Figure 7A**). When I tested for neutralization against the prototype strain RRV T48 in a focus reduction neutralization test (FRNT), I found that five mAbs had half maximal inhibitory concentration (IC_{50}) values less than 15 ng/mL, indicating highly potent neutralization in cell culture, whereas nine other mAbs had neutralization IC_{50} values less than 100 ng/mL (**Figure 7A, Table 2**). I observed two distinct neutralization profiles for these mAbs:

one group of seven mAbs left a residual fraction of non-neutralized virus with a 60 to 90% maximal reduction of infection (**Figure 7B, Figure 8**), whereas the second group of fourteen antibodies completely eliminated virus infection (**Figure 7C, Figure 8**). I also tested four antibodies in neutralization assays using a representative panel of five diverse clinical isolates of RRV and observed that they had comparable neutralization potencies compared to the T48 strain (**Figure 9, Table 2**).

A

Antibody	Donor #	Isotype	Light chain	RRV Neutralization		RRV Binding
				IC_{50} (ng/mL)	E_{max}	EC_{50} (ng/mL)
RRV-130	1	IgG1	λ	6 [3-10]	100	30 [27-56]
RRV-199	2	IgG1	λ	7 [3-19]	96	120 [84-172]
RRV-135	1	IgG1	λ	10 [6-14]	94	15 [7-31]
RRV-92	1	IgG1	λ	11 [3-57]	92	43 [34-54]
RRV-210	2	IgG1	λ	13 [8-22]	100	531 [435-648]
RRV-19	1	IgG1	κ	16 [13-23]	99	22 [16-30]
RRV-200	2	IgG1	κ	27 [18-42]	100	47 [32-70]
RRV-133	1	IgG1	λ	29 [21-41]	100	17 [10-28]
RRV-221	2	IgG1	κ	33 [7-217]	90	72 [54-96]
RRV-139	1	IgG1	κ	47 [14-135]	96	16 [8-33]
RRV-201	2	IgG1	λ	49 [21-112]	94	18 [10-33]
RRV-49	1	IgG1	λ	58 [26-128]	99	50 [34-74]
RRV-12	1	IgG1	λ	63 [8-1e+20]	70	9 [7-13]
RRV-196	2	IgG1	λ	75 [23-205]	96	208 [162-267]
RRV-86	1	IgG1	λ	174 [55-636]	65	2 [2-4]
RRV-34	1	IgG1	λ	285 [16-1e+20]	62	17 [8-37]
RRV-191	2	IgG1	κ	334 [141-905]	96	163 [113-234]
RRV-205	2	IgG1	λ	334 [70-2,290]	70	9 [3-27]
RRV-136	1	IgG1	κ	988 [157-1e+20]	68	307 [184-511]
RRV-207	2	IgG3	κ	1,490 [901-2,430]	93	120 [101-144]
RRV-6	1	IgG1	κ	2,290 [509-12,200]	67	79 [40-151]

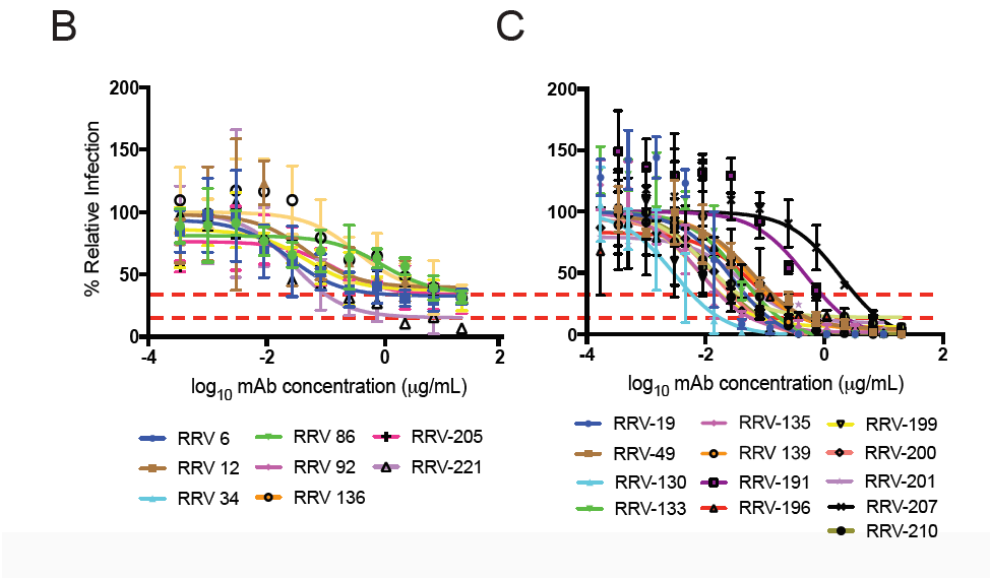

Figure 7. Antibodies generated against RRV bind and neutralize RRV. (**A**) Isotype, subclass, light chain designation (λ or κ), half maximal inhibitory concentration (IC_{50}) for neutralization, and half maximal effective concentration (EC_{50}) for binding are shown. Binding was measured using ELISA; neutralization was measured using a focus reduction neutralization test (FRNT). Both ELISA and FRNT were performed in triplicate, and 95% credible interval for EC_{50} and IC_{50} values are indicated in brackets. Curves and EC_{50} binding values were obtained using non-linear fit analysis using Prism software version 7 (GraphPad Software). IC_{50} neutralization values were obtained using 5 parameter logistic curves. Values are color-coded according to binding or neutralization potency, with a stronger binder or neutralizer indicated by a darker blue or green color, respectively. > indicates neutralization was not detected, when tested at concentrations up to 10,000 ng/mL. (**B**) Neutralization profiles of mAbs are divided into two groups, based on pattern of activity in a dilutional FRNT assay. Eight antibodies left a resistant fraction of 10 to 40% virus (based on E_{max} value), indicated by the red dotted lines and (**C**) thirteen antibodies completely eliminated virus. Error bars represent SD, and curves representative of multiple independent experiments are shown.

Table 2. **Summary of neutralization of different RRV strains**. The IC_{50}, or concentration that gives a 50% reduction with accompanying 95% credible intervals, is listed along with R^2, or percent of the variability explained by the regression fit, and E_{max}, the estimated percentage maximum neutralization.

RRV strain	MAb	Neutralization IC_{50} (ng/mL)	[95% credible interval]	R^2	E_{max}
T48	RRV-6	2,294	[509 – 12,228]	0.59	66
	RRV-12	63	[8.3 - > 2E5]	0.73	70
	RRV-19	16	[13 - 23]	0.92	99
	RRV-34	286	[16 - > 2E5]	0.48	61
	RRV-49	58	[26 – 128]	0.90	99
	RRV-86	174	[55 - 636]	0.72	65
	RRV-92	11	[2.7 - 57]	0.95	91
	RRV-130	5.7	[2.9 - 10]	0.78	101
	RRV-133	29	[21 - 41]	0.94	101
	RRV-135	10	[6.3 - 14]	0.88	93
	RRV-136	988	[157 - > 2E5]	0.73	67
	RRV-139	47	[14 - 135]	0.80	96
	RRV-191	334	[142 - 905]	0.79	96
	RRV-196	75	[23 - 205]	0.85	96
	RRV-199	6.7	[2.8 - 18]	0.86	95
	RRV-200	27	[18 - 42]	0.94	100
	RRV-201	49	[21 - 112]	0.86	93
	RRV-205	334	70 – 2,288]	0.56	70
	RRV-207	1,487	[901 – 2,429]	0.92	92
	RRV-210	13	[7.8 - 22]	0.87	100
	RRV-221	33	[6.8 - 217]	0.87	90
PW7	RRV-19	12	[8.2 - 16]	0.93	97
	RRV-92	18	[8.6 - 43]	0.81	81
	RRV-130	4.1	[1.3 - 8.4]	0.77	100
	RRV-135	12	[6.9 - 19]	0.85	94
SN11	RRV-19	10	[7 - 14]	0.92	96
	RRV-92	17	[11 - 34]	0.88	80
	RRV-130	9.0	[5.9 - 13]	0.9	99
	RRV-135	8.7	[5.9 - 13]	0.86	94
PW14	RRV-19	13	[6.9 - 28]	0.65	86
	RRV-92	70	[29 - 202]	0.86	74
	RRV-130	11	[8.5 - 14]	0.94	96
	RRV-135	14	[10 - 23]	0.89	92
2897601	RRV-19	12	[9.9 - 15]	0.95	95
	RRV-92	41	[16 - 147]	0.85	79
	RRV-130	13	[7.4 - 24]	0.84	98
	RRV-135	15	[8 - 38]	0.72	82
O'Regan	RRV-19	12	[9.2 - 14]	0.94	94
	RRV-92	105	[41 - 313]	0.79	81
	RRV-130	12	[9.5 - 16]	0.94	97
	RRV-135	17	[12 - 25]	0.94	96

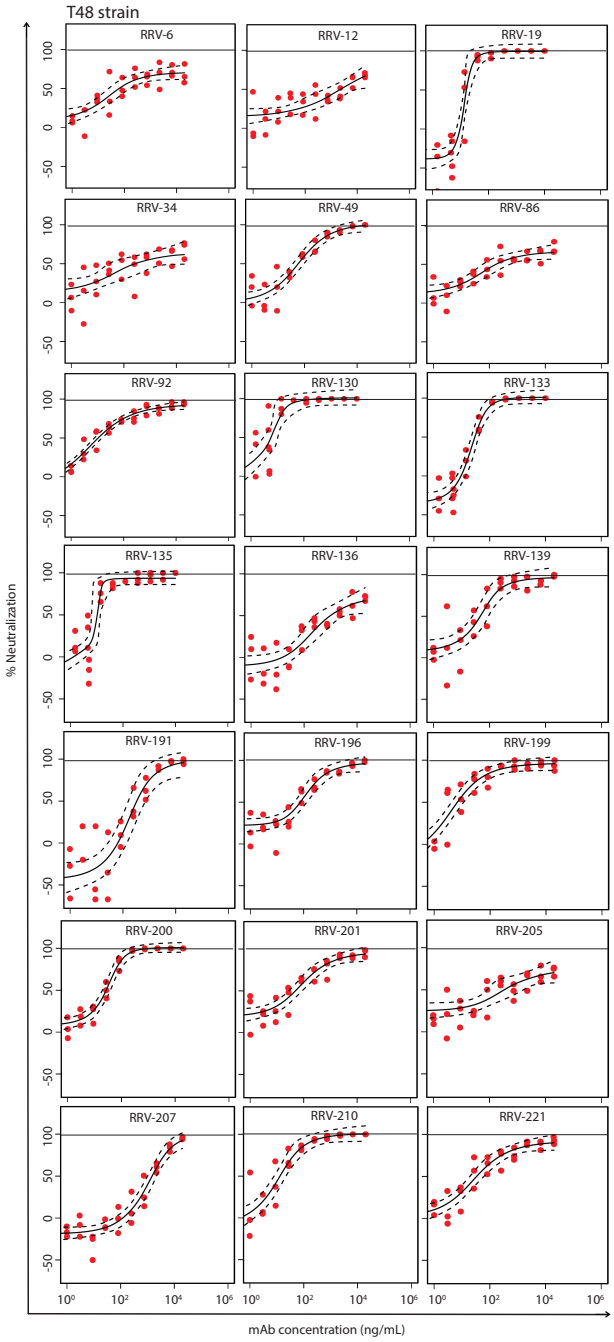

Figure 8. Neutralization activity of RRV mAbs against RRV strain T48. Red circles represent percent neutralization relative to control at different antibody concentrations. Logistic curves are indicated by solid lines, and 95% credible intervals are indicated by dashed lines. A line at 100% neutralization highlights mAbs that completely neutralize. Multiple experiments were performed in triplicate, and the best fit curve is shown.

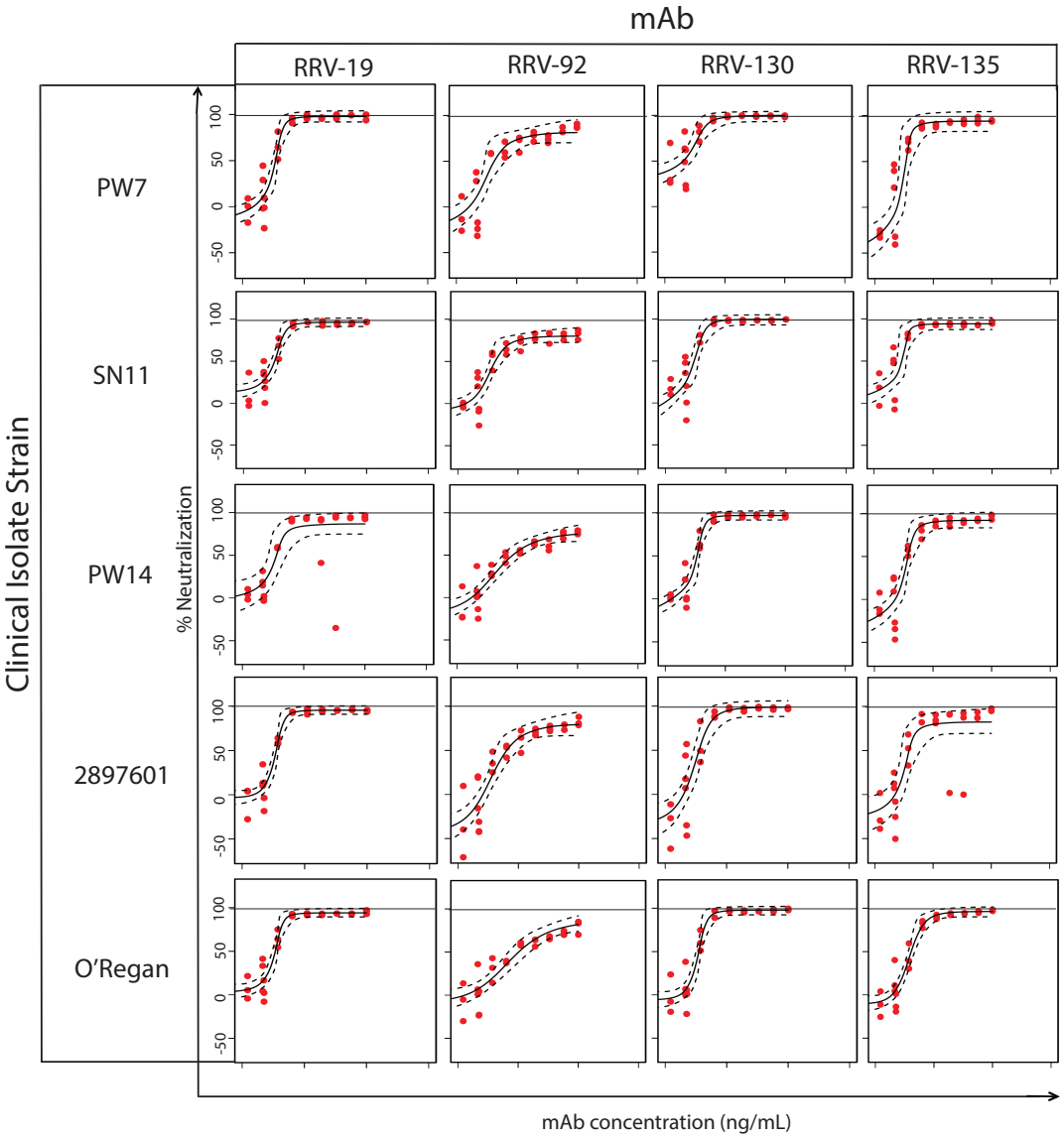

Figure 9. Neutralization profiles for five clinical isolate strains of RRV tested against four antibodies using a focus reduction neutralization test. RRV strains PW7 and SN11 were isolated from adult patients in 2009. RRV strain 2897601 (QML 2006) was isolated from an adult patient in 2006, and RRV strain O'Regan was isolated from an EP patient. The P7 and P14 isolates were sequenced, and four mutations in the E2 protein were identified in the P7 strain: I76L, D132N, S182P, and R251K; for the P14 strain, there are two mutations in the E2 protein: I67L and R251K (Aaskov et al., 1997; Liu et al., 2011; Wressnigg et al., 2015). Red circles represent percent neutralization relative to control at different antibody concentrations. Logistic curves are indicated by solid lines, and 95% credible intervals are indicated by dashed lines. Multiple experiments were performed in triplicate, and the best fit curve is shown.

Epitope mapping using alanine scanning mutagenesis and competition-binding assays

To identify the antigenic regions recognized by these neutralizing mAbs, I first performed alanine scanning mutagenesis using cell-surface expression of RRV E3-E2-6K-E1 structural proteins and flow cytometry to identify critical binding residues in the E2 glycoprotein. The library consisted of the first 300 residues of the E2 protein individually mutated to alanine, with alanine residues mutated to serine. I observed a loss of binding for eight mAbs, with residues spread across the A, B, and C domains, as well as arch region of the E2 protein (**Figure 10A, 11**). RRV-196 had loss-of-binding residues within the A domain alone, whereas RRV-92 and RRV-210 lost binding when residues were changed in the A, B and C domains, as well as arch region, of E2 (**Figure 10A, 10B**). Seven of the eight mAbs targeted regions within the B domain, and of those, three mAbs had loss-of-binding residues within the B domain alone. Within the B domain, residues 189, 206, and 221 showed decreased binding for two mAbs, and mutation of residue 211 resulted in loss-of-binding for six mAbs: RRV-86, RRV-92, RRV-130, RRV-205, RRV-210, and RRV-221 (**Figure 10A, 10B**). When I mapped these residues onto the surface of the structure of the related CHIKV E1/E2 heterodimer (PDB 3N42) (Voss et al., 2010), I found that most residues clustered within the surface-exposed region of the viral glycoprotein, with only a few located at the base of the heterodimer subunit in the C domain (**Figure 10C**).

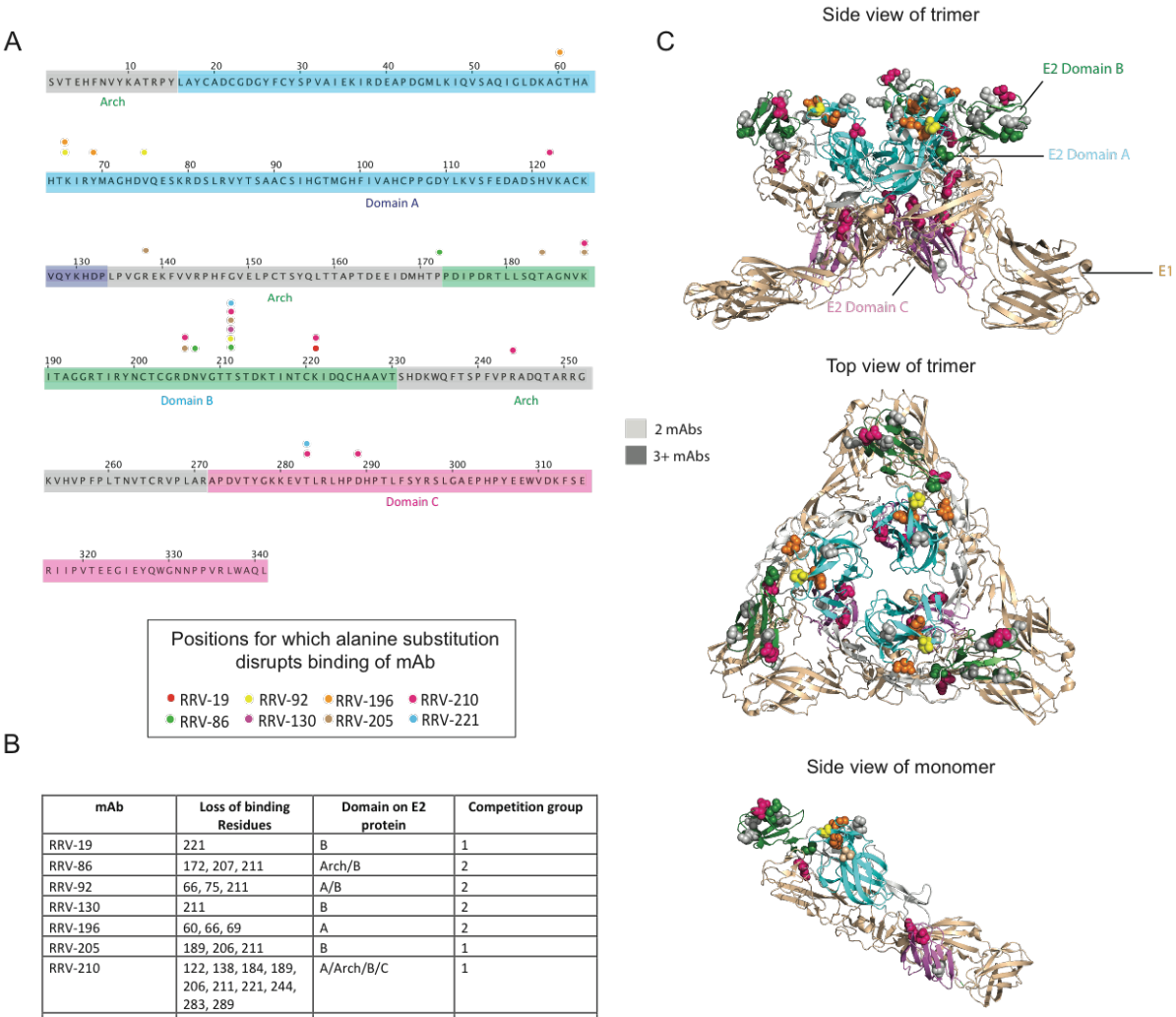

mAb	Loss of binding Residues	Domain on E2 protein	Competition group
RRV-19	221	B	1
RRV-86	172, 207, 211	Arch/B	2
RRV-92	66, 75, 211	A/B	2
RRV-130	211	B	2
RRV-196	60, 66, 69	A	2
RRV-205	189, 206, 211	B	1
RRV-210	122, 138, 184, 189, 206, 211, 221, 244, 283, 289	A/Arch/B/C	1
RRV-221	211, 283	B/C	1/2

Figure 10. Alanine scanning mutagenesis reveals E2 residues important for mAb binding.
(A) Amino acid sequence of E2 from the RRV T48 strain, indicating loss-of-binding residues determined through alanine scanning mutagenesis. Each amino acid residue is numbered according to its position within the E2 protein, with the A, B, and C domains along with the arch regions (Smith et al., 2015; Voss et al., 2010) color coded (grey, arch; dark blue, domain A; green, domain B; magenta, domain C). A circle above the sequence indicates the position of residues for which alanine substitution disrupts mAb binding, with each circle color corresponding to a different mAb. **(B)** Summary table with residues disrupted by alanine scanning mutagenesis, including the E2 domain in which they are found and the competition group to which the mAb belongs (see **Figure 14**) Two independent experiments were performed and values were averaged for loss-of-binding determination. A cutoff value of 10% was used, with the requirement that two other mAbs have binding of 50% or greater. **(C)** Loss-of-binding residues mapped onto the crystal structure of the CHIKV E1/E2 heterodimer (PDB 3N42), with three heterodimer subunits combined to represent the viral spike trimer. Top and side views of the trimer are shown, with residues important for mAb binding color coded as in (**A**) and shown as space-filling forms. The E2 protein is shown in green and the E1 protein in light brown, and each of the domains is labeled as in (**A**). A side view of a single heterodimer subunit is also shown (bottom).

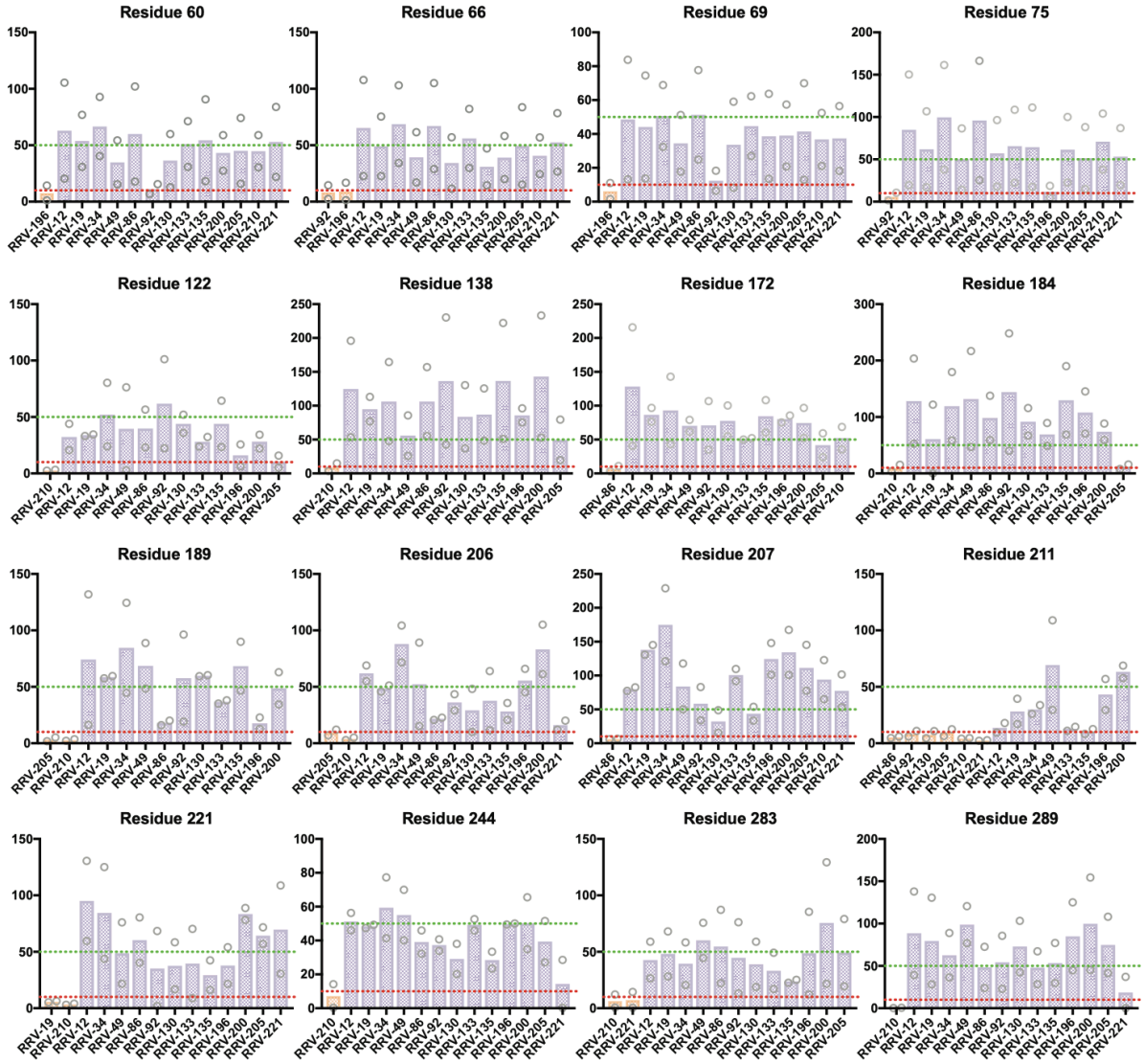

Figure 11. Alanine scanning mutagenesis antibody binding to mutant residues. Graphs showing percent binding of antibody to mutant residues relative to WT surface-expressed RRV proteins in alanine scanning mutagenesis. A cutoff value of 10% (indicated by red dotted line) was used to determine mAb loss-of-binding at a residue, with the requirement that two other mAbs have binding of 50% or greater (indicated by the green dotted line). The orange colored graphs indicate mAbs meeting this requirement. The bar graphs represent the mean of two experiments, with the values from each individual experiment indicated by the white dots.

As another method to distinguish antibody epitopes, I performed a quantitative competition-binding assay using biolayer interferometry (BLI). I used RRV-86 immobilized on Fc-specific anti-human IgG biosensor to capture virus-like particles (VLPs) expressing the full

set of structural proteins (C-E3-E2-6K-E1). I then added two antibodies sequentially, and the percent binding of the second antibody in the presence of saturating concentrations of the first was determined. Five out of twenty-one mAbs were excluded from the analysis due to undetectable or weak binding to VLPs in this format. Antibodies in the panel binned roughly into two competition-binding groups, with seven mAbs in the first group (red box), seven in the second group (blue boxes), and two in an overlapping group (grey boxes) (**Figure 12A**). The order of antibody addition affected the competition profile, as in some cases the first antibody blocked binding of the second antibody, but the reverse was not true, as with RRV-200 and RRV-34. This effect may be due in part to steric hindrance mediated by Fc regions in the full-length antibody during binding to the VLP. While there was no correlation between whether mAbs were completely neutralizing or not and their competition group, I did observe an association between the alanine scanning mutagenesis data and competition data. MAbs in the first competition group (red) showed predominant epitopes within the B domain (green) and C domain (magenta) when overlaid on the CHIKV E1/E2 trimer, whereas those in the second group (orange) mapped primarily to the A domain (dark blue) and arch regions (grey) **(Figure 12B**). Two mAbs had a competition profile that overlapped between the two groups, and additionally, some residues uncovered through the alanine scanning mutagenesis were targeted by mAbs within both competition groups (grey) (**Figure 12B**).

A

First antibody \ Second antibody	RRV-133	RRV-139	RRV-200	RRV-19	RRV-205	RRV-201	RRV-210	RRV-49	RRV-221	RRV-86	RRV-12	RRV-196	RRV-34	RRV-92	RRV-130	RRV-135
RRV-133	6	11	16	14	7	8	3	7	9	68	65	93	74	82	86	84
RRV-139	17	8	23	25	31	25	17	22	7	37	30	26	64	47	51	42
RRV-200	17	0	10	9	19	15	8	9	4	5	23	13	18	8	16	8
RRV-19	9	-9	-1	2	6	3	-2	7	-5	7	27	5	40	25	31	4
RRV-205	0	10	20	30	13	-5	-9	1	-5	14	55	74	1	19	23	24
RRV-201	13	7	22	13	22	11	5	5	3	56	78	98	71	64	70	64
RRV-210	27	4	52	20	41	32	19	14	17	19	104	116	16	11	15	17
RRV-49	39	42	45	53	32	24	12	4	-1	34	29	22	25	32	46	31
RRV-221	7	36	79	62	52	41	27	16	18	33	64	67	28	21	31	28
RRV-86	22	5	17	16	13	14	-1	-13		0	-3	2	-12	-10	-3	-12
RRV-12	59	4	18	18	69	59	33	9	13	-1	1	13	5	-1	-1	0
RRV-196	67	17	17	35	68	64	53	29	13	2	8	14	7	1	0	2
RRV-34	69	69	67	94	31	78	63	13	5	-3	-2	15	3	-3	-4	-7
RRV-92	73	57	55	80	86	86	52	29	11	2	6	17	5	2	10	3
RRV-130	44	30	30	54	59	55	48	39	15	3	6	14	4	2	9	2
RRV-135	86	25	31	62	98	92	72	30	13	3	3	16	5	1	0	1

B

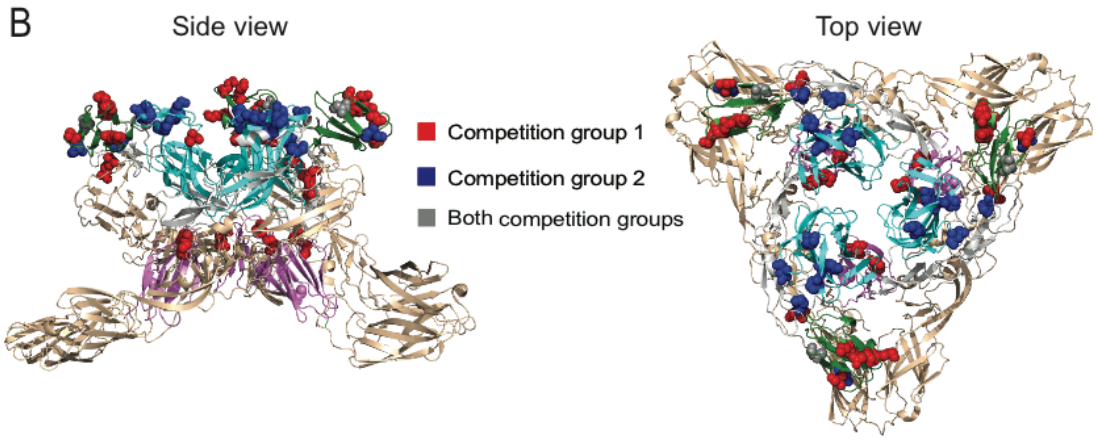

Figure 12. Epitope mapping studies to identify groups of mAbs recognizing similar major antigenic sites. (**A**) An Octet RED96 instrument (Pall FortéBio) was used to perform epitope binning studies using competition binding. RRV-86 was used as a capture antibody and was immobilized onto Fc-specific anti-human IgG biosensors for 2 min. After measuring the baseline signal, the biosensor tips were immersed into wells containing RRV VLPs for two minutes. After another baseline measurement, biosensors then were transferred to wells containing a first mAb at a concentration of 100 µg/mL for 5 min, before immersion in a solution containing a second mAb, also at a concentration of 100 µg/mL for 5 min. The percent competition of the second mAb in the presence of the first mAb was determined by comparing the maximal signal of binding for the second mAb in the presence of the first antibody to the maximal signal of the second mAb in the absence of competition. Competition was defined by reduction of the maximal binding score to <25% of un-competed binding (black boxes). A non-competing mAb was identified when maximal binding was >50% of un-competed binding (white boxes). A 25 to 50% reduction in maximal binding was considered intermediate competition (gray boxes). Some values are negative due to slight dissociation of the first antibody in the presence of the second. The colored boxes denote two overlapping asymmetrical competition groups. The blue dotted boxes highlight antibody self-competition. (**B**) Residues corresponding to mAbs in each competition group as determined through alanine scanning mutagenesis mapped onto the CHIKV E1/E2 trimer of heterodimers (PDB 3n42). Space-filling models for loss-of-binding residues in competition group 1 are shown in red, and loss-of-binding residues for competition group 2 in orange. A top view of the trimer is shown (left) as well as a side view (right).

Mechanisms of virus neutralization

To gain insight into the mechanism(s) of neutralization used by these mAbs, I performed pre- and post-attachment neutralization assays with representative mAbs from each of the competition-binding groups. RRV-19, RRV-133, and RRV-139 were chosen from group 1, and RRV-130 and RRV-135 were chosen from group 2. These mAbs have a range of neutralization potencies. In the pre-attachment assay, virus was incubated with antibody at 4°C before addition to Vero cell monolayers, also at 4°C. Virus not attached to the cells and unbound antibody were washed out, and then attached virus was allowed to internalize during a brief incubation period at 37°C. Cell monolayers were stained 18 h later, as in the FRNT. All six mAbs neutralized in the pre-attachment assay, indicating that these mAbs block either cell adherence or entry of virus (**Figure 13A**). In the post-attachment assay, which detects effects both on viral entry and on downstream steps such as fusion from the endosome, virus was adsorbed first to cells at 4°C. Excess virus was washed out before mAb was added, also at 4°C. After a brief incubation period at 37°C to allow virus internalization, cells were overlaid with methylcellulose, incubated, and then fixed and stained 18 h later. All mAbs also blocked at post-attachment steps, although post-attachment neutralization was slightly less potent than pre-attachment for RRV-130, RRV-133, RRV-135, and RRV-139 (**Figure 13A**).

To determine if some of the inhibitory activity in the post-attachment assay was due to antibody-mediated inhibition of RRV fusion to cell membranes after entering the endosome, I performed a fusion from without (FFWO) assay. This test, which measures fusion of virus with the plasma membrane under low pH conditions, has been used as a surrogate assay for determining antibody inhibition of alphavirus fusion in endosomes (Pal et al., 2013). I first added virus to cells at 4°C before adding mAbs. Subsequently, after removing unbound virus and antibody, I pulsed cells at 37°C in a low-pH medium to promote plasma membrane-mediated viral fusion. Virus that entered the cells was stained with fluorescent antibodies 14 h later and detected by flow cytometry. At a concentration of 10 μg/mL, I found that RRV-133, RRV-130,

RRV-135, RRV-139, and RRV-19 significantly reduced virus entry to cells under low-pH conditions (**Figure 13B, 13C**). Antibodies in both competition-binding groups inhibited fusion, so inhibition of fusion by mAbs does not seem to correlate with mapping to the A or B domain.

Recently, the cell surface protein Mxra8 was identified as a receptor for CHIKV and several other arthritogenic alphaviruses, including RRV, MAYV, and ONNV viruses (Zhang et al., 2018). To determine whether my RRV mAbs can block engagement of virus to this receptor, I performed a competition ELISA in which RRV virions were captured onto wells of a microtiter plate, and then mAbs were bound to virus before addition of a purified recombinant mouse Mxra8-Fc fusion protein. MAbs from each of the competition-binding groups blocked binding of Mxra8-Fc binding to RRV (**Figure 13D**). All mAbs that poorly blocked binding to Mxra8 had IC_{50} values of greater than 100 ng/mL, suggesting that neutralization potency might be related to effectiveness of Mxra8 blocking. However, we did not observe a difference in potency of Mxra8 blocking for those mAbs that did or did not leave a resistant fraction of virus in the neutralization assay. Based on the alanine mutagenesis data, the mAbs that blocked binding to Mxra8 contacted residues 60, 66, 69 and 75 in the A domain and residues 172, 207, 211, and 221 in the arch and B domain. I overlaid these residues (yellow) on the CHIKV E1/E2 heterodimer along with the known Mxra8 contact residues on E2: 5-6, 18, 26-29, 62-64, 71-72, 74-76, 119-121, 123, 144, 150, 157-160 178-182, 189, 191-193, 212-214, 221-223, 263-265, 267 (red) (Basore et al., 2019; Song et al., 2019; Zhang et al., 2018), showing that the footprint for these Mxra8-blocking mAbs was proximal to the binding site of the Mxra8 receptor (**Figure 13E**).

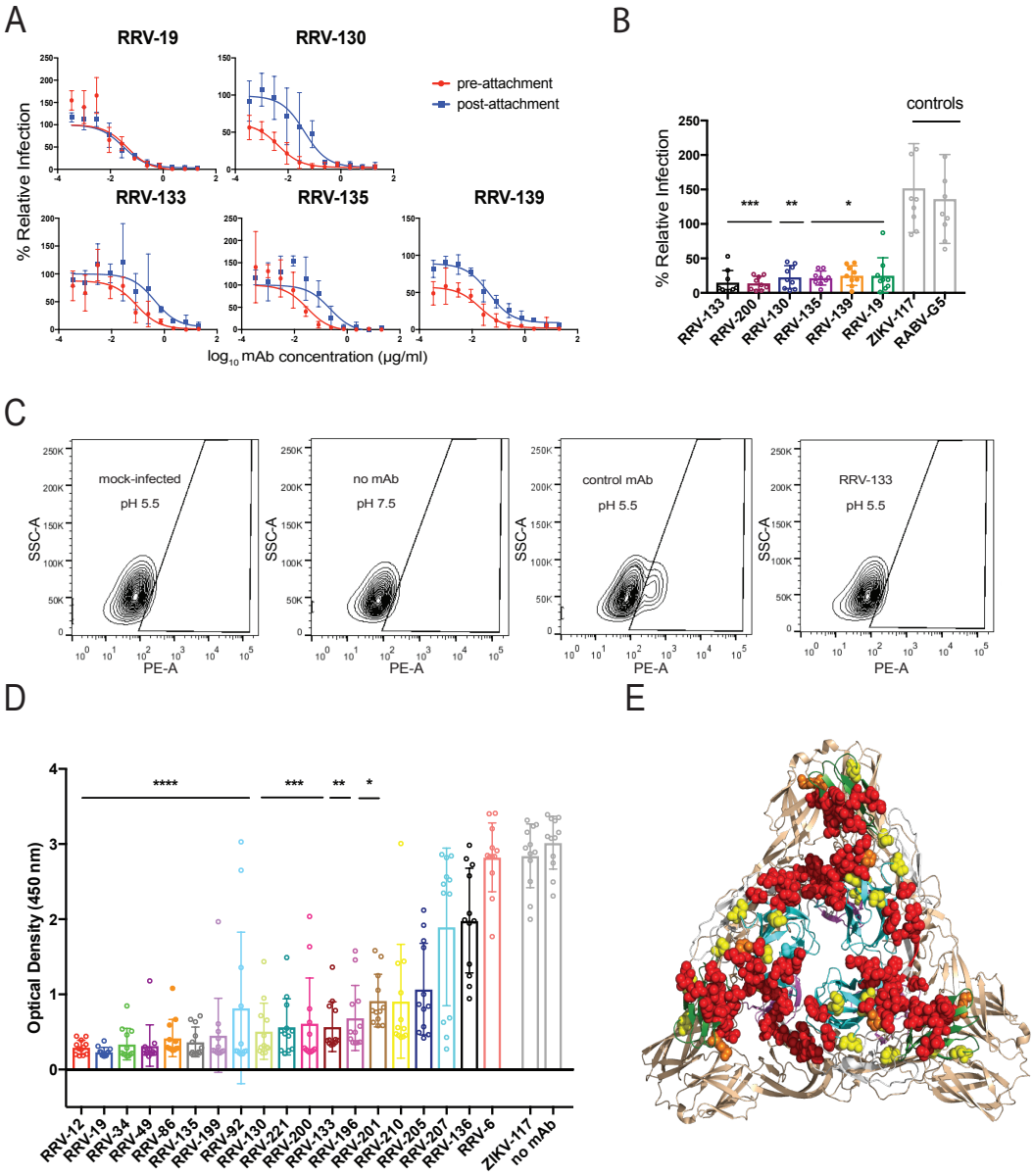

Figure 13. RRV mAbs neutralize through multiple mechanisms. (**A**) Pre-attachment and post-attachment neutralization assays were performed for representative mAbs from each competition group, and a focus-forming assay was used to quantify reduction in infection. In the pre-attachment assay, antibody was incubated with virus at 4°C before addition to Vero cells kept at 4°C. For the post-attachment assay, virus was applied to Vero cell monolayer cultures at 4°C before addition of antibody to cells at 4°C. Two independent experiments were performed in triplicate for each antibody, and representative curves are shown. (**B**) A fusion from without (FFWO) assay was used to measure antibody inhibition of virus fusion with the cell membrane under low pH conditions. Virus was adsorbed to Vero cell culture monolayers at 4°C for an hour before addition of antibody dilutions, also at 4°C, after removing excess virus. Cells then were exposed to a pH 5.5 medium or a control medium at neutral pH for two minutes and incubated at 37°C. The acidic pH medium was removed and cells were incubated for an

additional 14 h before fixing, permeabilizing, and staining for intracellular virus antigens before flow cytometric analysis. Intracellular virus was quantified by measuring percent PE-positive cells relative to a virus-only control. Three separate experiments were performed in triplicate for each antibody (Kruskal-Wallis one-way ANOVA with Dunn's post-test, with mean ± S.D. compared to virus-only control. (*p < 0.05, **p < 0.01, ***p < 0.001)). (**C**) Representative flow cytometry contour plots are shown for the FFWO assay. Mock-infected cells under a low-pH condition and cells with no antibody under a neutral pH condition (to ensure that virus only entered the cell through pH-mediated fusion) are shown as negative controls, and cells with a non-specific mAb (ZIKV-117) under a low pH condition are shown as a positive control. (**D**) Antibody blocking of RRV binding to mouse Mxra8-Fc fusion protein was determined through competition ELISA. Virus was captured on the plate with a human mAb before addition of RRV mAbs followed by Mxra8-mFc (mouse Fc). A loss of signal indicates competition of RRV mAbs with Mxra8-mFc for binding to virus. Three independent experiments were performed in quadruplicate (Kruskal-Wallis one-way ANOVA with Dunn's post-test, with mean ± S.D. compared to isotype control (*p < 0.05, **p < 0.01, ***p < 0.001, ****p < 0.0001)). (**E**) Residues that result in loss of Mxra8 binding to cell-surface-displayed chikungunya proteins are mapped onto the CHIKV E1/E2 trimer of heterodimers (PDB 3J2W) in red, and the alanine footprint of mAbs that block binding of mouse Mxra8-Fc protein to RRV are shown in yellow. Overlapping epitopes of RRV mAbs and Mxra8 contact residues are denoted in orange.

Therapeutic activity of mAbs *in vivo*

I selected ten antibodies with IC_{50} neutralization values below 100 ng/mL to test for protection in a highly susceptible, immunocompromised mouse model of RRV infection and disease. Four-week old male wild-type (WT) C57BL/6 mice were treated with 0.2 mg of MAR1-5A3 (a blocking anti-Ifnar1 mAb) (Sheehan et al., 2006) prior to inoculation with 10^3 FFU of RRV, and 100 µg of RRV mAb was administered via the intraperitoneal route one day after virus inoculation. When given a control mAb for treatment, all mice died after 7 days. In contrast, when given an RRV mAb, mortality was delayed over the course of three weeks (**Figure 14A**). The most effective mAb, RRV-19, protected 80% of mice, followed by RRV-139 at 70% protection, and RRV-86, at 60% protection. No difference in protection was seen between those mAbs that left a resistant fraction of virus (left) and those that neutralized completely (right), although the two most protective mAbs neutralized infection completely (**Figure 14A**).

Since RRV infection in humans is rarely fatal, RRV-19 and RRV-86, representing mAbs from different competition-binding groups, were tested in an immunocompetent mouse model of RRV-induced myositis where infection results in high viral burden in muscles and joint-associated tissues (Morrison et al., 2006). Four-week old male WT C57BL/6 mice were treated

with mAbs one day post-infection with 10^3 FFU of RRV. The gastrocnemius (calf muscle), ankle, spleen, and quadriceps were harvested three days after infection, and viral RNA burden was measured by qRT-PCR. Although both mAbs significantly reduced viral RNA in all tissues, RRV-19 was more effective in the ipsilateral and contralateral gastrocnemius, as well as the ipsilateral ankle and quadriceps (**Figure 14B**). RRV-19 and RRV-86 were equally effective in the contralateral ankle and quadriceps, as well as the spleen. While there was less than a 10-fold decrease in viral RNA burden in the ipsilateral ankle, this difference was statistically significant (**Figure 14B**).

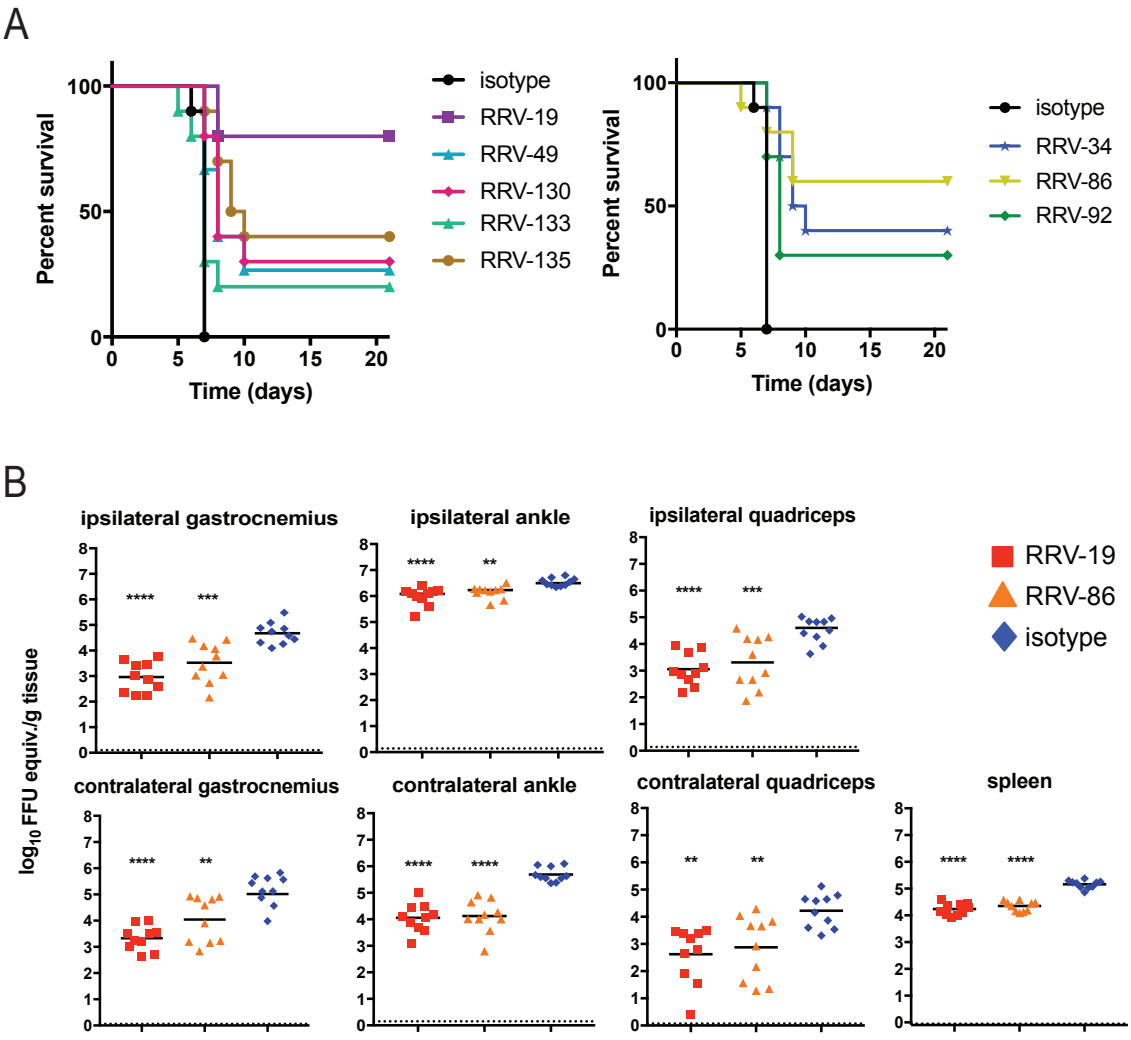

Figure 14. Therapeutic administration of anti-RRV mAbs in mice. (**A**) WT C57BL/6 mice were given 0.2 mg of anti-Ifnar1 mAb, and subsequently inoculated with 10^3 FFU of RRV in the footpad. At one day post-infection, 100 µg of RRV mAb was administered. Antibodies are grouped according to neutralization profiles, with those exhibiting incomplete neutralization *in vitro* on the left and those exhibiting complete neutralization *in vitro* on the right. Two independent experiments were performed, with a total of n = 10 for each antibody group. The isotype control in the two graphs are the same. Statistical analysis was performed using a log rank test with Bonferroni correction: RRV-19, $p < 0.0001$; RRV-34, $p < 0.0001$; RRV-49, $p = 0.0038$; RRV-86, $p = 0.0021$; RRV-92, $p = 0.0013$; RRV-130, $p = 0.0004$; RRV-133, $p = 0.3771$; RRV-135, $p < 0.0001$; RRV-139, $p < 0.0001$. (**B**) 100 µg of RRV-19, RRV-86, or an isotype control were administered one day post-infection to WT immunocompetent C57BL/6 mice, and the ipsilateral and contralateral gastrocnemius, quadriceps, ankle, or spleen tissues were collected at 3 days post-infection. Viral RNA was quantified through qRT-PCR. Two independent experiments were performed, with a total of n = 10 mice for each antibody group (one-way ANOVA with a Dunnett's post-test comparing each group to the isotype control; **p < 0.01, ***p < 0.001, ****p < 0.0001).

RRV disease severity was also measured in an immunocompetent mouse model using a previously published clinical scoring system (Morrison et al., 2011). Three-week-old male and female WT C57BL/6 mice were inoculated with 10^3 FFU of RRV strain T48 before intraperitoneal administration of 100 μg of RRV-19, RRV-86, or an isotype control mAb at one day post-infection. Mice were weighed, and a clinical score was assigned based on grip strength, gait, and righting reflex, as previously described (Haist et al., 2017). All mice receiving the anti-RRV mAbs were protected from weight loss and clinical disease, as compared to mice given the isotype control mAb (**Figure 15A**). In addition, viral RNA was quantified after harvest of the spleen, ipsilateral and contralateral gastrocnemius, quadriceps, and ankle tissues 18 days post-infection. A significant reduction in viral RNA was observed for administration of all mAbs except for RRV-19 in the contralateral calf and quad (**Figure 15B**).

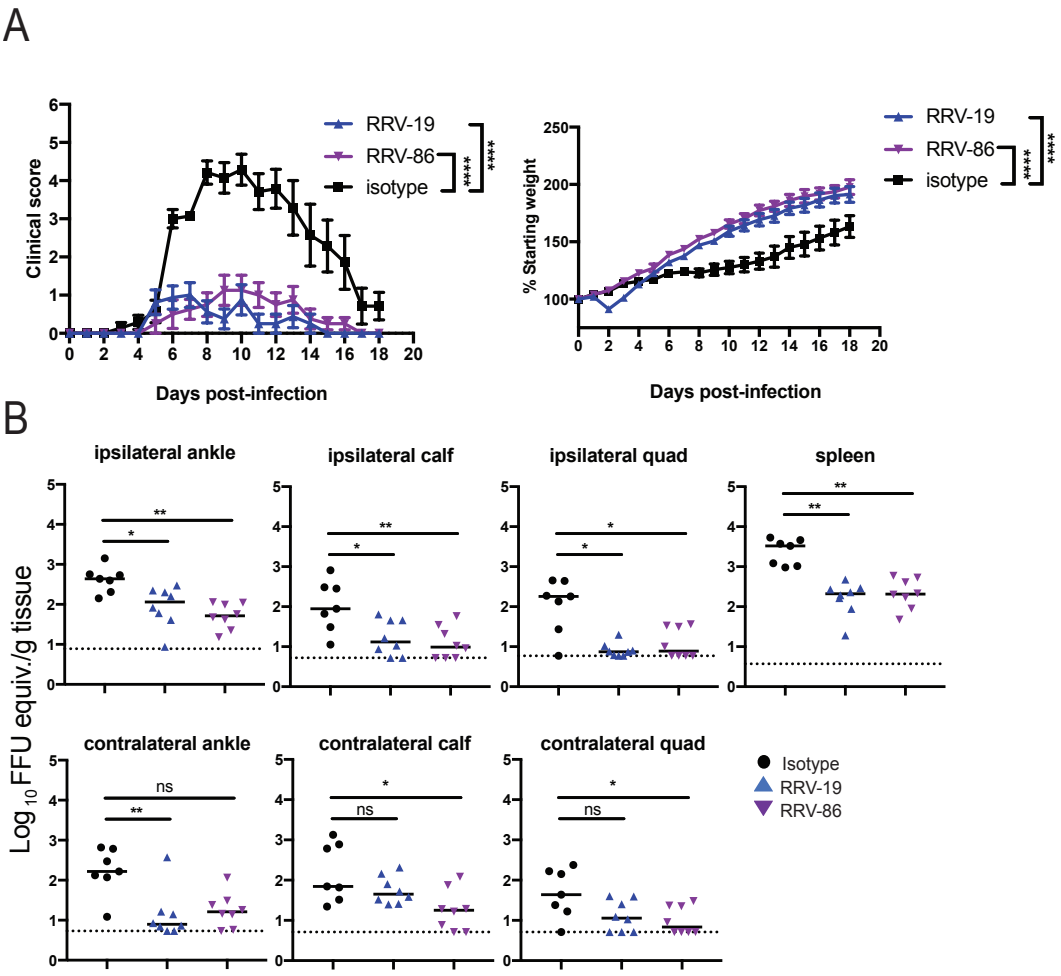

Figure 15. Therapeutic administration of anti-RRV mAbs improve clinical disease and reduce viral RNA burden in immunocompetent mice. (**A**) Three-week-old WT C57BL/6 mice were inoculated with 10^3 FFU of RRV strain T48 before intraperitoneal administration of 100 μg of antibody one day later. Mice were weighed each day over the course of 18 days and assigned a clinical score based on grip strength, gait, and righting reflex. Blind scoring of mice was performed using the following scoring system: 0, no disease; 1, mild defect in ipsilateral hind paw gripping; 2, mild defect in bilateral hind paw gripping; 3, bilateral loss in hind paw gripping; 4, bilateral loss in hind paw gripping with moderate hind limb weakness, observable mild altered gait, and difficulty or failure to right self; 5, bilateral loss in hind paw gripping with severe hind limb weakness, moderate altered gait, and loss of righting reflex; 6, bilateral loss in hind paw gripping with severe hind limb weakness, severely altered gait with possible dragging hind paw, and loss of righting reflex; 7, moribund. Two independent experiments were performed, with a total of n = 7-8 mice in each antibody group. Statistical analysis was performed using a one-way ANOVA of area under the curve test (****$p < 0.0001$). (**B**) Eighteen days post-infection, the spleen, ipsilateral and contralateral gastrocnemius, quadriceps, and ankle tissues were collected following extensive perfusion with PBS. Viral RNA was quantified through qRT-PCR and statistical analysis was performed using a Kruskal-Wallis multiple comparisons test (*$p < 0.05$, **$p < 0.01$; ns = not significant).

Discussion

These studies provide insight into the antibody response for the emerging pathogen RRV, using human mAbs isolated from naturally infected donors. The isolated mAbs recognize epitopes within the E2 glycoprotein, potently neutralize the RRV laboratory prototype strain in addition to five clinical isolates, and treat infection *in vivo* in a mouse model by reducing viral dissemination and clinical disease. I showed that a subset of mAbs neutralize at both pre-attachment and post-attachment stages, indicating that there are multiple mechanisms of neutralization for these mAbs. Additionally, nearly all neutralizing antibodies blocked binding of the receptor Mxra8 to RRV *in vitro*, and many also inhibited viral fusion with cell membranes. The majority of these mAbs had IC_{50} neutralization values less than 100 ng/mL, and several exhibited highly potent (<15 ng/mL) activity, which is similar in range to the best-in-class human neutralizing antibodies for the related CHIKV (Smith et al., 2015). For nearly half of these RRV mAbs, a 10 to 40% residual fraction of virus was not inhibited in neutralization assays. The molecular basis for this residual fraction of infectious virus remains unclear but could reflect particle heterogeneity due to incomplete maturation or release of the E3 precursor protein (Heidner et al., 1996; Zhang et al., 2011).

Through alanine scanning mutagenesis, I discovered multiple epitopes for these mAbs scattered across the A and B domains and the arch region, of the E2 protein. Because the alanine library only consisted of residues within the E2 protein, I did not test whether the mAbs contacted the E1 protein. Two main antigenic regions emerged between residues 60-75 in the A domain of E2 and 206-221 of the B domain. A major antigenic region has been suggested previously for RRV using three murine mAbs (Davies et al., 2000; Vrati et al., 1988). These antibodies were localized to the B domain and the adjacent arch region of the E2 protein, between residues 200 and 262, the position of two N-linked glycosylation sites (Nelson et al., 2016). The epitope for one of these mouse mAbs is at position 216 of the B domain, which is

within five residues of 221 and 211, two residues that were targeted by two or more human mAbs (Vrati et al., 1988). Additionally, residues 206 and 207 within the B domain appeared important for binding in the alanine scanning mutagenesis study. Residue 244, which is close to a mouse mAb epitope at position 246 (Davies et al., 2000) within the arch region connecting domains B and C, also emerged as a recognition site for one of the mAbs. Based on competition-binding studies, I assigned neutralizing antibodies into two major groups with similar profiles. Some asymmetry of competition was present in these groups, and the profiles of two mAbs overlapped between the two groups. While these two competition groups did not correlate perfectly with the alanine mutagenesis data, the majority of the mAbs in group 1 corresponded to residues within the B or C domains, whereas those in group 2 mapped primarily to domain A or the arch region between domains A and B. Although the C domain is not surface-exposed, it is probable that residues within this region stabilize the B domain, since the B domain undergoes a conformational change to uncover the fusion loop on the E1 protein after virus entry into the endosome (Fields and Kielian, 2013; Kielian et al., 2010; Li et al., 2010). Thus, mutating residues in this “hinge” region of domain C could affect mAb binding to domain B allosterically. Previously, neutralizing CHIKV antibodies have been shown to target analogous sites within the A, B, and arch regions of the E2 protein (Fox et al., 2015; Jin et al., 2015; Smith et al., 2015). These results indicate that both the A and B domains also are important antigenic sites for the human neutralizing antibody response directed against RRV. The knowledge of immunodominant sites on the virus recognized by potent neutralizing antibodies to RRV has implications for immunogen design, as there is currently no licensed vaccine available.

RRV is thought to have several possible receptors, including α1β1 integrin, which is nearly universally expressed on adherent cells, and Mxra8, a recently discovered receptor for multiple arthritogenic alphaviruses (La Linn et al., 2005; Zhang et al., 2018). A candidate receptor binding site could span across surface-exposed regions of both the A and B domains, as is hypothesized for Mxra8 (Zhang et al., 2018). The fact that mAbs from both competition groups

with epitopes in the A and B domains of the E2 protein inhibited binding to Mxra8 protein, supports this hypothesis. Several regions of the E2 protein that resulted in loss of Mxra8 binding to cell-surface-displayed CHIKV proteins are residues 62-64, 71-72, and 74-76 (Basore et al., 2019; Song et al., 2019; Zhang et al., 2018), which are close to loss-of-binding residues 66, 69, and 75, determined for Mxra8-blocking mAbs RRV-92 and RRV-196. Additionally, residues 207, 211, and 221 in the B domain of the E2 protein, which were revealed by alanine scanning mutagenesis as important for binding of RRV-19, RRV-86, RRV-92, RRV-130, and RRV-221, are in close proximity to residues 212-214 and 221-223 that are additional contact sites for Mxra8 (Basore et al., 2019; Song et al., 2019; Zhang et al., 2018).

In addition to attachment/entry inhibition and blockage of binding to Mxra8 receptor, I also observed post-attachment inhibition activity for a subset of mAbs tested, although in most cases, neutralization appeared to be more potent in the pre-attachment assays. During alphavirus infection of a cell under normal conditions, a decrease in pH within the endosome exposes the fusion loop on the E1 protein, which is usually shielded by the B domain of E2 (Fields and Kielian, 2013; Kielian et al., 2010; Li et al., 2010). While specific alanine scanning mapping data was not obtained for all of the fusion blocking mAbs, it is possible that these antibodies, which are from multiple competition-binding groups, stabilize the B domain to prevent uncovering of the fusion loop.

Therapeutic studies in mice with an acquired deficiency of type I IFN signaling revealed that all mAbs increased survival of the mice to some degree, and administration of three different mAbs resulted in a greater than 50% survival rate. Importantly, administration of two selected anti-RRV mAbs in immunocompetent WT mice improved clinical disease signs, as demonstrated by greater hind limb strength and hind paw gripping ability, and increased weight gain. Analysis of viral RNA levels present in several tissues showed that both anti-RRV mAbs tested reduced viral RNA burden in nearly all tissues examined. A combination mAb therapy has proven efficacious for CHIKV (Pal et al., 2013), so it is possible that pairing antibodies such

as RRV-19 and RRV-86, which are from different competition-binding groups, could reduce viral burden to a greater degree and prevent emergence of resistance. Additionally, since these mAbs have therapeutic benefit in animal models, they likely would have a protective effect in these models when administered at lower doses prophylactically, as was seen with CHIKV mAb studies (Pal et al., 2013; 2014; Smith et al., 2015).

Materials and methods

Source of human B cells

The first research subject was a 50-year old woman living in the U.S. who had a history of laboratory-confirmed infection in Australia in 1987. The second subject was a 32-year old male who was exposed to the virus during childhood in Australia in a clinically diagnosed but non-laboratory confirmed case of infection. Peripheral blood was obtained from the first donor in 2015 (28 years after infection) and from the second donor in 2017 (approximately 20 years after infection) with written informed consent following approval of the study by the Vanderbilt University Medical Center Institutional Review Board. Peripheral blood mononuclear cells (PBMCs) were isolated from both donors using density gradient centrifugation on Ficoll and were cryopreserved in liquid nitrogen until used in the experiments.

Generation of human hybridomas

Approximately 10^7 cryopreserved PBMCs were thawed and transformed with Epstein-Barr virus obtained from the supernatant of B95.8 cells in a suspension also containing a Chk2 inhibitor, cyclosporin A, and CpG, and the mixture was plated in a 384-well cell culture plate. After 7 days, transformed cells in each well were transferred to a well in 96-well plates containing a feeder layer of irradiated cells that were PBMCs obtained from discarded

leukofiltration devices (Nashville Red Cross). After an additional 5 days, the supernatants of expanded cells were screened for the presence of RRV-reactive antibodies using an enzyme-linked immunosorbent assay (ELISA), described below. Transformed B cells from wells containing supernatant with antibodies reactive to RRV were fused to the HMMA2.5 non-secreting myeloma cell line using an established electrofusion technique (Smith and Crowe, 2015). After fusion, the resulting mixture of hybridoma cells was resuspended in medium containing hypoxanthine, aminopterin, thymidine and oubain to select for hybrids of B cells and myeloma cells.

RRV ELISA screen

RRV strain T48 was propagated in Vero cells. The cell line was authenticated and tested monthly during culture for the presence of mycoplasma and found to be negative in all cases. Infected cell supernatants containing virus with a titer of approximately 5 x 10^6 FFU/mL were harvested when cytopathic effect was maximal, filtered through a 0.45 µm filter, then frozen and stored at –80°C until use. 384-well ELISA plates were coated with 25 µL of RRV strain T48 diluted 1:100 in PBS, and incubated for 1 h at 37°C. Plates were washed 5 times with PBS containing Tween (PBST) using an EL406 combination washer dispenser instrument (BioTek) and blocked for 1 h at room temperature with 5% milk powder and 2% goat serum, diluted in PBS. After washing 2 times with PBST, 25 µL of supernatants from hybridoma cultures or EBV-transformed cell lines were added to plates, which then were incubated for 1 h at room temperature. Plates were washed 4 times, and 25 µL of goat anti-human alkaline phosphatase-conjugated secondary antibodies (Meridian Life Science) diluted 1:5,000 in PBS was added to plates. After a 45-min incubation period, plates were washed 5 times and 25 µL of alkaline phosphatase substrate tablets (Sigma) diluted in Tris buffer with 1 M $MgCl_2$ was added. Optical density was read at 405 nm after 1 h using a Biotek plate reader.

Biolayer interferometry (BLI) competition-binding studies

An Octet RED96 BLI instrument (Pall FortéBio) was used to perform epitope binning studies using competition binding. One of the human antibodies (RRV-86) was used as a capture antibody and was immobilized onto Fc-specific anti-human IgG biosensors for 2 min. After measuring the baseline signal, the biosensor tips were immersed into wells containing RRV VLPs for 2 min. After another baseline measurement, biosensors then were transferred to wells containing a first mAb at a concentration of 100 µg/mL for 5 min, before immersion in a solution containing a second mAb, also at a concentration of 100 µg/mL for 5 min. The percent competition of the second mAb in the presence of the first mAb was determined by comparing the maximal signal of binding for the second mAb in the presence of the first antibody to the maximal signal of that mAb alone when separately tested uncompeted. Competition was defined by reduction of the maximal binding score to <20% of un-competed binding. A non-competing mAb was identified when maximal binding was >50% of un-competed binding. A 25 to 50% reduction in maximal binding was considered intermediate competition.

Generation of virus-like particles (VLPs)

RRV structural genes, capsid-E3-E2-6K-E1, encoding 3,783 bp with the addition of a Kozak sequence, were cloned into the pcDNA3.1(+) mammalian cell expression plasmid (GenScript). 293T cells (American Type Culture Collection [ATCC] Cat. No. CRL-11268) were transfected with 4 µg per 5 $\times 10^5$ cells of the plasmid using the Lipofectamine 2000 method according to the protocol of the manufacturer (ThermoFisher Scientific). Transfection was allowed to proceed for 48-72 h before supernatant was harvested and filtered through a 0.45 µm filter. VLPs were concentrated by ultracentrifugation at 110,000 g in a SW28 rotor for 2 h at 4°C through a 20% sucrose cushion using a Sorvall Discovery 90SE ultracentrifuge. The resulting pellet was resuspended in 250 µL of TNE buffer (0.01 M Tris-HCl, pH 7.2, 0.1 M NaCl, 0.001 M EDTA) and stored at 4°C.

Hybridoma cell line clone production

Two weeks after fusion, hybridoma cell lines were cloned by single-cell sorting using fluorescence-activated cell sorting on a BD FACSAria™ III sorting cytometer with aerosol containment, in the Vanderbilt University Medical Center Flow Cytometry Core. Approximately 2 weeks later, an ELISA screen was performed, and wells containing cloned cells secreting antibodies reactive to RRV were selected for expansion.

Purification of mAb IgG protein

Clonal cells secreting mAbs were grown in 75 cm^2 flasks to 70% confluency in hybridoma growth medium (ClonaCell-HY medium E from STEMCELL Technologies, 03805). The cells were expanded equally to four 225 cm^2 flasks for antibody expression in serum-free medium (GIBCO Hybridoma-SFM, Invitrogen, 12045084). The supernatant was harvested after 3 weeks and purified by affinity chromatography using protein G columns (GE Life Sciences, Protein G HP Columns). Purified IgG from hybridoma cell expression was used for all assays.

Focus reduction neutralization test

Vero cells (American Type Culture Collection [ATCC] Cat. No. CCL-81) were seeded in 96-well plates at 30,000 cells/well the day before use. Antibodies were diluted in 96-well U-bottom plates, with a 1:3 dilution series across the plate and a virus-only control in the left column. A solution containing infectious RRV was diluted to a concentration of 100 focus-forming units (FFU)/mL and mixed 1:1 by volume in a 96-well plate with antibody suspensions. The virus/antibody mixture was incubated for 1 h at 37°C before transfer to Vero cell monolayer cultures. Infection proceeded for 1.5 h and then a 1% methylcellulose overlay prepared in DMEM with 2% FBS was added to cells. After 18 h, 1% paraformaldehyde (PFA) prepared in PBS was used to fix cells for at least one hour. Plates were washed 3 times with PBS before

addition of a 1:6,000 dilution of anti-RRV mouse ascites fluid (ATCC Cat. No. VR-1246AF) prepared in cell permeabilizing buffer (PBS with 0.1% saponin and 0.1% bovine serum albumin). After incubation for at least 2 h at room temperature, plates were washed 3 times in permeabilizing buffer, and anti-mouse HRP-conjugated secondary (Kirkegaard & Perry Laboratories [KPL]) was added at a 1:2,000 dilution in permeabilizing buffer. Plates were incubated for 1 h at room temperature, and washed 3 times before addition of TrueBlue Peroxidase substrate (KPL) for 20 min. Plates were rinsed with dH_2O, and then plates were imaged with an ImmunoSpot® plate reader (Cellular Technology Limited [CTL]). Foci were counted with BioSpot 5.1 software (CTL), and the percent relative infection was calculated based on the virus-only control. Triplicate tests were performed for each antibody, and the results were averaged.

Fusion from without (FFWO) assay

Vero cells were seeded at 30,000 cells/well in 96-well plates the day before use in the assay. Before the start of assay, cells were washed once with binding medium (RPMI 1640, 0.2% BSA, 10 mM HEPES pH 7.4, and 20 mM NH_4Cl) at 4°C, and incubated for 15 min at 4°C. The T48 strain of RRV was concentrated to 10^8 FFU/mL using 100 kDa centrifugal filters (Amicon) Centricon. Virus was prepared in binding medium and added to cells at a multiplicity of infection (MOI) of 15 for 1 h at 4°C. Any remaining free virus was removed with two washes in binding medium. Antibodies were prepared in DMEM containing 2% FBS at 10 μg/mL concentrations and added to cells for 1 h at 4°C. Antibody was removed and fusion with the plasma membrane was initiated by the addition of fusion media (RPMI 1640, 0.2% BSA, 10 mM HEPES, and 30 mM succinic acid at pH 5.5) for 2 min at 37°C. Binding medium (RPMI 1640, 0.2% BSA, 10 mM HEPES at pH 7.4) was used in place of low pH fusion medium in controls wells to ensure that virus entry into cells only occurred due to pH-dependent plasma membrane fusion. After a 2-min incubation, medium was removed and cells were incubated in DMEM

supplemented with 5% FBS, 10 mM HEPES, and 20 mM NH_4Cl (pH 7.4). Fourteen hours later, cells were detached with trypsin, fixed with 1% PFA in PBS for 1 hour, and permeabilized with 0.1% saponin detergent solution. For staining prior to flow cytometry analysis, cells were incubated sequentially with RRV mouse ascites fluid (1:6000 dilution ATCC Cat. No. VR-1246AF) for 1 h and PE conjugated goat anti-mouse IgG secondary antibody for 1 h (ThermoFisher Scientific). Cells were analyzed on BD Fortessa flow cytometer with FlowJo software.

Alanine scanning mutagenesis for epitope mapping

The same C-E3-E2-6K-E1 construct used to generate VLPs (see above) was used to construct an alanine mutation library for mapping of antibody epitopes. The first 300 residues in the RRV E2 protein were mutated to alanine, and alanine codons were mutated to serine and synthesized as cDNA (Twist Bioscience). Each mutant was sequence verified and expressed on the surface of 293F cells for screening using an iQue high-throughput flow cytometer (Intellicyt). Loss of binding for each mAb was determined by measuring reduction in fluorescent signal as compared to signal in cells expressing WT protein. To differentiate loss of binding from absence of protein expression, at least two control antibodies with binding at greater than 50% were required for each residue. A cutoff value of less than 10% binding when normalized to WT was set to determine a loss of binding at each residue. An untransfected cell control for each antibody also was used to ensure specificity of binding.

ELISA-based Mxra8–Fc competition binding assay

RRV-86 (2 μg/mL) was diluted in PBS and immobilized onto a 384-well ELISA plate before incubation for 1 h at 37°C. The plate was washed four times with PBS containing Tween (PBST) using an EL406 combination washer dispenser instrument (BioTek) and blocked for 1 h at room temperature with 5% milk powder and 2% goat serum, diluted in PBS. RRV T48 strain was

diluted to 4 x 10^7 FFU/mL in PBS and 25 µL per well was added for 1 h at room temperature. After washing five times with PBST, RRV mAbs were diluted to 20 µg/mL in PBS and 25 µL of mAb was added to each well, except for control wells where just PBS was added. Blocking mAbs were incubated for 30 min at room temperature and were left in when 25 µL of Mxra8-Fc (mouse Fc region) (Zhang et al., 2018) fusion protein at a concentration of 10 µg/mL was added to each well. After incubation at room temperature for 1 h, the plate was washed four times with PBST and 25 µL per well of a goat anti-mouse HRP-conjugated anti-mouse Fc secondary antibody (SeraCare) was added at a 1:2,000 dilution. After five washes with PBST, plates were developed with TMB Substrate (ThermoFisher Scientific) and the reaction was stopped with H_2SO_4. Absorbance was read at 450 nm with a Biotek plate reader. A similarly prepared human mAb specific for Zika virus (ZIKV-117 (Sapparapu et al., 2016)) was included as a negative control antibody.

Mouse studies

All animal experiments and procedures were carried out in accordance with the recommendations in the Guide for the Care and Use of Laboratory Animals of the National Institutes of Health. The protocols were approved by the Institutional Animal Care and Use Committee at the Washington University School of Medicine (Assurance number A3381-01). Injections were performed under anesthesia that was induced and maintained with ketamine hydrochloride and xylazine, and all efforts were made to minimize animal suffering.

Survival studies. Four-week-old male WT C57BL/6 mice were treated with 0.2 mg of MAR1-5A3 (anti-Ifnar1 antibody) prior to inoculation with 10^3 FFU of WT RRV T48 strain in the footpad. The following day, 100 µg of anti-RRV antibody or an isotype control antibody to an unrelated viral target was administered to mice by intraperitoneal injection. Mice were observed over the course of 21 days for survival and moribund mice were euthanized.

Viral burden studies. Four-week-old male WT C57BL/6 mice were inoculated with 10^3 FFU of RRV strain T48 and then one day post-infection were given 100 μg of antibody by intraperitoneal injection. Three days post-infection, the ipsilateral and contralateral gastrocnemius, quadriceps, and ankle tissues were collected as well as the spleen following extensive perfusion with PBS. RNA was isolated from tissues using the RNeasy mini kit (Qiagen). Viral RNA was quantified by qRT-PCR using the TaqMan RNA to C_T one-step kit (Applied Biosystems) with nsp3 specific primers and compared to RNA isolated from viral stocks as a standard curve to determine FFU equivalents.

Clinical scoring studies. Three-week-old male and female WT C57BL/6 mice were inoculated with 10^3 FFU of RRV strain T48 and then one day post-infection were given 100 μg of antibody by intraperitoneal injection. Mice were weighed and assigned a clinical score based on grip strength, gait, and righting reflex, as previously described (Haist et al., 2017). Mice were scored blinded and as follows: 0, no disease; 1, mild defect in ipsilateral hind paw gripping; 2, mild defect in bilateral hind paw gripping; 3, bilateral loss in hind paw gripping; 4, bilateral loss in hind paw gripping with moderate hind limb weakness, observable mild altered gait, and difficulty or failure to right self; 5, bilateral loss in hind paw gripping with severe hind limb weakness, moderate altered gait, and loss of righting reflex; 6, bilateral loss in hind paw gripping with severe hind limb weakness, severely altered gait with possible dragging hind paw, and loss of righting reflex; 7, moribund. No mice received a score of 7 throughout the course of the experiment. Eighteen days post-infection, the spleen, ipsilateral and contralateral gastrocnemius, quadriceps, and ankle tissues were collected following extensive perfusion with PBS. Viral RNA was quantified as described above.

Statistical analyses

For the fusion from without and Mxra8 blockade assays, a Kruskal-Wallis one-way ANOVA with Dunn's post-test was used to determine significance. For survival studies in the

immunocompromised mouse model, statistical analysis was performed using a log rank test with Bonferroni correction, and for analysis of viral RNA titers in the immunocompetent mouse model, a one-way ANOVA with a Dunnett's post-test comparing each group to the isotype control was used. A one-way ANOVA of area under the curve test was used to determine statistical significance in the clinical disease mouse model, and a Kruskal-Wallis multiple comparisons test was used to determine significant reductions in viral RNA.

Logistic curve analysis used to calculate IC_{50} values for neutralization assays

The logistic growth curve we considered for concentration x includes five parameters β_1, β_2, β_3, β_4, and β_5. The function follows the following form:

$$f(x) = \beta_1 + \frac{\beta_2 - \beta_1}{1 + g_x \exp\left(\frac{\beta_3 - x}{\beta_4}\right) + (1 - g_x)\exp\left(\frac{\beta_3 - x}{\beta_5}\right)}$$

where

$$g_x = \frac{1}{1 + \exp\left(-\overline{C}_g(\beta_3 - x)\right)}$$

is a logistic weighting function varying smoothly between 0 and 1, centered about the 50% reduction point. If β_4 and β_5 are the same sign, then the mean curvature of g was determined by the reciprocal of the mean

$$\overline{C}_g = \frac{2}{|\beta_4 + \beta_5|}$$

β_1 is the lower asymptote; β_2 is the upper asymptote; β_3 is inflection point of the function which corresponds to a 50% reduction point; β_4 and β_5 controls the relative steepness or shallowness of the logistic curve (note that this parameterization does not assume symmetry).

CHAPTER III

HUMAN MONOCLONAL ANTIBODIES BROADLY PROTECT AGAINST INFECTION OF ARTHRITOGENIC ALPHAVIRUSES BY RECOGNIZING CONSERVED ELEMENTS OF THE MXRA8 RECEPTOR BINDING DOMAIN

Introduction

Because there is no licensed treatment or vaccine for arthritogenic viruses, there is a need to better define the epitopes recognized by protective antibodies. In particular, identifying broadly cross-reactive and neutralizing human antibodies could prove useful for revealing conserved epitopes that may be beneficial for the design of a universal alphavirus vaccine. Previously, murine mAbs were identified that broadly neutralized multiple alphaviruses, including CHIKV, MAYV, ONNV, RRV, and SFV (Earnest et al., 2019; Fox et al., 2015). These mAbs blocked multiple steps of the viral life cycle, including entry and egress, and one mAb, CHK-265, neutralized by binding to the B domain and possibly by cross-linking it to the A domain of an adjacent viral spike (Fox et al., 2015). However, few human broadly cross-reactive mAbs have been identified, and the their mechanism of neutralization is unknown (Fox et al., 2015).

In this chapter, I identify cross-reactive alphavirus antibodies from the B cells of immune human subjects and determine their epitopes and mechanism(s) of inhibition. I screened pre-existing plasma antibodies isolated from individuals with prior history of infection with RRV or CHIKV and identified six mAbs that cross-reacted with two or more arthritogenic alphaviruses. Next, I determined that these mAbs competed for binding to a common antigenic site and defined the molecular basis for recognition of CHIKV, RRV, MAYV, SAGV, GETV, and ONNV by a broadly neutralizing mAb, RRV-12. High resolution cryo-EM structures of RRV-12 in complex with CHIKV, RRV, or MAYV revealed that the epitope for this mAb lies at the distal end

of E2 protein B domain in a region with partial sequence conservation across multiple alphaviruses. This mAb showed efficacy *in vivo* against infection and disease when administered therapeutically in mouse challenge models of RRV or MAYV. Overall, this work provides insight into the humoral immune response to alphaviruses during human infection and identifies a shared epitope targeted by human antibodies. In addition to the use of RRV-12 as a possible therapy against multiple alphaviruses, the molecular and structural understanding of its binding site provided here could inform rational epitope-based vaccine design strategies.

I would like to acknowledge Andrew Miller in Richard Kuhn's at Purdue University for performing all structural studies and Julie Fox in Michael Diamond's group at Washington University in St. Louis for performing all mouse experiments.

Antibody-dependent enhancement

Antibody-dependent enhancement (ADE) is a phenomenon that has been observed for some viruses, particularly flaviviruses, whereby antibodies produced in a prior infection lead to a more severe subsequent infection. Antibodies against the initial virus serotype are often non-neutralizing towards virus of a different serotype, and instead facilitate increased uptake of virus by monocytes and macrophages via Fcγ receptors (Smatti et al., 2018). For RRV, antibody-dependent enhancement (ADE) has been demonstrated in a few *in vitro* studies in the presence of subneutralizing concentrations of antibody, and the mechanism is thought to involve specific inhibition of antiviral gene transcription after entry of the virus into macrophages (Lidbury and Mahalingam, 2000; Linn et al., 1996). However, during RRV vaccine trials, ADE was not observed in mice passive transfer studies, and neutralizing antibodies in the serum of vaccinated individuals conferred protection in mice (Holzer et al., 2011). It is thus unlikely that ADE occurs during alphavirus infections *in vivo*.

Isolation of human mAbs with broad cross-reactivity for multiple alphaviruses

I isolated a panel of human mAbs from two subjects. The first subject (mentioned in Chapter II) had a history of a laboratory-confirmed case of RRV that was acquired in Australia and the second came from a subject in Colombo, Sri Lanka with serological evidence of prior natural CHIKV infection. I screened supernatants of Epstein-Barr virus (EBV) transformed B cells from these donors for direct binding to RRV or MAYV by ELISA, respectively. B cells that secreted antibody reactive with either RRV or MAYV were fused to a myeloma line to establish stable hybridoma cell lines, which then were cloned through single-cell flow cytometric sorting.

Binding and neutralization profiles for mAbs

RRV-12, which was isolated from cells from the RRV-immune subject, and five mAbs isolated from the CHIKV-immune subject, were tested for binding and neutralization against six alphaviruses: CHIKV, RRV, ONNV, MAYV, GETV, and SAGV, chosen based on close evolutionary distance and availability (**Figure 16, 17**). Binding was tested with both a direct virus ELISA and protein ELISA using CHIKV and MAYV E2 proteins. While most half maximal binding (EC_{50}) values were found to be between 4 and 100 ng/mL for the virus ELISAs, the mAbs bound less well to recombinant soluble forms of the viral proteins, with EC_{50} values ranging from 35 to 1,269 ng/mL (**Table 3**). Notably, mAbs did not bind to ONNV in ELISA, although each of the mAbs neutralized this virus (**Table 3, Figure 18B and 19**). I used a focus reduction neutralization test (FRNT) to assess more quantitatively the neutralizing activity of mAbs against these six viruses, and found reasonable correspondence between binding and neutralization activity, as measured by half maximal inhibitory concentration (IC_{50}). However, whereas CHKV-70 bound strongly to CHIKV, MAYV, and RRV in a virus ELISA, it did not neutralize these viruses efficiently (**Table 3 and Figure 18**). As described previously (Heidner et al., 1996; Zhang et al., 2011), some mAbs were unable to neutralize infection completely and left a resistant fraction of infectious virus even when tested at high concentrations (**Table 4 and**

Figure 18B). In general, ONNV was the most potently neutralized, with only a small fraction of un-neutralized virus remaining (**Table 4 and Figure 18B, 19**).

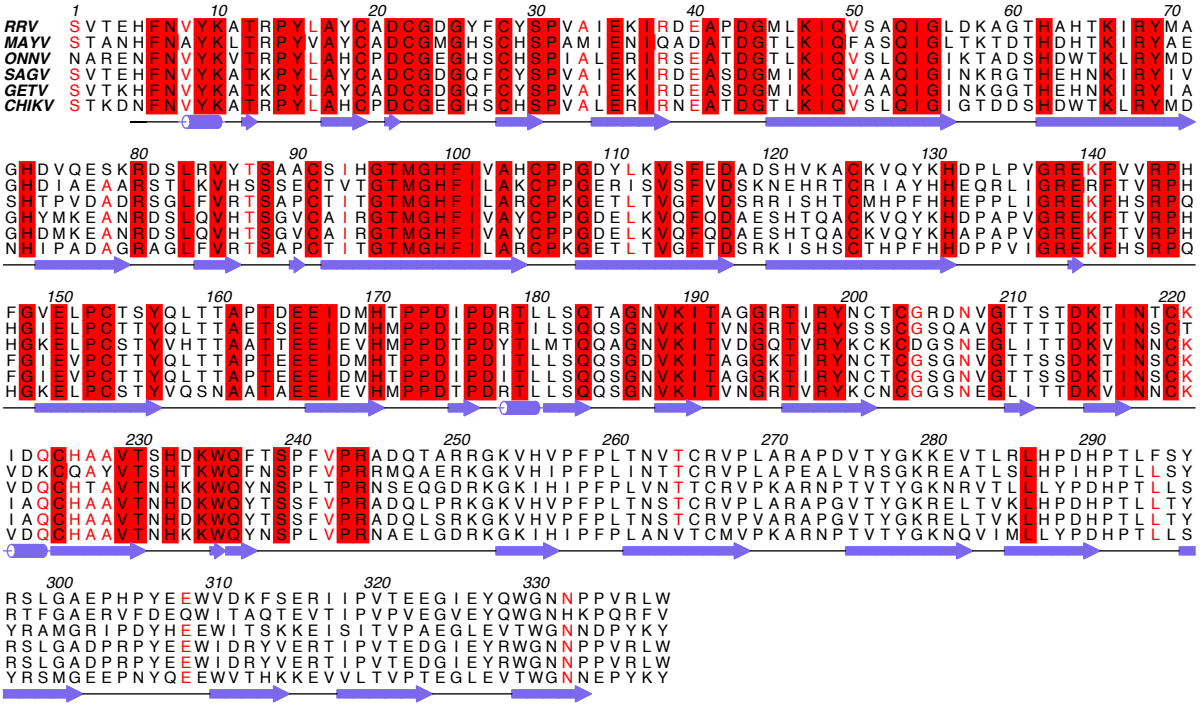

Figure 16. Sequence alignment of alphaviruses. E2 protein sequence alignment for six viruses generated using ALINE program (Bond and Schüttelkopf, 2009). Red highlighted residues indicate complete sequence conservation between the six viruses, while residues in red font indicate sequence conservation for five out of six viruses.

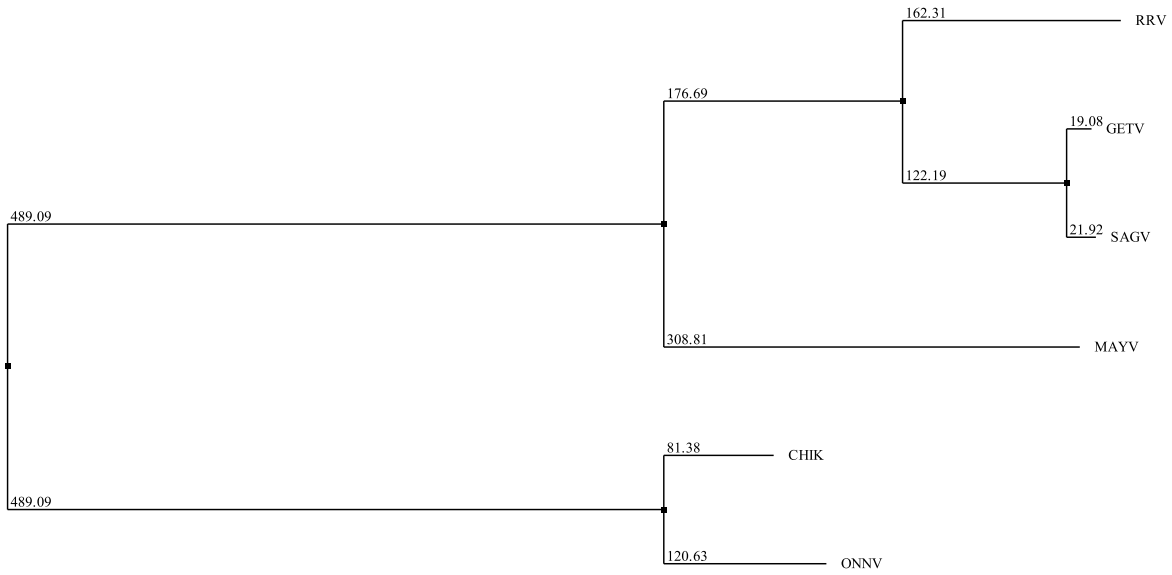

Figure 17. **Phylogenetic tree of related alphaviruses.** Phylogenetic tree generated using neighbor-joining tree function in Jalview multiple alignment editor. Numbers indicate the distances calculated for the amino acid sequences of the E2 protein from six viruses: RRV, SAGV, GETV, MAYV, ONNV, and CHIKV.

Table 3. Isotype, light chain designation (λ or κ), half maximal inhibitory concentration (IC_{50}) for neutralization, and half maximal effective concentration (EC_{50}) for binding. Binding was measured using a virus ELISA, and neutralization was measured using an FRNT. Both ELISA and FRNT were performed in triplicate, and curves and IC_{50} or EC_{50} binding values were obtained using non-linear fit analysis with top of curve constrained to 100 for neutralization, using Prism software version 7 (GraphPad Software). > indicates binding or neutralization was not detected when tested at concentrations up to 10,000 ng/mL. EC_{50} binding and IC_{50} neutralization values were calculated based on two independent experiments, performed in triplicate.

mAb	Donor	Isotype	LC	Binding to protein EC_{50} (ng/mL)		Binding to virus EC_{50} (ng/mL)					Neutralization IC_{50} (ng/mL)					
				CHIKV	MAYV	CHIKV	MAYV	RRV	SAGV	GETV	CHIKV	MAYV	RRV	SAGV	GETV	ONNV
RRV-12	RRV	IgG1	λ	103	85	59	6	4	7	14	25	56	38	18	12	3
CHIKV-77	CHIKV	IgG1	K	99	95	30	11	4	10	9	430	61	15	53	26	3
CHIKV-70	CHIKV	IgG1	K	43	27	32	13	7	>	>	>	470	146	>	>	19
CHIKV-62	CHIKV	IgG1	λ	181	168	76	59	>	20	18	17	23	>	275	306	17
CHIKV-105	CHIKV	IgG1	K	63	55	37	55	>	37	12	8	9	>	33	8	2
CHIKV-66	CHIKV	IgG1	K	1,259	>	1,581	1,489	>	>	>	112	494	>	>	>	1,020

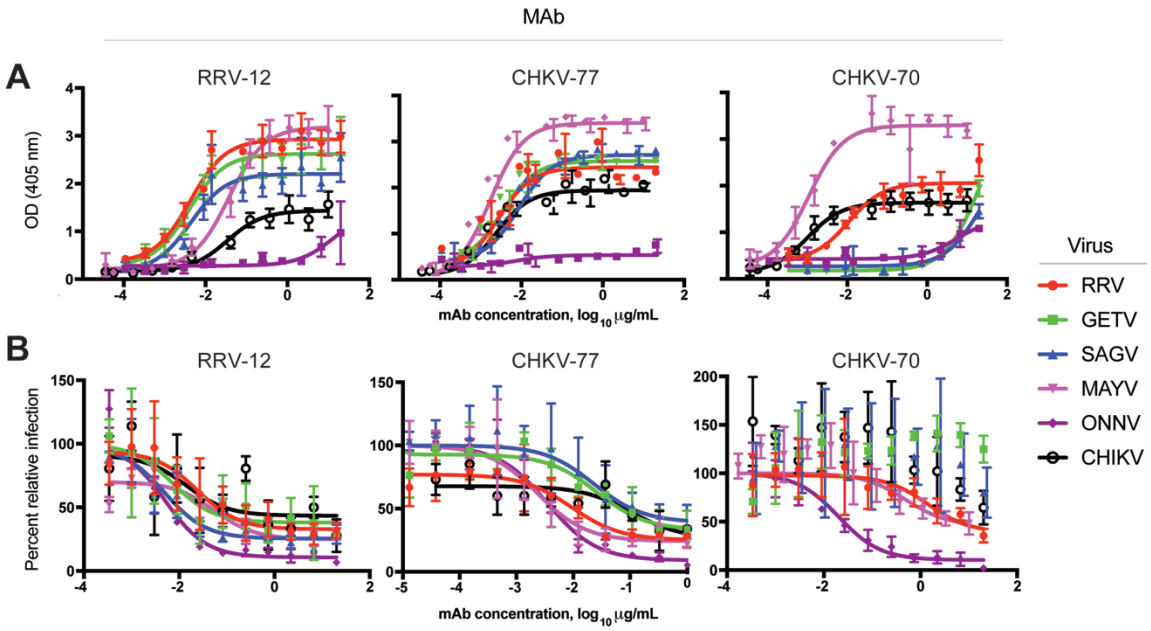

Figure 18. Antibodies generated from donors naturally infected with Ross River (RRV) or chikungunya (CHIKV) virus bind and neutralize RRV, Mayaro (MAYV), CHIKV, Sagiyama (SAGV), Getah (GETV), and O'nyong'nyong (ONNV) viruses. (A) Binding, or **(B)** neutralization profiles of three broadly neutralizing mAbs, as determined through ELISA or FRNT. Two independent experiments were performed, and representative binding and neutralization curves are shown, with error bars representing mean ± S.D. Binding was measured using a virus ELISA and neutralization was measured using a focus reduction neutralization test (FRNT). Both ELISA and FRNT were performed in triplicate, and curves and IC_{50} or EC_{50} binding values were obtained using non-linear fit analysis with top of curve constrained to 100 for neutralization, using Prism software version 7 (GraphPad Software).

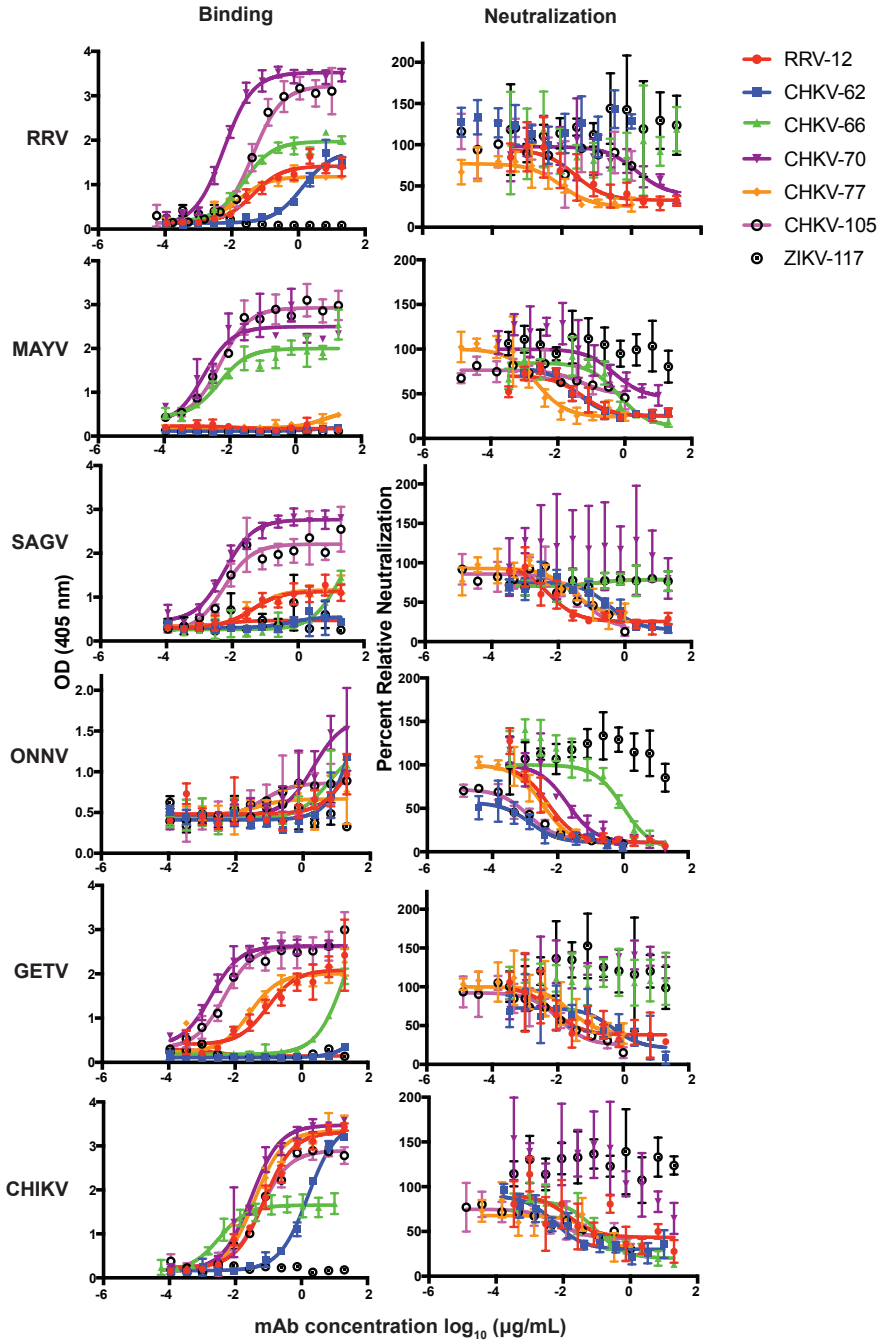

Figure 19. **Representative binding and neutralization curves for all mAbs against RRV, MAYV, SAGV, GETV, CHIKV, and ONNV.** Binding was determined through virus ELISA and neutralization through focus reduction neutralization test.

Table 4. Percent maximum neutralization for cross-neutralizing mAbs. Percent maximum neutralization for cross-reactive mAbs against CHIKV, MAYV, RRV, SAGV, GETV, and ONNV is given, as calculated by Prism software. A dash indicates that no neutralization was observed at a concentration of 10,000 ng/mL or less.

MAb	Percent maximum neutralization					
	CHIKV	MAYV	RRV	SAGV	GETV	ONNV
RRV-12	58	80	70	78	70	85
CHIKV-77	55	68	76	67	67	94
CHIKV-70	-	63	53	-	-	87
CHIKV-62	76	82	-	89	82	95
CHIKV-105	68	64	-	67	70	85
CHIKV-66	79	69	-	-	-	89

Biolayer interferometry competition-binding assays

To determine if these cross-reactive mAbs recognized a similar antigenic site, I performed competition-binding biolayer interferometry (BLI) assay using recombinant protein containing a histidine tag. I first immobilized protein on Anti-Penta-HIS (HIS1K) biosensors (Pall FortéBio) before adding two antibodies sequentially. The percent binding of the second antibody in the presence of saturating concentrations of the first antibody was compared to non-competed binding. As expected, each antibody competed with itself. A binding value of less than 25% was considered completely blocking, whereas values between 25 and 50% were considered partially blocking. CHKV-66 was excluded from the analysis because it did not bind avidly enough to E2 protein to assess competition. Virtually all of the cross-reactive mAbs competed for binding to a common antigenic site on CHIKV and MAYV E2 protein (**Figure 20A**).

Blockade of Mxra8 binding

To begin to determine if the cross-reactive human mAbs also blocked attachment to the Mxra8 receptor, I performed a competition binding ELISA with three of the viruses, RRV, MAYV,

and CHIKV. Viral particles were captured onto an ELISA plate, and mAbs were allowed to attach to virus before the addition of purified recombinant mouse Mxra8-Fc fusion protein. At a concentration of 10 μg/mL, RRV-12 and CHKV-70 substantially inhibited each of the three viruses from binding to Mxra8-Fc protein, as compared to a control antibody (**Figure 20B**). In comparison, CHKV-77 reduced Mxra-Fc binding only slightly, and this difference did not attain statistical significance. I also performed titration curves to test various concentrations of mAb and found that RRV-12 and CHKV-70 maximally blocked binding of RRV to Mxra8-Fc protein at a concentration of ~2 μg/mL, whereas for CHIKV, maximal inhibition occurred at < 1μg/mL, and for MAYV, maximal inhibition was observed at a higher concentration of ~7 μg/mL (**Figure 20C**). All mAbs tested most potently blocked Mxra8 binding to CHIKV, as evidenced by IC_{50} values and inhibition curves (**Figure 20D**).

A

Second mAb

First mAb	RRV-12	CHKV-77	CHKV-70	CHKV-62	CHKV-105
RRV-12	12	12	17	2	4
CHKV-77	3	8	23	4	9
CHKV-70	37	2	5	4	2
CHKV-62	1	11	29	6	7
CHKV-105	7	18	41	10	14

Second mAb

First mAb	RRV-12	CHKV-77	CHKV-70	CHKV-62	CHKV-105
RRV-12	8	16	19	9	5
CHKV-77	14	20	15	10	8
CHKV-70	44	9	4	24	22
CHKV-62	10	8	12	9	6
CHKV-105	5	6	12	9	3

B

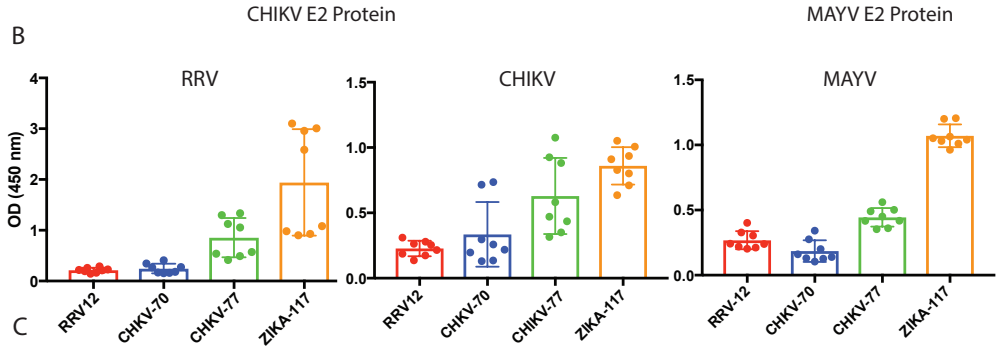

C

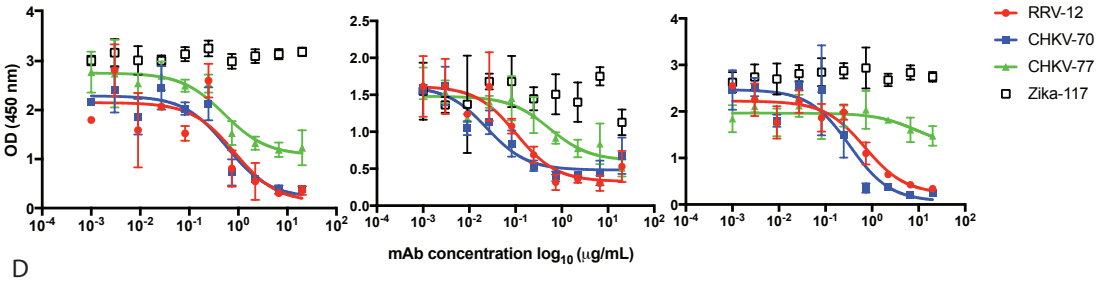

D

	IC_{50} value (ng/mL)		
	RRV	MAYV	CHIKV
RRV-12	632	478	145
CHKV-70	619	407	56
CHKV-77	819	5,387	300

Figure 20. **Cross-reactive mAbs compete for the same antigenic site and inhibit binding to Mxra8 receptor protein**. (**A**) An Octet RED96 instrument (Pall FortéBio) was used to perform epitope binning studies using competition binding. After a baseline measurement, Anti-Penta-HIS (HIS1K) biosensor tips were used to immobilize either CHIKV or MAYV E2 protein containing a histidine tag. After another baseline measurement, biosensors then were transferred to wells containing a first mAb at a concentration of 50 µg/mL for 5 min, before immersion in a solution containing a second mAb, also at a concentration of 50 µg/mL for 5 min. The percent competition of the second mAb in the presence of the first mAb was determined by comparing the maximal signal of binding for the second mAb in the presence of the first antibody to the maximal signal of the second mAb in the absence of competition. Competition was defined by reduction of the maximal binding score to <25% of un-competed binding (black boxes). A 25 to 50% reduction in maximal binding was considered intermediate competition (gray boxes). (**B**) Antibody blocking of virus binding to mouse Mxra8-Fc fusion protein was determined through competition ELISA. MAYV, CHIKV, or RRV were captured on the plate with a human mAb before addition of RRV mAbs followed by Mxra8-mFc (mouse Fc). A loss of signal indicates competition of RRV mAbs with Mxra8-mFc for binding to virus. Two independent experiments were performed in quadruplicate. (**C**) Dose-response curve of mAb inhibition of virus binding to mouse Mxra8-Fc fusion protein through competition ELISA. Two independent experiments were performed in triplicate and representative curves are shown. (**D**) Half maximal inhibitory values (IC_{50}) values for dose response curves, calculated based on the average of two independent experiments performed in triplicate.

RRV-12 mechanism of neutralization

I then chose one of the receptor-blocking mAbs for further testing to gain insight into the mechanism of neutralization. To determine if RRV-12 blocked a step in the viral entry pathway, we performed a variation on the FRNT in which virus was incubated with antibody at 37°C before addition to Vero cell monolayers, also at 37°C. Virus and antibody then were removed from cells with three washes before addition of a methylcellulose semisolid overlay. Eighteen hours later, the overlay was removed and cell monolayers were stained for viral antigen. Entry of RRV, MAYV, CHIKV, SAGV, GETV, and ONNV was reduced significantly compared to the isotype control mAb (**Figure 21A**). We then quantified viral foci size using another variation on the FRNT, where antibody was added directly to the methylcellulose layer after cells were incubated with virus at 37°C. When an ImmunoSpot® plate reader was used to calculate viral foci area after staining, we found that RRV-12 significantly reduced foci size for each of the viruses except ONNV (**Figure 21B, 21C**). In the absence of the methylcellulose overlay, viral spread occurred more substantially in the presence of the control antibody, whereas only antigen-positive cells were observed when RRV-12 was applied (**Figure 21D**). To further confirm mechanism of neutralization, we evaluated the inhibitory activity of RRV-12 against one virus, RRV, in pre- and post-attachment assays. In the pre-attachment assay, virus was incubated with antibody at 4°C before addition to Vero cell monolayers, also at 4°C. Virus not attached to the cells and unbound antibody were washed out, and attached virus was allowed to internalize during a brief incubation period at 37°C. The post-attachment assay was performed similarly, except excess virus was washed out before mAb was added, also at 4°C. For both assays, after virus internalization, cells were overlaid with methylcellulose, incubated, and then fixed and stained 18 h later. RRV-12 blocked at both pre- and post-attachment steps (**Figure 21E**). While the pre-attachment inhibition results supported our finding that RRV-12 blocks viral binding to Mxra8, we next tested if the observed post-attachment blockade could include steps

downstream from entry, such as fusion. We accomplished this by performing a fusion from without (FFWO) assay, which has previously been used as a surrogate assay to measure fusion of alphaviruses with the plasma membrane under low pH conditions (Jin et al., 2015; Pal et al., 2013; Smith et al., 2015). Virus was absorbed first to cells at 4°C before mAbs were added. After removing unbound virus and antibody, cells were pulsed at 37°C in a low-pH medium to promote plasma membrane-mediated viral fusion. Virus that entered the cells was stained with antibodies 14 h later and detected by flow cytometry. At a concentration of 10 μg/mL, RRV-12 did not inhibit fusion, with virus levels comparable to those of the negative control antibodies (**Figure 21F**). This result indicates that attachment, entry, and viral spread are the most likely mechanisms of inhibition utilized by RRV-12.

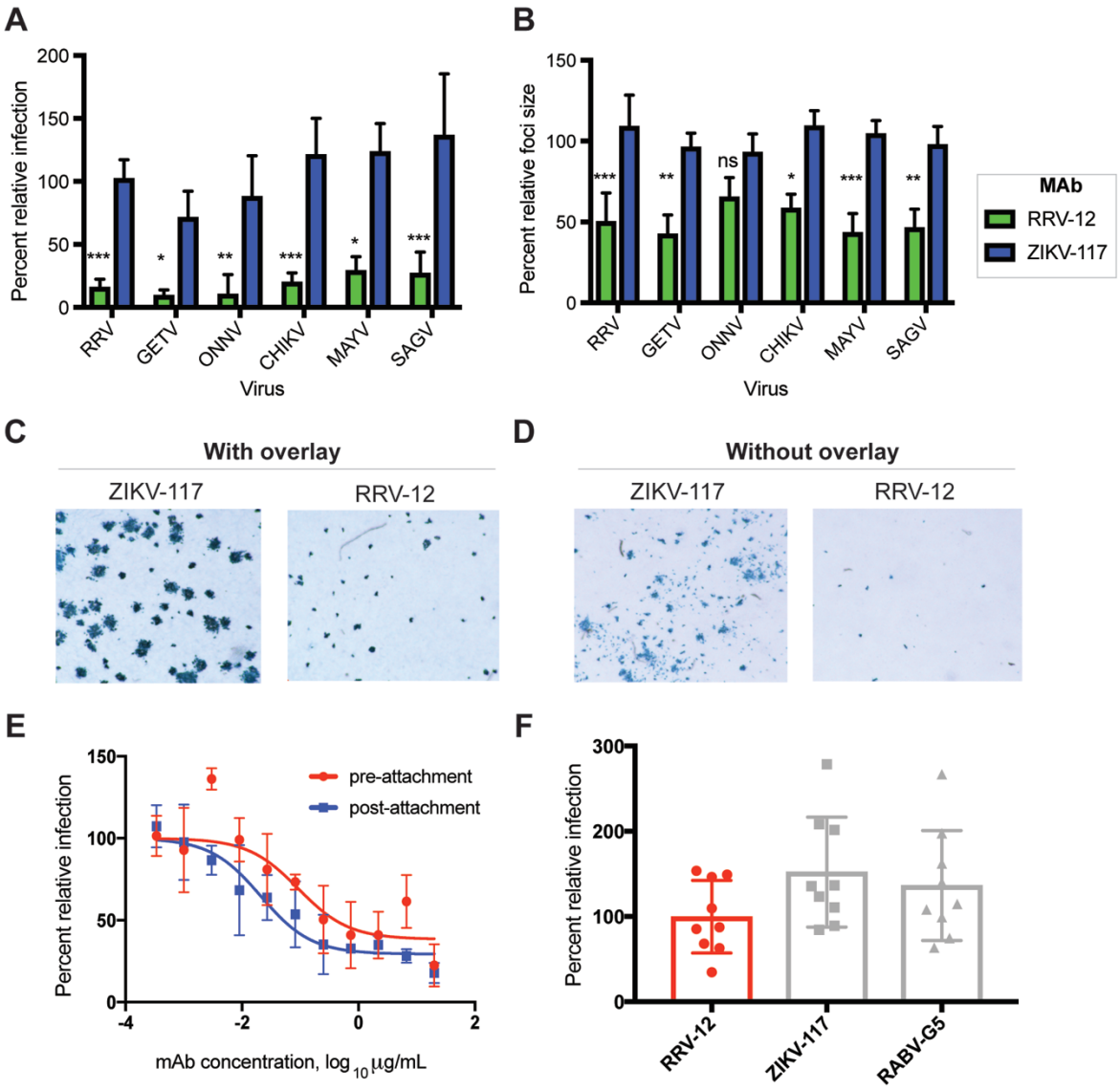

Figure 21. **RRV-12 blocks entry and cell-cell spread of RRV, MAYV, CHIKV, SAGV, GETV, and ONNV.** (**A**) RRV-12 blocks entry of RRV, MAYV, CHIKV, SAGV, GETV. Antibody at a concentration of 20 µg/mL was incubated 1:1 with virus for 1 h at 37°C before addition to Vero cells for 1 h, also at 37°C. Antibody was then removed with 3 washes in media before addition of a methylcellulose overlay. Cells were incubated at 37°C for 18 h before fixing and immunostaining. Foci were imaged and counted with a CTL unit. Three independent experiments were performed with triplicate samples in each experiment. (Kruskal-Wallis one-way ANOVA with Kruskal-Wallis post-test, with mean ± S.D. compared to isotype control (*$p < 0.05$, **$p < 0.01$, ***$p < 0.001$, ****$p < 0.0001$) (**B**) RRV-12 blocks cell-to-cell spread of RRV, MAYV, CHIKV, SAGV, GETV, and ONNV as measured through reduction of foci size. Virus was added to Vero cells for 1 h at 37°C before addition of 20 µg/mL of antibody diluted in methylcellulose overlay. After 18 h, cells were fixed, immunostained, and foci size was measured with a CTL unit. Three independent experiments were performed with triplicate samples in each experiment. (Kruskal-Wallis one-way ANOVA with Kruskal-Wallis post-test, with mean ± S.D. compared to isotype control (*$p < 0.05$, **$p < 0.01$, ***$p < 0.001$, ****$p < 0.0001$)) (**C**) Representative images of RRV-12 reduction of foci size for RRV infection as compared to a control antibody, with antibody added to methylcellulose overlay (left) and with antibody in the absence of methylcellulose overlay (right). Antibody concentrations were at 20 µg/mL and

immunostaining was performed as in FRNT. (**D**) Pre-attachment and post-attachment neutralization assay for RRV-12. In the pre-attachment assay, antibody was incubated with virus at 4°C before addition to Vero cells kept at 4°C. For the post-attachment assay, virus was applied to Vero cell monolayer cultures at 4°C before addition of antibody to cells at 4°C. Two independent experiments were performed in triplicate for each antibody, and representative curves are shown. (**E**) A fusion from without (FFWO) assay was used to measure antibody inhibition of virus fusion with the cell membrane under low pH conditions. Virus was adsorbed to Vero cell culture monolayers at 4°C for an hour before addition of antibody dilutions, also at 4°C, after removing excess virus. Cells then were exposed to a pH 5.5 medium or a control medium at neutral pH for two minutes and incubated at 37°C. The acidic pH medium was removed and cells were incubated for an additional 14 h before fixing, permeabilizing, and staining for intracellular virus antigens before flow cytometric analysis. Intracellular virus was quantified by measuring percent PE-positive cells relative to a virus-only control. Three separate experiments were performed in triplicates for each antibody.

RRV-12 targets a partially conserved E2 B domain epitope

To gain structural insight into the cross-reactivity of RRV-12, Fab fragments of RRV-12 were bound to RRV, CHIKV, or MAYV virions and analyzed by cryo-EM and single-particle reconstruction. Cryo-EM micrographs of each virus incubated with Fab RRV-12 demonstrated intact particles suitable for further analysis. Following single-particle reconstruction, structures for each virus/Fab RRV-12 complex were determined to a resolution of 6.3Å for RRV, 5.3Å for CHIKV, 5.3Å for MAYV, and 4.8 Å for native MAYV (**Figure 22A**).

The location of Fab RRV-12 binding sites on each virus was determined from the fitted coordinates of viral glycoprotein E2 structures and the Fab CHK-265 model (Fox et al., 2015). The position of CHIKV E3 was determined by alignment of a CHIKV E2-E3 structure derived from PDB 6NK7 (Basore et al., 2019) to the E2 ectodomain structure fit of the RRV-12 bound CHIKV density map. In comparison with the other RRV-12 bound viruses, E3 was only found to be present in the CHIKV structure. The positions of RRV and MAYV E2, and CHIKV E2, E3 and Fab structures relative to each other in the context of the density maps were analyzed to map regions of the virus surface within 6Å of the Fab structure (**Figure 22B**).

These results revealed that the RRV-12 Fab bound to similar regions of the E2 B domain from all three viruses at both the i3 axis and q3 axis trimers (**Figure 22B**), with each epitope on the surface being fully occupied. The Fab CDR loops are predicted to bind to a region of the E2

B domain spanning residues: RRV E2 183-187, 218-221, and 223; CHIKV E2 179-184, 198-200, 213-219; and MAYV E2 184-187 and 219-221 (**Figure 22B, Figure 23A**). A sequence alignment of RRV, CHIKV, MAYV, ONNV, SAGV, and GETV E2 B domain amino acid sequences revealed a partially conserved region on the E2 B domain composed of residues 183-187 and 217-222 shared between all the viruses (**Figure 23C**).

Density associated with the constant region of the Fab appears to cross-link neighboring spikes (**Figure 22C).** Analysis of fitted E2, E3 and Fab constant domain positions in the context of the density maps were used to map residues to the three virus surfaces. Residues RRV 7 (E2 β-ribbon), 59 and 60 (A domain), MAYV 7 and 10 (E2 β-ribbon), and 60 (A domain) are within 6Å of the constant domain (**Figure 22B, Figure 23A, B)**. These contacts are primarily due to the angle of Fab binding, which brings the constant domain near the virus surfaces (**Figure 24**). A gap exists in the density between the RRV and MAYV surface and the constant domain (**Figure 24**) suggesting at least a weak and/or transient interaction not observable with single particle reconstructions. For these reasons, residues on RRV and MAYV surfaces are most likely not a primary factor in Fab binding but may participate in transiently positioning the Fab.

For CHIKV, areas of E3 density contact the Fab density near the junction of the antibody variable and constant domains (**Figure 24**). E3 residues 8-10, 12, 14-17, and 19-25 are within 6Å of the antibody variable domain, and residues 52-53 are within 6Å of the antibody constant domain (**Figure 22B, Figure 25A, B**). Like RRV and MAYV, a gap is present between the CHIKV viral surface and the Fab constant domain, and the angle of Fab binding is similar (**Figure 24**). The contacts on the CHIKV surface result from occupation by E3 on a position that is empty on RRV and MAYV (**Figure 24**). E3 appears to lie directly underneath the Fab (**Figure 24**). Likely, these contacts on the surface of CHIKV are not critical residues in the cross-reactive epitope since the Fab binds similar regions on the E2 B domain on RRV and MAYV in the absence of E3 compared to CHIKV.

The position of Mxra8 in the asymmetric unit relative to CHIKV E2 (Basore et al., 2019) PDB 6NK7) was mapped to the asymmetric units of RRV-12-bound virions in the RRV, MAYV or CHIKV structures. Residues of the virus surface within 6Å of the Mxra8 position in the asymmetric unit were mapped (**Figure 22B**). Residues 25-28 and 61-63 of RRV, 22-24 and 115 of CHIKV, and 25-27 and 192 of MAYV are located on the A domain of E2 near the B domain Fab contacts and do not overlap predicted residues of the RRV-12 epitope (**Figure 23A, B**). Residues 61-63 and 158-160 of RRV, 142, 155, and 156 of CHIKV, and 55, 59-65, 157-161 and 262-2640 of MAYV are located on the strand of an adjacent E2 within the trimer. E1 residues 85-87 RRV, 83-85, 97, 98, and 226 CHIKV are within 6Å of the position of Mxra8 in the asymmetric unit of each virus (**Figure 23A, B**). A comparison of the structures of Mxra8 or RRV-12 bound to the CHIKV E2 B domain reveals that Mxra8 and RRV-12 do not bind to the same regions of E2; however, binding of one protein may occlude the binding of the other (**Figure 24**).

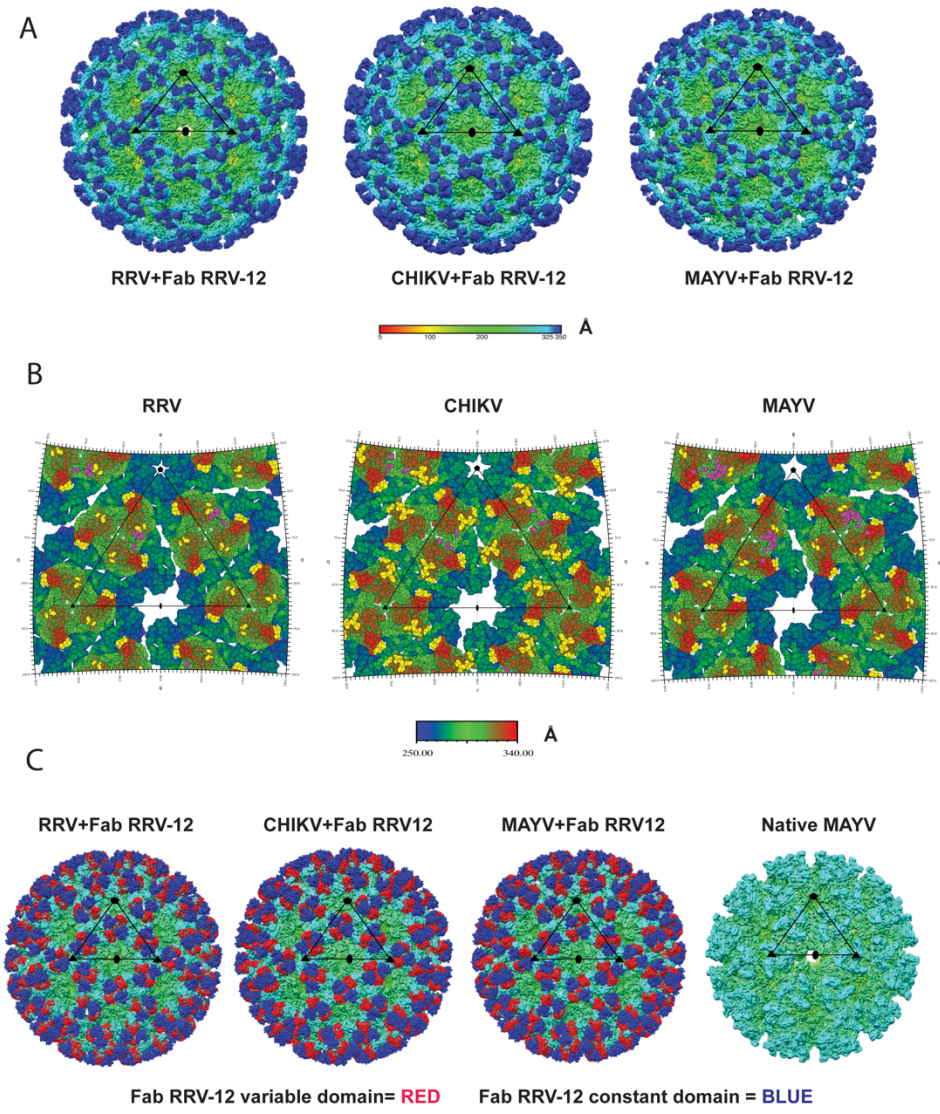

Figure 22. Structural analysis of Fab RRV-12 binding to RRV, CHIKV, and MAYV by cryo-EM. (**A**) Cryo EM density maps of RRV, CHIKV, and MAYV viruses bound by Fab RRV-12. Each map was determined by single particle reconstruction using icosahedral averaging. The scale bar represents the radial distance by color in Angstroms. The superimposed black triangle represents the asymmetric unit. Symmetry axes are indicated by a pentagon for the five-fold axis, by triangles for the icosahedral three-fold axis, and by an oval for the two-fold axis. Resolution of each map is determined at 0.143 on Fourier Shell correlation curves. The resolution of each map is 6.3 Å for RRV and 5.3 Å for both CHIKV and MAYV. (**B**) RIVEM road maps of the viral surface. Scale bar indicates radial distance from the center in Angstroms. Residues highlighted in yellow are on the E2 B domain and are located within 6 Å or less to the Fab structure. Highlighted residues indicate each B domain of each i3 and q3 trimer is fully occupied. (**C**) Cryo-density maps of RRV, CHIKV, and MAYV bound with Fab RRV-12 and a native MAYV structure. Fab constant or variable domains are colored blue or red respectively. The remaining density of each structure is colored based on radial distance from the center of the particle, see scale bar in (**A**).

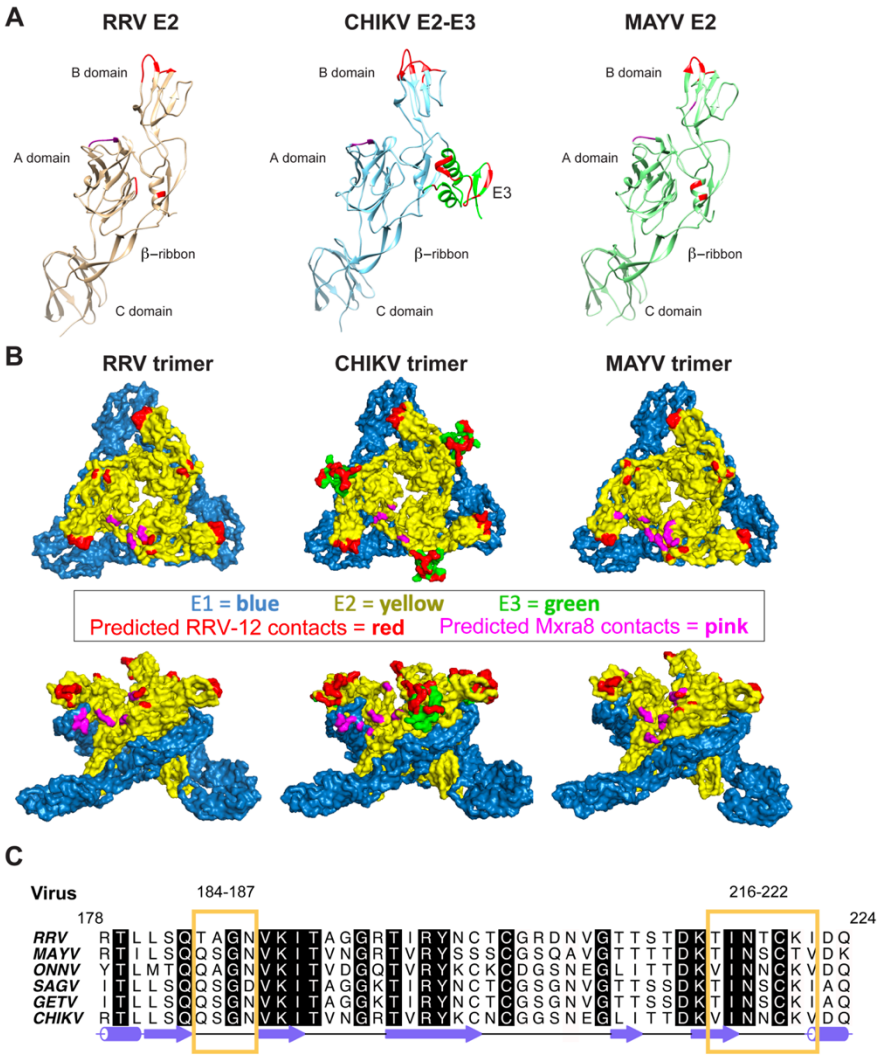

Figure 23. Fab RRV-12 targets the E2 B-domain. (**A**) Ribbon diagrams of E2 ectodomain structure from each virus. Regions of the B-domain highlighted in red are the predicted epitope. Highlighted regions span residues RRV 183-187 and 218-222, CHIKV E2 183-188 and 217-224, and MAYV E2 184-187 and 219-221. (**B**) Surface shaded representation of CHIKV E1/E2 trimer (PDB 3N42) as viewed down the center of the spike (left panel) or from the side of the spike (right panel). Fab RRV-12 footprint is orange and the E2 B-domain is cyan. The E2 A-domain is blue, and the C-domain is pink. The β-ribbon is green. (**C**) Sequence alignment of E2 B-domain region 172-228 from viruses CHIKV, ONNV, MAYV, RRV, SAGV, GETV. Red boxes outline a semi-conserved region between all these viruses containing residues of Fab RRV-12 epitope.

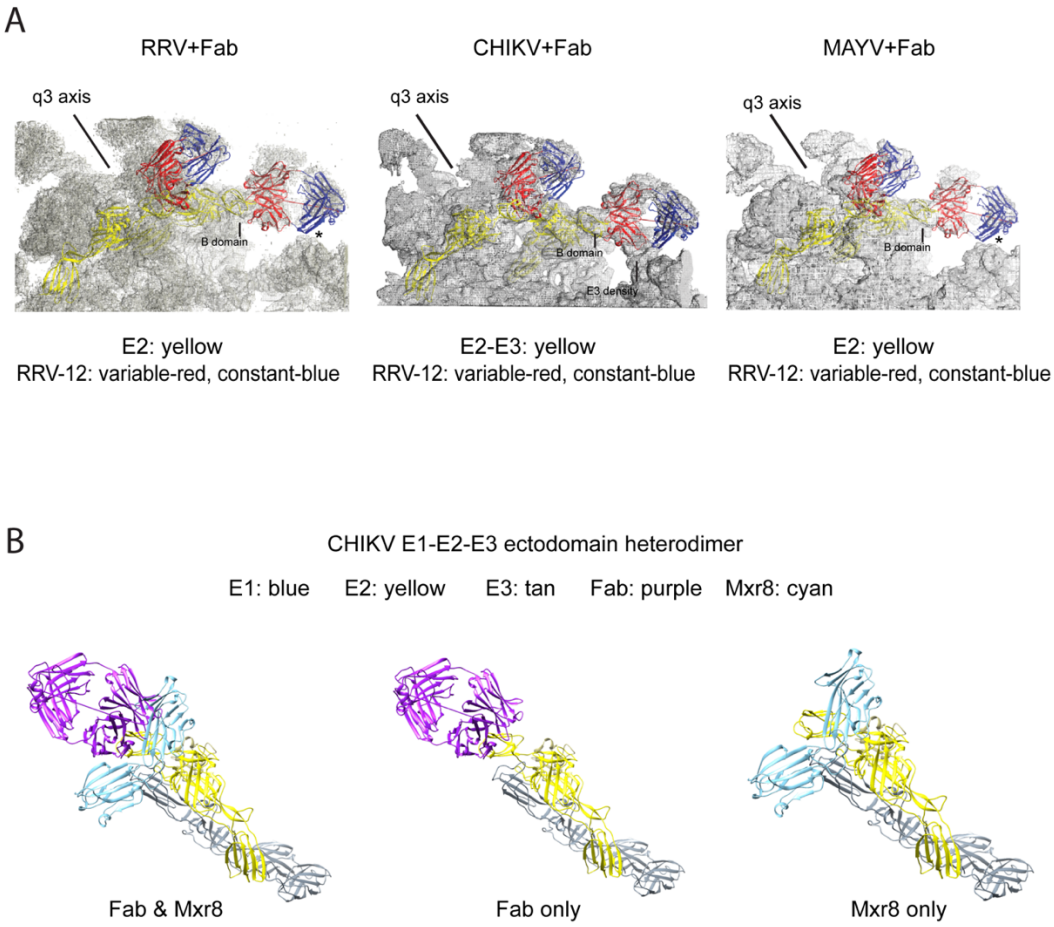

Figure 24. RRV-12 constant domain is near the viral surface. (A) The density of each Fab bound virus asymmetric unit was extracted with PHENIX (Liebschner et al., 2019). Fitted E2 structures are yellow; the Fab variable domains are red and constant domains are blue. The q3 axis of the asymmetric unit, the B domain, and E3 on CHIKV are all labeled. The asterisk on RRV and MAYV indicates space between the constant domain of the Fab and viral surface. **(B)** RRV-12 and Mxra8 binding potentially occlude one another. The CHIKV E1-E2-E3 ectodomain heterodimer shown with either Mxra8 or RRV-12 bound and both Fab and Mxra8 bound. E1 is blue, E2 is yellow, E3 is tan, Fab is purple, and Mxra8 is cyan.

RRV-12 therapeutic activity *in vivo*

To determine the efficacy of RRV-12 *in vivo*, protective activity was first tested in an immunocompetent mouse model of RRV infection. Four-week old male WT C57BL/6 mice were treated with 100 μg of mAbs one day after infection with 10^3 FFU of RRV strain T48. The gastrocnemius (calf) muscle, ankle, spleen, and quadriceps muscle were harvested at 3 days post-infection (dpi), and viral RNA levels were measured by qRT-PCR. RRV-12 significantly

reduced viral burden in all tissues except for the ipsilateral ankle (**Figure 25A**). Next, the importance of Fc effector functions was tested by comparing the therapeutic efficacy of RRV-12 IgG and IgG-LALA Fc, the latter having diminished capacity for FcγR binding (Hessell et al., 2007), in immunocompetent mice (Arduin et al., 2015; Saunders, 2019). Notably, no significant differences were observed between RRV infection in animals treated with intact or LALA forms of RRV-12 (**Figure 25B**). The therapeutic efficacy of RRV-12 was then tested in a stringent immunocompromised mouse model of RRV infection and disease. Four-week old male wild-type C57BL/6 mice were treated with 0.2 mg of MAR1-5A3 (Sheehan et al., 2006), an anti-Ifnar1 blocking mAb, prior to inoculation with 10^3 FFU of RRV. One hundred micrograms of RRV mAb via an intraperitoneal route one day after virus inoculation. When mice were given a control mAb, death was observed after 7 days; however, RRV-12 protected 40% of mice from death over the three-week time course (**Figure 25C**). The therapeutic efficacy of RRV-12 was also tested in an immunocompetent mouse challenge model of MAYV (Earnest et al., 2019). RRV-12 reduced MAYV viral burden in all tissues examined, including in the ipsilateral ankle, which was not seen in the RRV model. Finally, a clinical scoring system was used to measure severity of RRV disease in WT immunocompetent juvenile mice. Three-week-old WT C57BL/6 mice were inoculated with 10^3 FFU of RRV strain T48, and 100 μg of RRV-12 or an isotype control mAb was administered via intraperitoneal injection one day later. Mice were weighed and monitored over the course of 18 days and a clinical score was assigned based on grip strength, gait, and righting reflex, as previously described (Haist et al., 2017). Mice that received RRV-12 had marked improvement in clinical score compared to mice treated with the control (**Figure 26A**). In addition, a significant reduction in viral RNA was observed in all tissues examined, including the spleen, ipsilateral and contralateral gastrocnemius, quadriceps, and ankle tissues harvested at 18 dpi (**Figure 26B**).

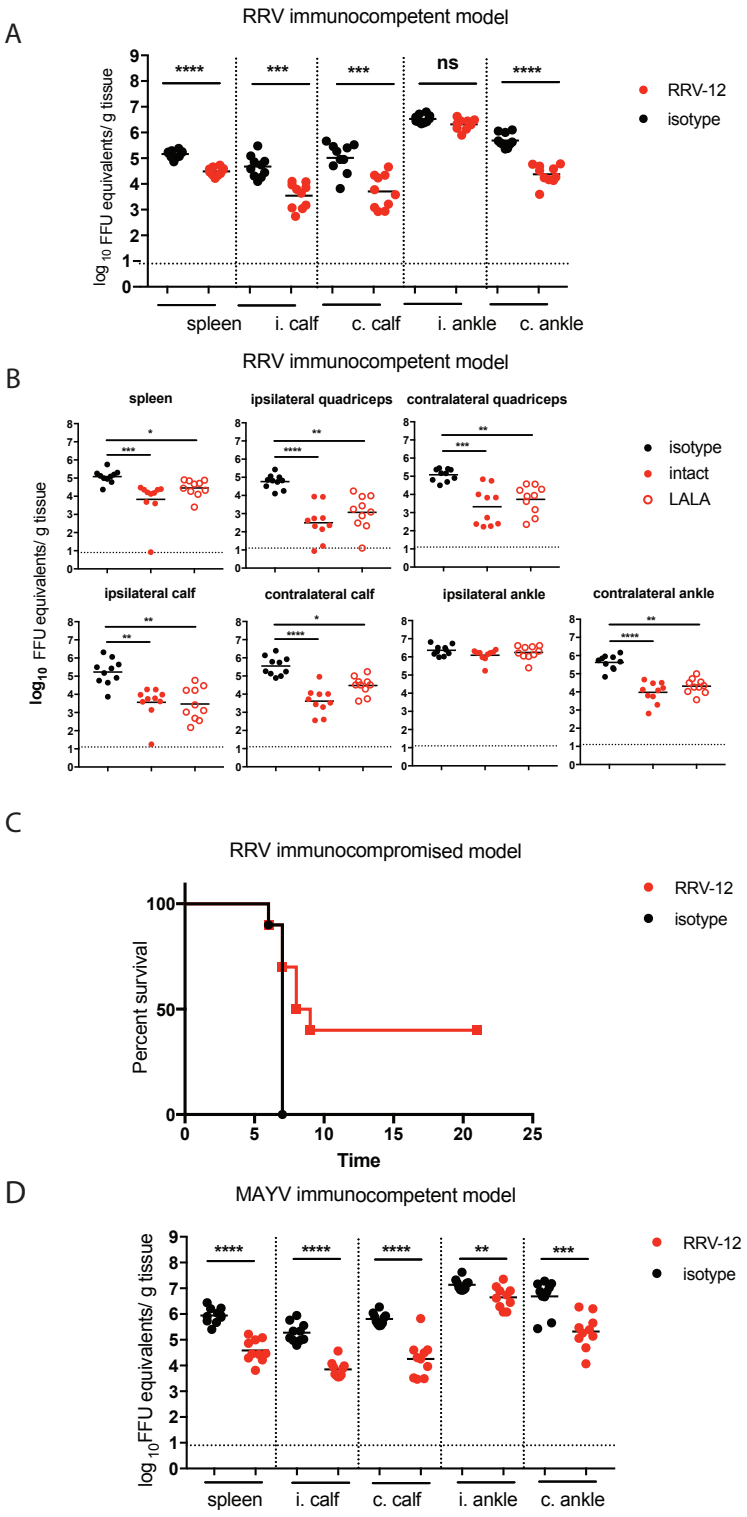

Figure 25. Protective activity of RRV-12 *in vivo* against RRV and MAYV. (**A**) RRV-12 reduces viral infection in immunocompetent WT model of RRV infection. RRV-12 (100 μg) was administered at 1 dpi, and ipsilateral and contralateral gastrocnemius, quadriceps, ankle, or spleen tissues were collected 3 dpi

for measurement of viral RNA through qRT-PCR. Two independent experiments were performed, with ten mice per antibody for each group (one-way ANOVA with a Dunnett's post-test comparing each group to the isotype control; **p < 0.01, ***p < 0.001, ****p < 0.0001). (**B**) RRV-12 LALA mutant and RRV-12 intact mAb have similar therapeutic effect in immunocompetent mouse model of RRV infection. RRV-12 (100 µg) was administered at 1 dpi to WT mice, and ipsilateral and contralateral gastrocnemius, quadriceps, ankle, or spleen tissues were collected 3 dpi for measurement of viral RNA through qRT-PCR. Two independent experiments were performed, with ten mice per antibody for each group (one-way ANOVA with a Dunnett's post-test comparing each group to the isotype control; **p < 0.01, ***p < 0.001, ****p < 0.0001). (**C**) RRV-12 increases survival when administered therapeutically after RRV infection in an immunocompromised mouse model. Mice were given 0.5 mg of anti-Ifnar1 antibody, and subsequently inoculated with 10^3 FFU of RRV in the footpad. At 1 dpi, 100 µg of RRV antibody was administered, and mice survival was monitored for three weeks. Two independent experiments were performed, with five mice per antibody for each group. (**D**) RRV-12 reduces viral burden in an immunocompetent model of MAYV infection in mice. As described above, RRV-12 (100 µg) was administered 1 dpi in WT mice, and ipsilateral and contralateral gastrocnemius, quadriceps, ankle, or spleen tissues were collected 3 dpi for measurement of viral RNA by qRT-PCR. Two independent experiments were performed, with a total of ten mice for each antibody group (one-way ANOVA with a Dunnett's post-test comparing each group to the isotype control; **p < 0.01, ***p < 0.001, ****p < 0.0001).

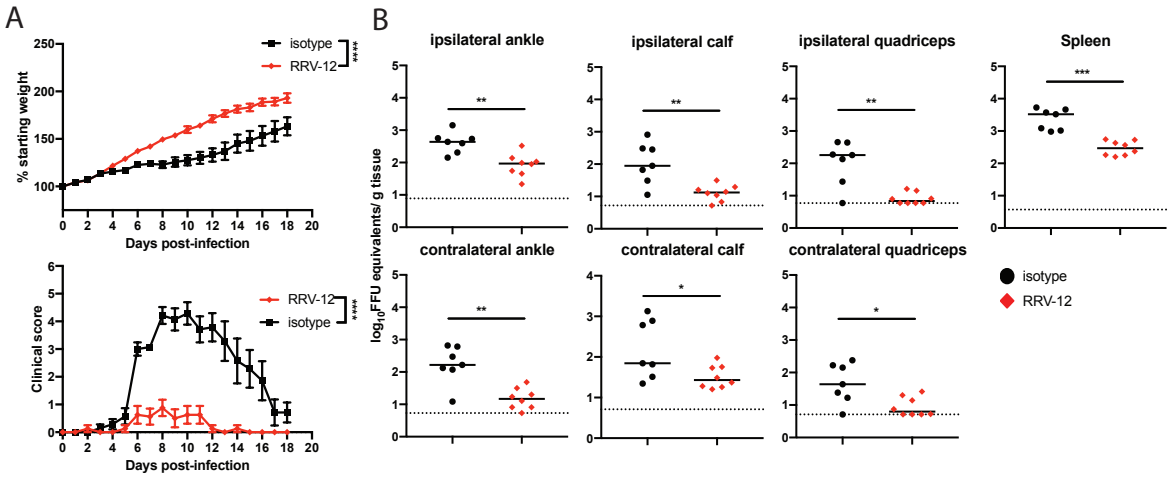

Figure 26. RRV-12 improves clinical disease and reduces viral RNA burden when given therapeutically in a WT mouse model. (**A**) Three-week-old WT C57BL/6 mice were inoculated with 10^3 FFU of RRV strain T48 before administration of 100 µg antibody by intraperitoneal injection at 24 hpi. Mice were then weighed each day over the course of 18 days and assigned a clinical score based on grip strength, gait, and righting reflex. Blind scoring of mice was performed using the following scoring system: 0, no disease; 1, mild defect in ipsilateral hind paw gripping; 2, mild defect in bilateral hind paw gripping; 3, bilateral loss in hind paw gripping; 4, bilateral loss in hind paw gripping with moderate hind limb weakness, observable mild altered gait, and difficulty or failure to right self; 5, bilateral loss in hind paw gripping with severe hind limb weakness, moderate altered gait, and loss of righting reflex; 6, bilateral loss in hind paw gripping with severe hind limb weakness, severely altered gait with possible dragging hind paw, and loss of righting reflex; 7, moribund. Two independent experiments were performed, for a total of n=8 mice in each antibody group. Statistical analysis was performed using a one-way ANOVA of area under the curve test (****p < 0.0001). (**B**) Eighteen days post-infection, the spleen, ipsilateral and contralateral gastrocnemius, quadriceps, and ankle tissues were collected following extensive perfusion with PBS. Viral RNA was quantified through qRT-PCR and statistical analysis was performed using a Kruskal-Wallis multiple comparisons test (*p < 0.05, **p < 0.01; ns = not significant).

Discussion

Here, I identified cross-reactive neutralizing antibodies generated from two individuals from different geographic areas with prior history of infection with CHIKV or RRV. Two of these antibodies broadly neutralized six different arthritogenic alphaviruses: RRV, CHIKV, MAYV, ONNV, SAGV, and GETV. These cross-reactive mAbs competed for a similar antigenic site and blocked binding of virus to Mxra8-Fc fusion protein. Cryo-EM analysis of Fab fragments of RRV-12 bound to CHIKV, MAYV, and RRV revealed engagement to a conserved epitope at the distal end of the B domain. In addition to blocking attachment to Mxra8 receptor, I found that RRV-12 blocked viral entry and prevented cell-cell spread of virus. Finally, when tested in mouse models of RRV and MAYV infection, RRV-12 reduced viral titer in multiple tissues and improved clinical outcome.

Previously, two human antibody reactive against several alphaviruses, 8I4 and 2H1, were reported, although these mAbs neutralized infection of only RRV, MAYV, and SFV, and with moderate potency (Fox et al., 2015). A cross-reactive murine antibody, CHK-265, also was described previously that potently neutralizes CHIK and MAYV, but it inhibited RRV, SFV, and ONNV to a lesser extent (Fox et al., 2015). A cryo-EM structure of CHK-265 Fab in complex with CHIKV revealed that CHK-265 binds principally to the B domain at residues 182-189, 203-206, and 214-218 (Fox et al., 2015). The structure for CHK-265 also suggested that the mechanism of neutralization might involve a tethering of the B domain to an additional contact site in the A domain at residues 71-72 on an adjacent spike. Although the CHKV-265 epitope nearly completely overlaps the RRV-12 binding site defined here at residues 184-187 and 216-222, the footprint for RRV-12 includes fewer residues, and does not appear to include the A domain, indicating a slightly different orientation of engagement. The location of both RRV-12 and CHK-265 binding sites within the same B domain region suggests that this epitope is important for recognition of broadly neutralizing mAbs. For the viruses I tested, complete

sequence conservation of the B domain is observed at residues 186, 217-218, and 220 within the footprint of RRV-12. While a region of high sequence conservation among alphaviruses also is observed at residues 95-101 in the A domain, it is possible that broadly neutralizing mAbs may target the B domain more frequently, since its position at the distal end of the E2 protein allows for accessibility on the viral spike.

RRV-12 and CHKV-70 blocked binding to Mxra8 protein in a competition ELISA. Mxra8 contacts residues within the A and B domains, as well as arch regions of the E2 protein. In particular, the Mxra8 footprint on the B domain includes residues 178-182, 189, 191-193, 212-214, and 221-223 (Basore et al., 2019; Zhang et al., 2018). These residues overlap with, or are adjacent to, the binding site determined for RRV-12 at residues 184-187 and 216-222. Of note, CHKV-77 did not inhibit binding to Mxra8-Fc protein in a competition ELISA, even though its neutralization potency as measured by IC_{50} value was similar to that of RRV-12. I speculate that CHKV-77 most likely recognizes a spatially distinct epitope in the E2 B domain, even though it competes with RRV-12 in both the MAYV and CHIKV protein BLI competition binding assays. The neutralization mechanism of CHKV-77 may be similar to that of other B domain neutralizing antibodies, such as those inhibiting entry, fusion, and egress (Earnest et al., 2019; Fox et al., 2015; Lee et al., 2011). My finding that RRV-12 inhibits entry is consistent with several other alphavirus antibodies that block infection through this mechanism (Fox et al., 2015; Jin et al., 2015; Pal et al., 2013). RRV-12, however, did not inhibit plasma membrane-mediated fusion, an assay that is a surrogate for endosomal fusion (Pal et al., 2013). This result agrees with the finding that broadly neutralizing murine mAbs primarily block alphavirus infection principally by preventing entry and attachment (Fox et al., 2015).

I discovered a unique focus reduction phenotype for RRV-12, suggesting that it also limits cell-to-cell spread of virus. This phenotype has also been described in other virus systems, for example the case of the influenza heterosubtypic HA-specific human mAb FluA-20 that is not neutralizing *in vitro* but is protective *in vivo* (Bangaru et al., 2019). There are several means by

which cell-to-cell alphavirus spread may be inhibited by antibodies. During CHIKV infection, neutralizing mAbs against the E2 protein have been found to block envelopment of nucleocapsids driven by the E1/E2 glycoprotein, thus preventing viral budding (Jin et al., 2018). Alternatively, viral particles may be released from the cell, yet have reduced infectivity. Mutations in the B domain of RRV, including a cysteine-to-serine mutation at residue 220, were shown to reduce levels of E2 incorporation in viral particles, thereby leading to fewer infectious particles, possibly through destabilization of E2-nucleocapsid interactions (Snyder et al., 2012). Finally, antibodies binding to the B domain may inhibit cell-to-cell spread of alphaviruses (Lee et al., 2011). During the budding process, alphaviruses form actin- and tubulin-containing protrusions that function in protecting virions from inhibitory membrane-associated proteins and preventing superinfection of the same cell (Brown et al., 2018). These structures do not fuse with the neighboring cell, but instead concentrate virus near the cell membrane. E2-nucleocapsid interactions are important for formation of these protrusions, and it is therefore possible that conformational changes induced by antibody binding to the distal region of the B domain may affect interactions of the transmembrane portion of the B domain with the nucleocapsid (Brown et al., 2018; Martinez and Kielian, 2016). Further study will be required to define which of these inhibition mechanisms RRV-12 utilizes.

These *in vivo* results demonstrate that RRV-12 is protective in both RRV and MAYV mouse models of infection, and reduces clinical disease in an immunocompetent RRV mouse model when administered therapeutically. When a LALA Fc variant of RRV-12 was tested *in vivo*, diminished protection was not observed as compared to intact IgG, suggesting that Fc effector functions may not be essential for protection. Previously, CHIKV and RRV mAbs have demonstrated promising therapeutic activity in wild-type or immunocompromised mouse models (Fox et al., 2015; Jin and Simmons, 2019; Pal et al., 2013; Smith et al., 2015). However, these mAbs exhibited nearly complete elimination of virus *in vitro*, and therefore it was surprising that RRV-12 demonstrated comparable levels of protection despite a resistant fraction of ~40% of

virus in the FRNT. This phenomenon has been reported previously for alphavirus mAbs, and while the exact cause is unknown, particle heterogeneity due to maturation differences or partial retention of cleaved E3 precursor protein have been suggested as possible contributing factors (Heidner et al., 1996; Zhang et al., 2011). This result suggests that incompletely neutralizing mAbs still should be considered as therapeutic candidates.

In addition to intraperitoneal administration of antibodies in mouse models, other forms of antibody delivery have shown promise for alphaviruses. A single dose of a potently neutralizing human anti-CHIKV mAb delivered as lipid-encapsulated mRNA conferred protection against viral infection and arthritis in mice and macaques (Kose et al., 2019; Roussel et al., 2006). The description here of a broadly neutralizing human mAb that protects against disease in multiple mouse models could provide another such candidate for mRNA delivery. Additionally, the knowledge provided here of antibody mechanism and binding epitope on the E2 B domain could aid efforts to design a broadly protective alphavirus vaccine.

Materials and methods

Source of human B cells

The RRV-immune subject was a 50-year old woman living in the U.S. who had a history of laboratory-confirmed infection in Australia in 1987, as described in Powell *et al* (in submission). Peripheral blood was obtained from this subject in the U.S. in 2015 (28 years after infection) after written informed consent with approval from the Vanderbilt University Medical Center Institutional Review Board. Peripheral blood mononuclear cells (PBMCs) were isolated using density gradient centrifugation on Ficoll and were cryopreserved in liquid nitrogen until used in the experiments. The other blood sample was collected in 2015 from an adult subject in Colombo, Sri Lanka with serological evidence of prior CHIKV infection (>1/5,000 serum neutralizing antibody titer to CHIKV using virus replicon particles based on the Sri Lankan strain

SL15649 (Morrison et al., 2011). CHIKV infection was common in Colombo during the years 2006 to 2008. The studies in Sri Lanka were approved by the Ethics Review Committee of the Medical Faculty, University of Colombo, Sri Lanka [serving as the National Institutes of Health (NIH)–approved Institutional Review Board (IRB) for Genetech Research Institute] and the IRB of Vanderbilt University Medical Center. The blood sample was a discarded buffy coat from a routine blood donation at the National Blood Center in Colombo, Sri Lanka. The sample was de-identified before removal from the National Blood Center. PBMCs and a plasma sample were separated at Genetech Research Institute by density gradient centrifugation and then cryopreserved and stored on liquid nitrogen until transfer to Vanderbilt using a liquid nitrogen dry shipper.

Cell lines

Vero (monkey, sex unspecified), cell lines were obtained from the American Type Culture Collection (ATCC CCL-81). Vero cells were cultured in Dulbecco's Modified Eagle Medium (DMEM) (ThermoFisher Scientific) supplemented with 5% fetal bovine serum (FBS; HyClone) at 5% CO_2, 37°C. BHK21 cell lines were obtained from (ATCC CCL-10) and cultured in 10% FBS (Sigma) and Minimal Essential Media (MEM, ThermoFisher Scientific).

Viruses

Ross River virus strain T48, chikungunya virus strain 181/25, O'nyong'nyong virus strain MP30, Mayaro virus strain TR VL-4675, Sagiyama virus strain M6-Mag 132, and Getah virus strain MM 2021 were obtained from the World Reference Center for Emerging Viruses and Arboviruses at UTMB.

Mouse models

Three-week-old male and female WT C57BL/6J were used for clinical disease model studies and four-week-old male WT C57BL/6J mice were used for acute virological and survival studies. Mice were housed in microisolator cages and provided food and water ad libitum. All animal experiments and procedures were carried out in accordance with the recommendations in the Guide for the Care and Use of Laboratory Animals of the National Institutes of Health. The protocols were approved by the Institutional Animal Care and Use Committee at the Washington University School of Medicine (Assurance number A3381-01). Injections were performed under anesthesia that was induced and maintained with ketamine hydrochloride (80 mg/kg) and xylazine (15 mg/kg), and all efforts were made to minimize animal suffering.

Generation of human hybridomas

Approximately 10^7 cryopreserved PBMCs were thawed and transformed with Epstein-Barr virus obtained from the supernatant of B95.8 cells in a suspension also containing a Chk2 inhibitor, cyclosporin A, and CpG, and the mixture was plated in a 384-well cell culture plate. After 7 days, transformed cells were transferred to 96-well plates containing a feeder layer of irradiated cells that were PBMCs obtained from discarded leukofiltration devices (Nashville Red Cross). After an additional 5 days, the supernatants of expanded cells were screened for the presence of RRV- or MAYV-reactive antibodies using an enzyme-linked immunosorbent assay (ELISA), described below. Transformed B cells from wells containing supernatant with antibodies reactive to RRV or MAYV were fused to the HMMA2.5 non-secreting myeloma cell line using an established electrofusion technique (Smith and Crowe, 2015). Subsequently, the resulting mixture of hybridoma cells was resuspended in medium containing hypoxanthine, aminopterin, thymidine and oubain to select for hybrids of B cells and myeloma cells.

Virus ELISA screen

RRV strain T48 was propagated in monolayer cultures of Vero cells. The cell line was authenticated and tested monthly during culture for the presence of mycoplasma and found to be negative in all cases. Infected cell supernatants containing virus with a titer of approximately 5 x 10^6 FFU/mL were harvested when cytopathic effect was maximal, filtered through a 0.45 µm filter, then frozen and stored at –80°C until use. 384-well ELISA plates were directly coated with 25 µL of RRV strain T48 harvested directly from cell supernatants, diluted 1:100 in PBS, and incubated for 1 h at 37°C. Plates were washed 5 times with PBS containing Tween (PBST) using an EL406 combination washer dispenser instrument (BioTek) and blocked for 1 h at room temperature with 5% milk powder and 2% goat serum, diluted in PBS. After washing 2 times with PBST, 25 µL of supernatants from hybridoma cultures or EBV-transformed cell lines were added to plates, which then were incubated for 1 h at room temperature. Plates were washed 4 times, and 25 µL of goat anti-human alkaline phosphatase-conjugated secondary antibodies (Meridian Life Science) diluted 1:5,000 in PBS was added to plates. After a 45-min incubation period, plates were washed 5 times and 25 µL of alkaline phosphatase substrate tablets (Sigma) diluted in Tris buffer with 1M $MgCl_2$ was added. Optical density was read at 405 nm after 1 h using a Biotek plate reader.

BLI competition-binding studies

An Octet RED96 BLI instrument (Pall FortéBio) was used to perform epitope binning studies using competition binding. Anti-Penta-HIS (HIS1K) biosensor tips were used to immbolize either CHIKV or MAYV E2 protein containing a hexahistidine tag. After measuring the baseline signal, the biosensor tips were immersed into wells containing mAb for 2 min. After another baseline measurement, biosensors then were transferred to wells containing a first mAb at a concentration of 50 µg/mL for 5 min, before immersion in a solution containing a second mAb, also at a concentration of 50 µg/mL for 5 min. The percent competition of the second mAb

in the presence of the first mAb was determined by comparing the maximal signal of binding for the second mAb in the presence of the first antibody to the maximal signal of that mAb alone when separately tested uncompeted. Competition was defined by reduction of the maximal binding score to <25% of un-competed binding. An intermediate competing mAb was identified when a 25 to 50% reduction in maximal binding was observed.

Hybridoma cell line clone production

Two weeks after fusion, hybridoma cell lines were cloned by single-cell sorting using fluorescence-activated cell sorting on a BD FACSAria™ III sorting cytometer with aerosol containment, in the Vanderbilt University Medical Center Flow Cytometry Core. Approximately 2 weeks later, an ELISA screen was performed, and wells containing cloned cells secreting antibodies reactive to RRV or MAYV were selected for expansion.

Purification of mAb IgG protein

Clonal cells secreting mAbs were grown in 75 cm^2 flasks to 70% confluency in hybridoma growth medium (ClonaCell-HY medium E from STEMCELL Technologies, 03805). The cells were expanded equally to four 225 cm^2 flasks for antibody expression in serum-free medium (GIBCO Hybridoma-SFM, Invitrogen, 12045084). The supernatant was harvested after 3 weeks and purified by affinity chromatography using protein G columns (GE Life Sciences, Protein G HP Columns). Purified IgG from hybridoma cell expression was used for all assays.

Focus reduction neutralization test

Vero cells (American Type Culture Collection [ATCC] Cat. No. CCL-81) were seeded in 96-well plates at 30,000 cells/well the day before use. Antibodies were diluted in 96-well U-bottom plates, with a 1:3 dilution series across the plate and a virus-only control in the left column. A solution containing infectious virus (RRV, MAYV, CHIKV, ONNV, SAGV, or GETV)

was diluted to a concentration of 100 focus-forming units (FFU)/mL and mixed 1:1 by volume in a 96-well plate with antibody suspensions. The virus/antibody mixture was incubated for 1 h at 37°C before transfer to Vero cell monolayer cultures. Infection was allowed to proceed for 1 h and then 1% methylcellulose overlay prepared in DMEM with 2% FBS was added to cells. After 18 h, 1% paraformaldehyde (PFA) prepared in PBS was used to fix cells for at least one hour. Plates were washed 3 times with PBS before addition of a 1:6,000 dilution of anti-RRV mouse ascites fluid (ATCC Cat. No. VR-1246AF), anti-MAYV mouse ascites fluid (ATCC Cat. No. [V-507-701-562) or anti-CHIKV mouse ascites fluid (ATCC Cat. No. V-548-701-562), prepared in cell permeabilizing buffer (PBS with 0.1% saponin and 0.1% bovine serum albumin). After incubation for at least 2 h at room temperature, plates were washed 3 times in permeabilizing buffer, and anti-mouse HRP-conjugated secondary (Kirkegaard & Perry Laboratories [KPL]) was added at a 1:2,000 dilution in permeabilizing buffer. Plates were incubated for 1 h at room temperature, and washed 3 times before addition of TrueBlue Peroxidase substrate (KPL) for 20 min. Plates were rinsed with dH_2O, and then plates were imaged with an ImmunoSpot® plate reader (Cellular Technology Limited [CTL]). Foci were counted with BioSpot 5.1 software (CTL), and the percent relative infection was calculated based on the virus-only control. Triplicate tests were performed for each antibody, and the results were averaged.

Entry and fusion inhibition, and foci reduction assays

Entry inhibition was performed as a variation of the FRNT. As described above, Vero cells were seeded in 96-well plates at 30,000 cells/well the day before use. Virus and antibody at a concentration of 20 µg/mL were mixed 1:1 and incubated together for 1 h at 37°C before transfer to Vero cell monolayer cultures. Infection was allowed to proceed for 1 h and importantly, antibody and virus were removed with three washes in medium. A 1% methylcellulose overlay prepared in DMEM with 2% FBS was then added to cells and staining was performed similarly to the FRNT. Plates were imaged with an ImmunoSpot® plate reader

(Cellular Technology Limited [CTL]). Foci were counted with BioSpot 5.1 software (CTL), and the percent relative infection was calculated based on the virus-only control. Triplicate tests were performed for each antibody and each virus, and the results were averaged.

A fusion from without (FFWO) assay was performed in which Vero cells were seeded at 30,000 cells/well in 96-well plates the day before use in the assay. Cells were washed once with binding medium (RPMI 1640, 0.2% BSA, 10 mM HEPES pH 7.4, and 20 mM NH_4Cl) at 4°C, and incubated for 15 min at 4°C. The T48 strain of RRV was concentrated to 10^8 FFU/mL using 100 kDa centrifugal filters (Amicon) Centricon. Virus was prepared in binding medium and added to cells at a multiplicity of infection (MOI) of 15 for 1 h at 4°C. Any remaining free virus was removed with two washes in binding medium. Antibodies were prepared in DMEM containing 2% FBS at 10 μg/mL concentrations and added to cells for 1 h at 4°C. Antibody was removed and fusion with the plasma membrane was initiated by the addition of fusion media (RPMI 1640, 0.2% BSA, 10 mM HEPES, and 30 mM succinic acid at pH 5.5) for 2 min at 37°C. Binding medium (RPMI 1640, 0.2% BSA, 10 mM HEPES at pH 7.4) was used in place of low pH fusion medium in controls wells to ensure that virus entry into cells only occurred due to pH-dependent plasma membrane fusion. After a 2-min incubation, medium was removed and cells were incubated in DMEM supplemented with 5% FBS, 10 mM HEPES, and 20 mM NH_4Cl (pH 7.4). Fourteen hours later, cells were detached with trypsin, fixed with 1% PFA in PBS for 1 hour, and permeabilized with 0.1% saponin detergent solution. For staining prior to flow cytometry analysis, cells were incubated sequentially with RRV mouse ascites fluid (1:6000 dilution ATCC Cat. No. VR-1246AF) for 1 h and PE conjugated goat anti-mouse IgG secondary antibody for 1 h (ThermoFisher). Cells were analyzed on BD Fortessa flow cytometer with FlowJo software.

An FRNT was performed in which antibody was added at a concentration of 20 μg/mL to the methylcellulose semisolid overlay. Virus first was allowed to infect cells for 1 h at 37°C before addition of antibody in the overlay. Staining was performed 18 h later, as in the FRNT. A variation of this assay also was performed in which antibody was added after viral infection of

cells for 1 h at 37°C. Virus was washed out with 3 washes in medium, and mAb at a concentration of 20 µg/mL was added to cells without the addition of methylcellulose. Images were taken post-staining using the CTL reader.

Virus purification and cryo-EM

RRV, CHIKV, and MAYV were propagated in BHK21 cell cultures. For each purification, approximately 2 x 10^8 BHK21 cells were inoculated with a MOI of approximately 0.1. Infected cell supernatant medium was collected between 24 and 36 h after inoculation, and was clarified by centrifugation at 2,744 x *g* for 30 min at 4°C. Virions were concentrated through a 28% sucrose cushion in TNE buffer (50 mM Tris pH 7.4, 200 mM NaCl, 1.0 mM EDTA) by ultra-centrifugation at 178,305 x *g* for 2 h at 4°C. Particles were resuspended in residual supernatant by rocking gently for 1 h at room temperature. Virus particles were concentrated further and purified based on size and density with a 5 to 55% continuous OptiPrep gradient (Sigma, catalog number D1655) and ultracentrifugation was performed at 178,305 x *g* for 2 h at 4°C. The virus-containing band was extracted, buffer exchanged, and concentrated into TNE buffer with an Amicon Ultra-4 100 kDa molecular weight cutoff centrifugal filter (Millipore-Sigma, catalog number Z648043-24EA) to a final volume of 0.05 mL. Fab fragments of mAb RRV-12 IgG were generated with the Pierce Fab Preparation Kit (ThermoFisher, catalog number 44985) according to the manufacturer's recommendations. Purified virus and Fab fragment complexes were incubated at a 2:1 molar ratio of Fab to E2 glycoprotein overnight at 4°C. Virus-Fab samples and native MAYV samples were flash frozen on Ultrathin carbon Lacey grids, 400 mesh copper (Ted Pella, catalog number 01824) in liquid ethane with a Gatan CP3 cryo-plunge. Virus-Fab complexes and native MAYV were imaged with a ThermoFisher Scientific Titan Krios, magnification 18,000x, and a pixel size of 1.6Å for RRV and 0.81Å for CHIKV, and both native and Fab bound MAYV. Images were collected with a Gatan K2 Summit direct electron detector and Leginon software package (Suloway et al., 2005). Micrographs were processed

with MotionCor2 (Zheng et al., 2017), and the CTF function was calculated with CTFFIND4 (Rohou and Grigorieff, 2015). Template-based particle selection was done with FindEM (Roseman, 2004), and non-reference 2D classification was performed with RELION. The final particle numbers used in single particle reconstructions were as follows: 9,559 RRV-Fab, 10,395 CHIKV-Fab, 18,410 MAYV-Fab and 20,592 native MAYV. Single particle reconstructions were performed according to the 'gold standard' method using jspr (Guo and Jiang, 2014). Briefly, particles were divided equally into two randomly selected independent particle sets. Two *de novo* models were generated from random sets of 1,000 particles. One *de novo* model was assigned to one of the particle sets. The other *de novo* model was assigned to the other particle set. Each independent dataset was refined iteratively assuming icosahedral symmetry. Refinement resulted in two independent models that converge on the same structure. Following corrections for astigmatism, elliptical distortion, defocus and the masking of the disordered nucleocapsid core, the final models of each independent data set were combined into a single final model. The average resolution of each map calculated at 0.143 from FSC curves was 6.3Å for RRV, 5.3Å for CHIKV, 5.3Å for MAYV, and 4.8 Å for native MAYV.

Based upon resolution values between 5-6Å for all three of the Fab bound virus density maps, the alpha carbon backbone of the alphavirus E1, E2 structural glycoproteins and the Fab model CHK-265 (Fox et al., 2015) were used to identify and interpret the maps. The crystal structure of the CHIKV E1/E2 dimer, RCSB PDB 3N42, (Voss et al., 2010) was used to analyze the CHIKV Fab-bound model. Homology models of both RRV and MAYV E1 and E2 glycoproteins generated with I-TASSER (Roy et al., 2010; Yang et al., 2015; Zhang, 2008), were used to analyze the RRV and MAYV Fab-bound models. The alpha carbon backbone of the RRV and MAYV E1 and E2 structures were aligned to the alpha carbon backbone of the CHIKV E1 and E2 crystal structures. The RMSD calculated in PyMOL for each alignment is 1.6 $Å^3$ for E1 RRV:CHIKV and 2.0 $Å^3$ for E2 RRV:CHIKV. The RMSD values for MAYV E1 and E2 aligned to CHIKV E1 and E2 are 1.6 $Å^3$for E1 and 2.1 $Å^3$ for E2. The alpha carbon backbone of

a model of both the constant and variable domains of Fab CHK-265 was fitted to all three virus-Fab complexes. Homology models of the variable light (VL) and variable heavy (VH) domains of RRV-12 were generated from the primary amino acid sequence of each domain with I-TASSER. In order to confirm Fab CHK-265 was a suitable substitute for RRV-12, the alpha carbon backbone of the RRV-12 variable domains were aligned to the Fab CHK-265 alpha carbon variable domain backbone with PyMOL. The RMSD is 0.94Å^3 for the VH domain alignment and 0.51Å^3 for the VL domain alignment. The constant region of RRV-12 was not available at the time of this study.

The protein structures of E1, E2, E3 and Fab were fit to the density maps sequentially using Chimera (Pettersen et al., 2004) and EMfit (Rossmann et al., 2001). Based upon the domain structures defined for the CHIKV E1/E2 dimer crystal structure (Voss et al., 2010), E1 was fit as a three-domain structure: domains I, II, and III, and E2 was fit as a four-domain structure using domains A, B, C and β-ribbon. Fab CHK-265 was fit as a four-domain structure using heavy chain constant and variable domains, and light chain constant and variable domains. Fitting was performed assuming icosahedral symmetry for a *T=4* virus particle. Goodness of fit of each domain of each protein was analyzed by average density heights, sumf, at each T number 1-4 and average sumf value for all T numbers. Each fitting produced a difference map and coordinates of the protein structure's position relative to the density. The backbone of CHIKV E3 structure was positioned in the CHIKV RRV-12 bound density map using a backbone E2-E3 structure from PDB 6NK7 aligned to the EMfit CHIKV E2 structure with Chimera and Coot. The RMSD, calculated in PYMOL, of the E2 region of the E2-E3 structure aligned to the CHIKV density map is 1.6Å^3. Using the fitted coordinates of the Fab and E2 relative to one another for RRV and MAYV and E2 and E3 for CHIKV, residues of E2 for RRV and MAYV and residues of E2 and E3 for CHIKV located 6Å or less from the Fab structure were identified with PyMOL. The residues in this region of the E2 B domain were mapped to the

surface of each of the three viruses with RIVEM (Xiao and Rossmann, 2007) and predicted to be the epitope.

The position of Mxra8 was mapped to the RRV-12 bound structures of RRV, MAYV, and CHIKV based upon its position in the asymmetric unit in PDB 6NK7 and EMDB 9395 (Basore et al., 2019). A combined E2, E3, and Mxra8 model was extracted from the asymmetric unit of the CHIKV virus structure bound with Mxra8. The combined structure was converted to backbone atoms only with PyMOL. The position of Mxra8 from that virus structure was mapped to the asymmetric unit of RRV-12 bound viruses RRV and MAYV relative to CHIKV with Chimera, PyMOL, and COOT. An asymmetric unit of each virus with both Mxra8 and RRV-12 bound was generated and used as the template for determining and mapping the residues of the virus surface within 6Å of either the Fab or Mxra8 with RIVEM.

ELISA-based Mxra8–Fc competition-binding assay

RRV-12 (2 µg/mL) was diluted in PBS and immobilized onto a 384-well ELISA plate before incubation for 1 h at 37°C. The plate was washed four times with PBS containing Tween (PBST) using an EL406 combination washer dispenser instrument (BioTek) and blocked for 1 h at room temperature with 5% milk powder and 2% goat serum, diluted in PBS. RRV, MAYV, or CHIKV were diluted to approximately 10^7 FFU/mL in PBS and 25 µL per well was added for 1 h at room temperature. After washing five times with PBST, RRV mAbs were diluted to 20 µg/mL in PBS and 25 µL of mAb was added to each well, except for control wells where just PBS was added. Blocking mAbs were incubated for 30 min at room temperature and 25 µL of Mxra8-Fc (mouse Fc region) (Zhang et al., 2018) fusion protein at a concentration of 10 µg/mL was then added to each well. After incubation at room temperature for an hour, the plate was washed four times with PBST and 25 µL per well of a goat anti-mouse HRP-conjugated anti-mouse Fc secondary antibody (SeraCare) was added at a 1:2,000 dilution. After five washes with PBST, plates were developed with TMB Substrate (ThermoFisher Scientific) and the reaction was

stopped with H_2SO_4. Absorbance was read at 450 nm with a Biotek plate reader. A similarly prepared human mAb specific for Zika virus (ZIKV-117 (Sapparapu et al., 2016) was included as a negative control antibody. Titration curves for antibody blockage of Mxra8 were generated similarly.

Mouse studies

Survival studies. Four-week-old male WT C57BL/6J mice were treated with 0.2 mg of MAR1-5A3 (anti-Ifnar1 antibody) prior to inoculation with 10^3 FFU of WT RRV T48 strain in the footpad. The following day, 100 µg of RRV antibody or an isotype control antibody to an unrelated viral target was administered to mice by intraperitoneal injection. Mice were observed over the course of 21 days for survival and moribund mice were euthanized.

Virological studies. Four-week-old male WT C57BL/6J mice were inoculated with 10^3 FFU of RRV strain T48 or MAYV strain BeH407 and then 24 hours post-infection were given 100 µg antibody by intraperitoneal injection. Three days post-infection, the ipsilateral and contralateral gastrocnemius and quadriceps muscles, and ankle tissues were collected as well as the spleen following extensive perfusion with PBS. RNA was isolated from tissues using the RNeasy mini kit (Qiagen). Viral RNA was quantified by qRT-PCR using the TaqMan RNA to C_T one-step kit (Applied Biosystems) with RRV nsp3 specific primers (Forward: 5′- GTG TTC TCC GGA GGT AAA GAT AG -3′, Reverse: 5′- TCG CGG CAA TAG ATG ACT AC -3′) and probe (5′- /56-FAM/ACC TGT TTA/ZEN/CCG CAA TGG ACA CCA/ 3IABkFQ/ -3′) or MAYV specific primers and probe (Earnest et al., 2019) and compared to RNA isolated from viral stocks as a standard curve to determine FFU equivalents.

Clinical scoring studies. Three-week-old male and female WT C57BL/6J mice were inoculated with 10^3 FFU of RRV strain T48 and then 24 hpi were given 100 µg antibody by intraperitoneal injection. Mice were weighed and assigned a clinical score based on grip

strength, gait, and righting reflex, as previously described (Haist et al., 2017). Mice were scored blinded and as follows: 0, no disease; 1, mild defect in ipsilateral hind paw gripping; 2, mild defect in bilateral hind paw gripping; 3, bilateral loss in hind paw gripping; 4, bilateral loss in hind paw gripping with moderate hind limb weakness, observable mild altered gait, and difficulty or failure to right self; 5, bilateral loss in hind paw gripping with severe hind limb weakness, moderate altered gait, and loss of righting reflex; 6, bilateral loss in hind paw gripping with severe hind limb weakness, severely altered gait with possible dragging hind paw, and loss of righting reflex; 7, moribund. No mice received a score of 7 throughout the course of the experiment. Eighteen days post-infection, the spleen, ipsilateral and contralateral gastrocnemius, quadriceps, and ankle tissues were collected following extensive perfusion with PBS. Viral RNA was quantified as described above.

Quantification and statistical analyses

Statistical analyses are described in the figure legends. All analyses were performed using Prism software (GraphPad Software). For quantification of viral RNA in RRV and MAYV WT mouse models, statistical analysis was performed using a one-way ANOVA with a Dunnett's post-test comparing each group to the isotype control (**$p < 0.01$, ***$p < 0.001$, ****$p < 0.0001$). Two independent experiments were performed, with ten mice per antibody for each group. For clinical disease studies in mice, two independent experiments were performed, with a total of n=7-8 mice in each antibody group. Statistical analysis was performed using a student's t-test of area under the curve analysis (****$p < 0.0001$) for clinical disease scoring, and a Mann Whitney test (*$p < 0.05$, **$p < 0.01$, ***$p < 0.001$) for analysis of viral RNA. For the lethal challenge immunocompromised RRV mouse model, two independent experiments were performed, with n=10 mice per antibody for each group, and statistical analysis was performed using a log rank test with Bonferroni correction, $p = 0.0057$.

For mechanistic assays determining reduction in foci number and size due to RRV-12, three independent experiments were performed with triplicate samples in each experiment. A one-way ANOVA with Kruskal-Wallis post-test was used for statistical analysis, with mean ± S.D. compared to a ZIKV-117 control (*$p < 0.05$, **$p < 0.01$, ***$p < 0.001$, ****$p < 0.0001$).

CHAPTER IV

HUMAN ANTIBODY RESPONSE TO MAYARO VIRUS

Introduction

Mayaro is an emerging arbovirus, and has been called a neglected threat with potential to cause a worldwide epidemic, as was seen for chikungunya (Levi and Vignuzzi, 2019). It is thus important to better understand mechanisms of protective immunity, including main antigenic sites targeted by neutralizing antibodies. While several studies have generated broadly neutralizing human and mouse alphavirus mAbs, including the work of Fox et al. as well as the work I describe in chapter III, no studies to date have produced and characterized MAYV-specific human mAbs. Previously, in the context of serology studies, polyclonal MAYV antibodies were found to target both the E1 and E2 proteins (Smith et al., 2018). Additionally, mouse mAbs were found to potently block infection at post-attachment steps, including preventing viral fusion with the endosome and egress from the cell. These mAbs primarily bound to regions of the E2 B domain, with a small fraction targeting the E1 protein (Earnest et al., 2019).

In this chapter, I describe a panel of human mAbs isolated from an individual who was naturally infected with MAYV. These mAbs neutralize MAYV infectivity in cell culture, and some compete with mouse mAbs in a competition ELISA, revealing the presence of distinct antigenic sites, including a possible new one. Although additional work is necessary to further understand mechanism of neutralization, in preliminary experiments these mAbs blocked binding of MAYV to the Mxra8 receptor.

Generation of MAYV-specific mAbs and characterization of binding and neutralization

I generated neutralizing mAbs against MAYV from a blood sample collected from a 67-year old male donor who had recently acquired a MAYV infection. I first transformed B cells with Epstein-Barr virus (EBV) before directly coating ELISA plates with MAYV virus and screening supernatant from the transformed B cells for reactivity against virus. In total, I isolated 11 antibodies that are MAYV-specific and do not cross-react with other alphaviruses. All mAbs bound virus in ELISA, but only five recognized MAYV E2 protein in addition to virus (**Table 5, Figure 27**). Six mAbs were potent neutralizers with IC_{50} values < 100 ng/mL, while five were not as potent with IC_{50} values > 1,000 ng/mL. All mAbs were of isotype IgG1, except for MAYV-125, which was IgG3 (**Table 5**).

Table 5. Half maximal binding and neutralization values for MAYV mAbs. Both recombinant E2 protein and virus were used for determination of EC¬50 values via ELISA, while an FRNT was performed for determination of the IC50 neutralization values.

			Neutralization (ng/mL)	Binding (ng/mL)	
mAb	Isotype	Light Chain	IC_{50}	virus EC_{50}	protein EC_{50}
MAYV-114	IgG1	K	3	5	>
MAYV-141	IgG1	K	10	23	>
MAYV-164	IgG1	λ	12	21	>
MAYV-138	IgG1	K	24	30	>
MAYV-128	IgG1	K	28	20	186
MAYV-111	IgG1	K	48	8	44
MAYV-116	IgG1	K	1,711	9	8
MAYV-139	IgG1	λ	1,973	25	>
MAYV-161	IgG1	K	2,302	30	>
MAYV-171	IgG1	λ	5,721	19	8,086
MAYV-125	IgG3	K	6,280	722	525

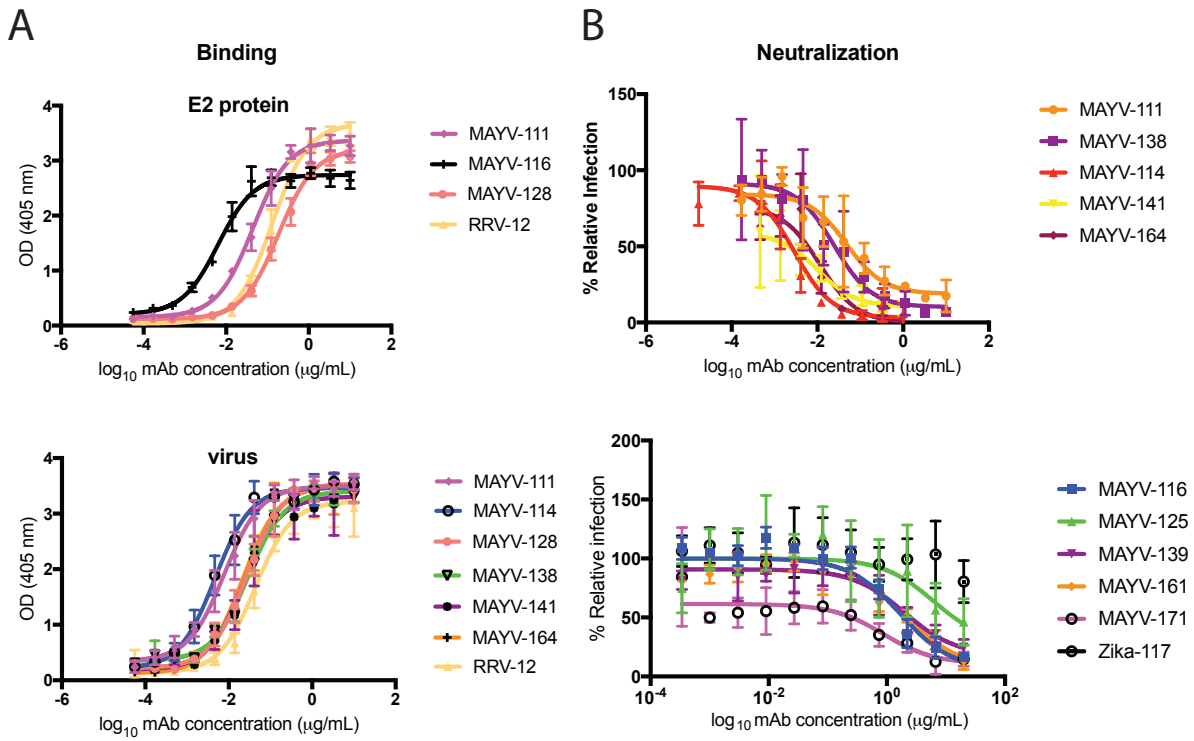

Figure 27. Binding and neutralization of MAYV mAbs. (**A**) ELISA binding curves of mAbs to both MAYV E2 protein and virus. (**B**) Neutralization profiles of mAbs, as determined by focus reduction neutralization test. Potently neutraling mAbs are shown in the top graph, while weaker neutralizers are shown in the lower graph.

Determination of main antigenic sites via competition ELISA

In order to determine binding epitopes for these MAYV mAbs, I performed a competition virus ELISA, using mouse MAYV mAbs with known binding sites as controls. MAbs were biotinylated and ELISA plates were coated with virus, before addition first of an unlabeled mAb and subsequently, the biotinylated mAb. If the first mAb competes with the second mAb for the same binding site, a reduction in signal will be seen as compared to signal observed for labeled antibody alone. I found that these mAbs binned into roughly five competition groups, two of which included mouse mAbs with known epitopes (**Figure 28**). MAYV-111 competed with three

mouse mAbs that target the B domain: MAY-130, MAY-147, MAY-125, while MAYV-139, MAYV-161, MAYV-164, and MAYV-171 competed with MAY-131, which most likely targets the E1 protein (Earnest et al., 2019). MAY-53 overlapped slightly with the B domain competition group, but was designated as a separate group due to its recognition of the A domain of E2 (Earnest et al., unpublished data), along with MAYV-64, which showed asymmetric binding. Human mAbs MAYV-114 and MAYV-141 may target a new site on the virus, since their binding profile was distinct.

mAb	MAYV-111	MAY-130	MAY-147	MAY-125	MAY-53	MAY-131	MAYV-139	MAYV-161	MAYV-164	MAYV-171	MAYV-114	MAYV-141	MAY-64
MAYV-111	7	6	9	31	56	29	21	45	22	27	66	7	20
MAY-130	16	1	-4	-2	18	110	51	108	110	83	106	50	6
MAY-147	99	52	5	17	46	117	53	61	97	68	127	47	30
MAY-125	55	45	16	26	18	144	79	57	40	60	71	43	14
MAY-53	93	89	112	75	-4	162	74	115	101	107	119	55	5
MAY-131	74	94	101	73	24	12	28	4	28	29	76	50	-13
MAYV-139	98	127	82	72	232	10	19	29	25	45	55	76	21
MAYV-161	85	99	88	59	72	3	28	-3	4	42	73	49	33
MAYV-164	86	121	61	41	89	3	29	0	35	29	35	52	32
MAYV-171	83	106	93	79	74	5	5	10	5	1	24	35	39
MAYV-114	63	71	27	54	80	38	2	-6	18	5	4	14	14
MAYV-141	11	25	7	5	71	38	2	-4	0	10	12	5	21
MAY-64	101	105	106	86	37	155	81	110	122	97	112	65	-4

Figure 28. **Competition ELISA for MAYV mAbs.** MAYV mAbs bin into roughly five groups, as determined via virus competition ELISA. Mouse mAbs previously mapped by (Earnest et al., 2019) are highlighted in yellow. Un-labeled mAb was first added at a saturating concentration of 100 µg/mL for 1 h at room temperature. Biotinylated mAb was then added without a wash step at a concentration of 50 µg/mL. After 1 h, antibody was washed out and anti-biotin HRP-conjugated secondary was added. Plates were developed with TMB substrate and absorbance was read at 450 nm. Background was subtracted and percent competition was determined with the formula: (average binding value – background)/ (labeled mAb alone) x 100. Black boxes indicate 0-35% binding (strong competition) of second mAb in the presence of the first, gray boxes indicate 35-65% binding (intermediate competition), and white boxes indicate > 65% binding (low competition).

Determination of Mxra8 receptor blocking

To gain insight into mAb mechanism of inhibition, I next performed a Mxra8 competition ELISA, as has been described in previous chapters, in which ELISA plates were coated with MAYV before addition of mAbs and a purified recombinant mouse Mxra8-Fc fusion protein. Seven mAbs blocked attachment of virus to recombinant receptor and not all of these mAbs were potent neutralizers (**Figure 29**). Specifically, MAYV-139, MAYV-161, and MAYV-171 all were potent Mxra8 blockers, but had IC_{50} values greater than 1,000 ng/mL, perhaps indicating the presence of multiple viral receptors or additional means of inhibition for the most potently neutralizing mAbs.

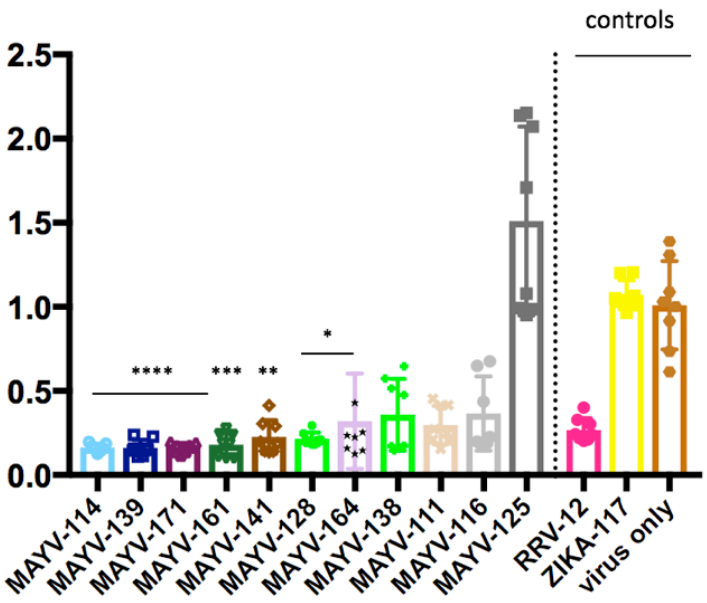

Figure 29. MAYV mAbs inhibit binding of virus to Mxra8-Fc fusion protein via competition ELISA. MAYV was captured on the plate with a human mAb before addition of MAYV mAbs followed by Mxra8-mFc (mouse Fc). A loss of signal indicates competition of RRV mAbs with Mxra8-mFc for binding to virus. Two independent experiments were performed in quadruplicate (Kruskal-Wallis one-way ANOVA with Kruskal-Wallis post-test, with mean ± S.D. compared to isotype control (*p < 0.05, **p < 0.01, ***p < 0.001, ****p < 0.0001).

Discussion

Here, I describe the first human mAbs generated against MAYV virus. Unlike my panel of RRV-specific mAbs, these mAbs bound to both and virus and protein, although increased neutralization potency seemed to correlate with poor recombinant protein recognition in ELISA. Two of the most potent neutralizing mAbs belonged to the same competition group, which did not include any of the previously mapped mouse mAbs (Earnest et al., 2019). Only one mAb, MAYV-111, competed with E2 B domain mouse mAbs, suggesting that perhaps this site is not a main target during human infection. Instead, most mAbs competed with mouse mAb MAY-131, which is suspected to recognize E1 instead of E2. While further study is necessary to verify E1 recognition of these human mAbs, this result could support the finding of Earnest et al. that E1 is a target of neutralizing antibodies, since one human mAb in this competition group, MAYV-164, neutralizes infection well *in vitro*. Additionally, my results indicate that Mxra8 blockage is a means of inhibition for MAYV mAbs, though likely not the only mechanism. Future studies will utilize a luciferase reporter MAYV to probe further into mechanism of inhibition, including experiments testing for fusion inhibition and antibody inhibition of virus release from the cell.

Materials and methods

MAb isolation, MAYV ELISA screen, FRNT, and ELISA-based Mxra8–Fc competition binding assay were performed as described in Chapters II and III.

Competition ELISA

Antibodies were first biotinylated in 96-well plate format using EZ-Link NHS-PEG_4-Biotin Kit (ThermoFisher Scientific, #21329) and Zeba Desalting Plates, 7kDa cutoff (ThermoFisher Scientific, #89808). 384-well ELISA plates were directly coated with MAYV at a concentration of

~ 1 x 10^5 FFU/mL. Plates were incubated for 1 h at 37°C, and blocked for 1 h in 5% milk powder and 2% goat serum, diluted in PBS. Un-labeled mAb was first added at a saturating concentration of 100 µg/mL for 1 h at room temperature. Un-labeled mAb was left in, and biotinylated mAb was then added at a concentration of 50 µg/mL. After 1 h, antibody was then washed out with PBST and an anti-biotin HRP-conjugated secondary antibody was added. After additional washes in PBST, TMB Substrate (ThermoFisher Scientific), plates were developed with TMB Substrate (ThermoFisher Scientific), the reaction was stopped with H_2SO_4, and absorbance was read at 450 nm with a Biotek plate reader. During data analysis, background on the ELISA plate was subtracted, and the following formula was used to calculate percent competition: (average binding value – background)/ (labeled mAb alone) x 100. Triplicates for each sample were used.

CHAPTER V

SUMMARY AND FUTURE DIRECTIONS

Thesis summary

Alphaviruses are a large group of mosquito-transmitted viruses that cause disease globally. In addition to acute symptoms of rash and fever, Old World alphaviruses cause severe musculoskeletal disease with arthralgia persisting from months to years, and there is no current vaccine or effective treatment available. Antibody therapies have shown promise for both preventing and treating disease caused by CHIKV in studies using mouse and primate models of infection. Most of these antibodies bind to surface-exposed regions of the E2 protein on the glycoprotein spike, and block infection by inhibiting multiple steps in the viral replication cycle. However, little is known about the human antibody response to other arthritogenic alphaviruses, including RRV, MAYV, and ONNV. Additionally, knowledge of conserved epitopes in the human antibody response against alphaviruses is lacking, and only one study has provided such information for mouse antibodies.

I first focused on generating a panel of antibodies from two RRV-immune donors. My goal was to determine the epitopes for these mAbs and to understand mechanism of neutralization, since no other human mAbs against RRV exist and only limited characterization work has been performed for a few mouse mAbs. I also wanted to test these mAb *in vivo* to determine if *in vitro* neutralization potency correlated with protection from clinical disease in mice. I generated 21 neutralizing mAbs against RRV, and found that these mAbs targeted epitopes within the A and B domains of the E2 protein. In addition, these mAbs blocked binding to newly discovered receptor Mxra8, but also blocked at post-attachment steps, including fusion. In a mouse model of RRV infection, two mAbs, one that completely neutralized virus *in vitro* and one that left a 35% fraction of un-neutralized virus, protected immunodeficient mice from lethal virus infection,

and significantly reduced viral RNA burden, clinical symptoms, and weight loss in an immunocompetent model. These results show that neutralization *in vitro* correlates with protection, and provide possible RRV-specific therapeutic candidates.

To determine whether alphavirus mAbs could bind in a cross-reactive manner to the E1/E2 glycoprotein, I screened both the mAb panel I isolated from RRV-immune donors, as well as mAbs isolated from a CHIKV-immune donor, for binding and neutralization against six arthritogenic alphaviruses. I found that six mAbs were cross-reactive, but only two neutralized all viruses in a focus reduction neutralization test. In addition, these mAbs competed for the same antigenic site in an Octet competition assay, and two inhibited binding of MAYV, RRV, and CHIKV to Mxra8.

We then chose to perform further structural studies on one of these mAbs, RRV-12, to determine the binding footprint on the glycoprotein. Three cyro-EM structures of RRV-12 in complex with MAYV, RRV, and CHIKV revealed a binding site within a conserved region of the E2 B domain, and binding did not appear to cross-link viral spikes. Furthermore, I performed mechanistic tests that revealed that this antibody did not inhibit fusion, but did reduce viral entry and cell-to-cell spread. To further understand whether this mAb may possibly be a therapeutic candidate, we tested it in both MAYV and RRV mouse models of infection, and found that viral RNA was reduced in multiple tissues after therapeutic administration. In addition, in the RRV model, clinical symptoms were greatly reduced. Knowledge of a human broadly neutralizing mAb epitope will advance rational vaccine design and provide a potential therapeutic candidate against multiple alphaviruses.

In Chapter IV, I describe 11 neutralizing mAbs generated from a donor infected with MAYV virus. Although additional characterization work remains to be performed, I used a competition virus ELISA to determine that these mAbs targeted three distinct antigenic regions on the glycoprotein, one of which did not compete with current mouse mAbs. Some of these mAbs

bound recombinant protein in addition to virus, although the more potently neutralizing ones did not bind to protein. In addition, six mAbs significantly reduced attachment of MAYV to Mxra8.

Collectively, the findings I present in this thesis advance our understanding of the human antibody response against alphaviruses, and provide insight into epitopes, mechanisms of neutralization, and *in vitro* predictors of protection in animal models. This knowledge could contribute to the design of immunogens eliciting broad-spectrum antibody responses and may advance mAb candidates for therapeutic consideration. In addition, this work sheds light on targets of the immune response for emerging viruses with pandemic potential.

Future directions

Use of HDX to investigate incomplete neutralization and mAb epitopes

In chapters II and III, I discussed a common phenotype seen in the focus reduction neutralization tests, where antibodies failed to completely neutralize virus, and instead left a 10-50% “resistant” fraction. However, when I tested RRV-12 neutralization potency against an RRV with a double mutation engineered at sites 82 and 86 within the A domain of the E2 protein (Silva et al., 2014), I found that nearly all of this resistant fraction disappeared (**Figure 30A**). I hypothesize that this complete neutralization phenotype may be due to increased stability of the viral particle caused by introduction of positively-charged residues within the center of the trimer (**Figure 30B)**. These mutations may stabilize the B domain, which shields the fusion loop protein on E1, therefore resulting in increased potency of neutralization for some B domain antibodies. However, further work is needed to better understand the mechanism by which this occurs.

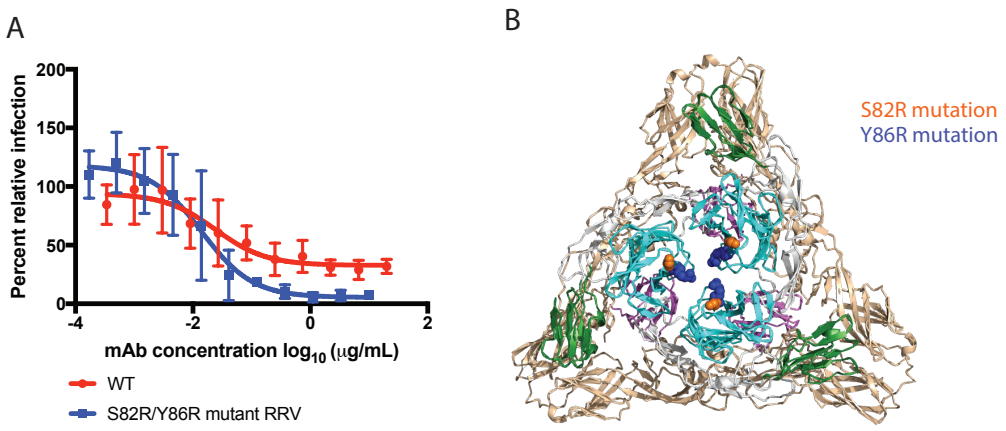

Figure 30. **RRV-12 reduces resistant fraction of virus for RRV with a double mutation in the A domain of the E2 glycoprotein**. (**A**) An FRNT was performed to test neutralization of S82/Y86 mutant virus or WT virus by mAb RRV-12. (**B**) Location of S82R/Y86R mutation within the A domain of the E2 protein mapped to chikungunya virus E1/E2 trimer of heterodimers (PDB 3n42). The A domain of E2 is indicated in cyan, the B domain in green, and the C domain in magenta. The S82R mutation is indicated in orange, and the Y86R mutation in dark blue.

One method that could be used to probe the mechanism of this phenomenon is hydrogen-deuterium exchange (HDX). HDX can be used to measure dynamic movement of viral particles under a variety of conditions, including changes in viral proteins due to temperature or binding of antibodies (Lim et al., 2017). In particular, the glycoprotein of a number of viruses, including HIV, Ebola, hepatitis C, and influenza, has been examined with HDX to determine conformational dynamics that occur during recognition by antibodies and small molecule inhibitors (Bale et al., 2011; Guttman and Lee, 2016; Guttman et al., 2015; Khan et al., 2014; Kim et al., 2011). This technique involves incubation of a protein in buffer containing deuterium, which results in the exchange of any amide protons with deuterium. Use of an acid protease stops the exchange, and digests the proteins into peptides that can then be analyzed using mass spectrometry to determine mass shifts due to deuterium labeling (**Figure 31**). To understand why RRV-12 is better neutralized by the mutant RRV virus, we could compare

mutant virus bound to antibody with WT virus bound to antibody, focusing especially on the B domain and any differences in conformation. While challenges remain for performing HDX with intact virus, recent studies have successfully accomplished analyses of surface envelope proteins on intact enveloped viruses (Bereszczak et al., 2013; Garcia et al., 2015; Lim et al., 2017). One drawback of HDX is lower resolution compared to X-ray crystallography or NMR. However, these other techniques provide only snapshots of proteins in a single conformation, while HDX can provide information on protein dynamics over a time course (Wei et al., 2014).

In addition to revealing structural dynamics of viral proteins, HDX has also been used to determine antibody epitopes (Bangaru et al., 2019; Terral et al., 2017). In Chapter IV, I discussed MAYV antibodies that compete with current mouse mAbs, but for which the specific binding site remains unknown. As a next step, I could use HDX to probe binding footprint. For antibodies such as MAYV-111, MAYV-128, and MAYV-116, that bind to E2 protein, this experiment could be simplified with the use of protein instead of virus.

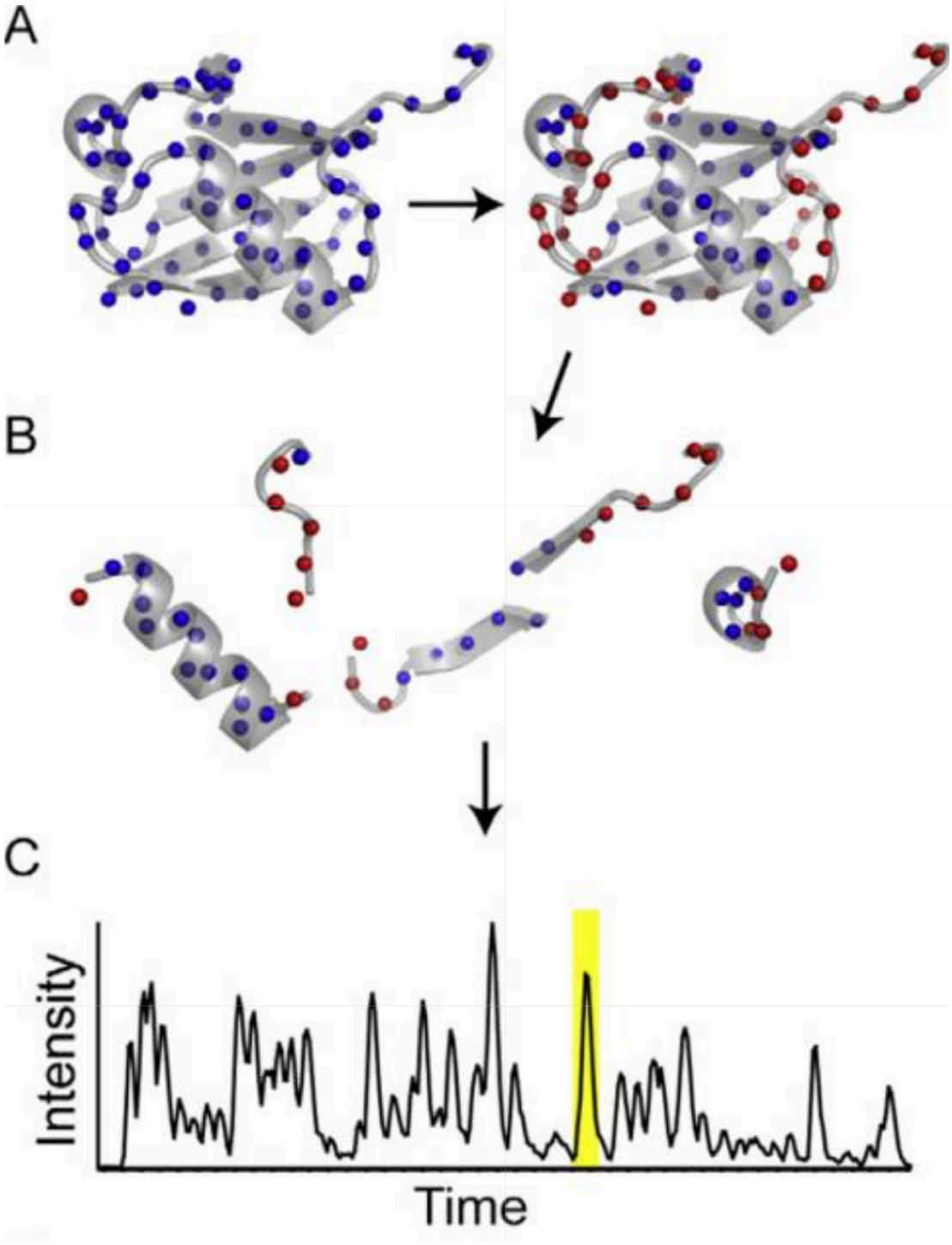

Figure 31. **Overview of HDX-MS. (A)** Protein is first incubated in a buffer containing deuterium to allow for exchange with amide protons. (**B**) The exchange is then slowed and an acid protease used to digest the protein into peptides. (**C**) Mass spectrometry is then performed to determine mass shift resulting from deuterium incorporation. Modified from (Guttman et al., 2016).

Testing MAYV mAbs *in vivo*

When MAYV mAbs were administered to mice in both musculoskeletal disease and lethal disease models, effector functions were found to be crucial for protection (Earnest et al., 2019). Specifically, administration of mouse mAbs engineered to have a N297Q heavy-chain N-linked glycosylation mutation in the constant region, known to abrogate binding to both FcγR receptors and C1q of complement, resulted in mouse death, as compared to a non-variant IgG1. Intriguingly, antibodies with similar neutralization profiles and mechanisms of inhibition were found to confer differing degrees of protection *in vivo.* Protection was instead better predicted by mAb binding avidity to infected cells as well as ability to promote Fc effector functions such as phagocytosis *in vitro* (Earnest et al., 2019). Based on these results, it would be interesting to investigate whether my human MAYV mAbs have similar patterns of protection *in vivo.* To accomplish this, I would first test binding of mAbs to MAYV-infected cells via flow cytometry, and would then select the best binders for testing *in vivo*. I would include both non-variant IgG1 and N297Q variants, and both antibody forms would be administered to immunodeficient mice (lethal challenge model) and WT mice (musculoskeletal model) therapeutically one day post-infection. If a difference in protection is observed between the aglycosyl variant and the non-variant, these results could further be confirmed by testing IgG1 mAbs in γ-chain–deficient (FcRγ−/−) mice, with the hypothesis that protection would be worse in mice lacking activating FcγRs than in WT mice.

Determining mechanism of cell-to-cell inhibition for RRV-12

In Chapter III, I discussed a phenotype for RRV-12, where foci size is significantly reduced in the FRNT. I speculated that this could be due to a number of mechanisms, including antibody blockage of viral release from the cell, a decrease in infectivity of viral particles, or prevention of cell-to-cell spread of virus along intercellular extensions. Visualization of virus budding through transmission electron microscopy (TEM) with gold labeling could shed light on

mechanism of mAb inhibition. To do this, Vero cells would be infected with an alphavirus (RRV, CHIKV, MAYV, ONNV, SAGV, or GETV) and then treated with RRV-12 IgG, an isotype control IgG, or mouse mAb CHK-265, known to inhibit alphaviral egress. The antibodies would all be labeled with gold particles to enable localization during virus budding. For visualization with TEM, ultra-thin sections would be cut and collected on a grid before staining with a metal stain. The resulting images will reveal if antibodies tether viral particles to the cell, or alternatively, if defects in particle assembly prevent budding from occurring.

Implications for rational vaccine design

Knowledge of the epitope of broadly neutralizing mAb RRV-12 has potential to aid in the development of an alphavirus vaccine that would elicit high titers of broadly neutralizing mAbs. Such structure-based approaches have previously been employed in vaccine design for HIV, influenza, RSV, and HCV (Correia et al., 2011; 2014; Fleishman et al., 2011; He et al., 2015; McLellan et al., 2011; Ofek et al., 2010; Zhou et al., 2014). This approach involves grafting the epitope targeted by the mAb onto a protein scaffold backbone that is specifically designed to accommodate the epitope, chosen with aid from computer algorithms that search large databases (He et al., 2015). For example, a scaffold-based design approach was used to engineer antigens that resemble the linear epitopes recognized by two broadly neutralizing HIV mAbs (Correia et al., 2011). More recently, this rational design strategy was applied in the development of an HCV vaccine, and yielded promising results in preclinical studies (He et al., 2015). Several properties of ferritin, including its self-assembly into nanoparticles, thermal and chemical stability, and three-fold axis symmetry with eight units, make it an ideal scaffold choice for epitope presentation (López-Sagaseta et al., 2016). While a traditional inactivated or live-attenuated vaccine passaged in cell culture typically elicits a polyclonal response, or a mixture of neutralizing and non-neutralizing antibodies that bind to a variety of epitopes covering the viral surface, a rationally designed vaccine composed of a carefully selected epitope attached to

a protein scaffold is likely to elicit high titers of mAbs specific to one antigenic site. Such an approach would be ideal for focusing the immune response on producing broadly protective antibodies. Though challenges remain for implementation of this strategy, including the transplantation and stabilization of epitopes that may be discontinuous (Kulp and Schief, 2013), it is a promising option in the search for a universal alphavirus vaccine.

Need for better animal models

Currently, three main models exist for evaluation of arthritogenic alphavirus disease in mice: a lethal neonatal challenge model, an immunocompromised lethal disease (*Ifnαr*−/−) model, and an arthritis model (Haese et al., 2016). In addition, rhesus macaque models that mimic clinical disease in humans have been employed, where macaques show signs of fever, joint swelling in the wrist and ankle, and rash (Broeckel et al., 2017; Pal et al., 2013; 2014). While these models have offered insight into viral pathogenesis while providing a way to select potential therapeutic candidates for further evaluation, several limitations remain to be addressed. For humans, the viremic period typically extends from day 4 to day 12 after onset of symptoms; however, the viremic phase is shorter in mice and macaques, with peak viral titers lasting from approximately day 2 to day 6 after infection (Labadie et al., 2010; Morrison et al., 2011). Thus far, antibodies have been given therapeutically in animals during this short viremic window. However, a future challenge that must be addressed before clinical use of anti-alphavirus mAbs is time of administration. Although the antibodies I presented in the preceding chapters were effective during the period of peak viremia, administration of mAbs to patients within this time window would necessitate more rapid diagnostic procedures, such as virus identification through qRT-PCR, instead of the current predominant diagnostic method of paired serology testing (Farmer and Suhrbier, 2019). It is not clear whether mAbs would retain efficacy beyond this narrow treatment window in order to reduce inflammation and swelling of joints that may persist for weeks after infection. While viral RNA has been detected in joint tissues of

C57BL/6 mice up to 16 weeks post-infection, infectious virus has not been isolated at time points beyond 7-10 days post-infection, and mice recover hindpaw gripping function at around 17 days post-infection (Hawman et al., 2013). We therefore need animal models that better reproduce the chronic symptoms of arthritis present in humans so that efficacy of administering mAbs post-viremia can be evaluated.

Study of non-neutralizing mAbs

While neutralizing mAbs were traditionally thought to be the "gold-standard" for conferring protection *in vivo*, studies have increasingly shown that non-neutralizing antibodies also have important properties that contribute to protection. For instance, non-neutralizing mAbs have been reported to confer protection for influenza, HIV, and Ebola, in part through activation of effector functions such as ADCC and ADCP (Henry Dunand et al., 2016; Lewis et al., 2015; Zeitlin et al., 2011). Because of this, it is no longer advantageous to bias screening strategies to select only for potently neutralizing mAbs. In the screening strategies that I present in Chapters II-IV, I may have unintentionally biased the screen to select for neutralizing mAbs, since I identified very few non-neutralizing mAbs. I suspect this result may have occurred due to screening solely with live virus in the ELISA assay, since coating ELISA plates with virus presents conformational epitopes that are perhaps more likely to be targeted by a select set of neutralizing mAbs. Interestingly, most of the mAbs I generated, with the exception of less potently neutralizing MAYV mAbs, do not bind to recombinant protein. Therefore, I hypothesize that I might have generated a much larger panel of non-neutralizing mAbs had I screened with recombinant protein in addition to virus. A further direction for this work would be to carry out the ELISA screen of hybridoma supernatants using both virus and protein, and to compare the mAbs generated from each screening strategy to determine if one strategy favors either category of mAb. Any non-neutralizing mAbs generated could then be analyzed for effector functions, and the resulting data could be used to select a subset for *in vivo* protection studies.

REFERENCES

Aaskov, J.G., Mataika, J.U., Lawrence, G.W., Rabukawaqa, V., Tucker, M.M., Miles, J.A., and Dalglish, D.A. (1981). An epidemic of Ross River virus infection in Fiji, 1979. Am J Trop Med Hyg *30*, 1053–1059.

Aaskov, J., Williams, L., and Yu, S. (1997). A candidate Ross River virus vaccine: preclinical evaluation. Vaccine *15*, 1396–1404.

Abu Bakar, F., and Ng, L.F.P. (2018). Nonstructural proteins of alphavirus-potential targets for drug development. Viruses *10*, 71.

Ackerman, M.E., Mikhailova, A., Brown, E.P., Dowell, K.G., Walker, B.D., Bailey-Kellogg, C., Suscovich, T.J., and Alter, G. (2016). Polyfunctional HIV-Specific Antibody responses are associated with spontaneous HIV control. PLoS Pathogens *12*, e1005315.

Acosta-Ampudia, Y., Monsalve, D.M., Rodríguez, Y., Pacheco, Y., Anaya, J.-M., and Ramírez-Santana, C. (2018). Mayaro: an emerging viral threat? Emerg Microbes Infect *7*, 163–11.

Aguilar, P.V., Estrada-Franco, J.G., Navarro-Lopez, R., Ferro, C., Haddow, A.D., and Weaver, S.C. (2011). Endemic Venezuelan equine encephalitis in the Americas: hidden under the dengue umbrella. Future Virol *6*, 721–740.

Aichinger, G., Ehrlich, H.J., Aaskov, J.G., Fritsch, S., Thomasser, C., Draxler, W., Wolzt, M., Müller, M., Pinl, F., Van Damme, P., et al. (2011). Safety and immunogenicity of an inactivated whole virus Vero cell-derived Ross River virus vaccine: a randomized trial. Vaccine *29*, 9376–9384.

Akahata, W., Yang, Z.-Y., Andersen, H., Sun, S., Holdaway, H.A., Kong, W.-P., Lewis, M.G., Higgs, S., Rossmann, M.G., Rao, S., et al. (2010). A virus-like particle vaccine for epidemic Chikungunya virus protects nonhuman primates against infection. Nat Med *16*, 334–338.

Akhrymuk, I., Frolov, I., and Frolova, E.I. (2016). Both RIG-I and MDA5 detect alphavirus replication in concentration-dependent mode. Virology *487*, 230–241.

Arduin, E., Arora, S., Bamert, P.R., Kuiper, T., Popp, S., Geisse, S., Grau, R., Calzascia, T., Zenke, G., and Kovarik, J. (2015). Highly reduced binding to high and low affinity mouse Fc gamma receptors by L234A/L235A and N297A Fc mutations engineered into mouse IgG2a. Mol Immunol *63*, 456–463.

Arias-Goeta, C., Mousson, L., Rougeon, F., and Failloux, A.-B. (2013). Dissemination and transmission of the E1-226V variant of chikungunya virus in Aedes albopictus are controlled at the midgut barrier level. PLoS One *8*, e57548.

Assunção-Miranda, I., Bozza, M.T., and Da Poian, A.T. (2010). Pro-inflammatory response resulting from sindbis virus infection of human macrophages: implications for the pathogenesis of viral arthritis. J Med Virol *82*, 164–174.

Assunção-Miranda, I., Cruz-Oliveira, C., and Da Poian, A.T. (2013). Molecular mechanisms involved in the pathogenesis of alphavirus-induced arthritis. Biomed Res Int *2013*, 973516–11.

Bahl, K., Senn, J.J., Yuzhakov, O., Bulychev, A., Brito, L.A., Hassett, K.J., Laska, M.E., Smith, M., Almarsson, Ö., Thompson, J., et al. (2017). Preclinical and clinical demonstration of immunogenicity by mRNA vaccines against H10N8 and H7N9 influenza viruses. Mol Ther *25*, 1316–1327.

Bale, S., Liu, T., Li, S., Wang, Y., Abelson, D., Fusco, M., Woods, V.L., and Saphire, E.O. (2011). Ebola virus glycoprotein needs an additional trigger, beyond proteolytic priming for membrane fusion. PLoS Neglect Trop D *5*, e1395.

Bangaru, S., Lang, S., Schotsaert, M., Vanderven, H.A., Zhu, X., Kose, N., Bombardi, R., Finn, J.A., Kent, S.J., Gilchuk, P., et al. (2019). A site of vulnerability on the influenza virus hemagglutinin head domain trimer interface. Cell *177*, 1136–1152.e18.

Basore, K., Kim, A.S., Nelson, C.A., Zhang, R., Smith, B.K., Uranga, C., Vang, Lo, Cheng, M., Gross, M.L., Smith, J., et al. (2019). Cryo-EM Structure of chikungunya virus in complex with the Mxra8 receptor. Cell *177*, 1725–1737.e16.

Bereszczak, J.Z., Rose, R.J., van Duijn, E., Watts, N.R., Wingfield, P.T., Steven, A.C., and Heck, A.J.R. (2013). Epitope-distal effects accompany the binding of two distinct antibodies to hepatitis B virus capsids. J Am Chem Soc *135*, 6504–6512.

Boere, W.A., Benaissa-Trouw, B.J., Harmsen, T., Erich, T., Kraaijeveld, C.A., and Snippe, H. (1985). Mechanisms of monoclonal antibody-mediated protection against virulent Semliki Forest virus. J Virol *54*, 546–551.

Bond, C.S., and Schüttelkopf, A.W. (2009). ALINE: a WYSIWYG protein-sequence alignment editor for publication-quality alignments. Acta Crystallogr D Biol Crystallogr *65*, 510–512.

Broeckel, R., Fox, J.M., Haese, N., Kreklywich, C.N., Sukulpovi-Petty, S., Legasse, A., Smith, P.P., Denton, M., Corvey, C., Krishnan, S., et al. (2017). Therapeutic administration of a recombinant human monoclonal antibody reduces the severity of chikungunya virus disease in rhesus macaques. PLoS Neglect Trop D *11*, e0005637.

Brown, R.S., Wan, J.J., and Kielian, M. (2018). The alphavirus exit pathway: what we know and what we wish we knew. Viruses *10*, 89.

Brummer-Korvenkontio, M., Vapalahti, O., Kuusisto, P., Saikku, P., Manni, T., Koskela, P., Nygren, T., Brummer-Korvenkontio, H., and Vaheri, A. (2002). Epidemiology of Sindbis virus infections in Finland 1981-96: possible factors explaining a peculiar disease pattern. Epidemiol Infect *129*, 335–345.

Burrack, K.S., Montgomery, S.A., Homann, D., and Morrison, T.E. (2015). CD8+ T cells control Ross River virus infection in musculoskeletal tissues of infected mice. J Immunol *194*, 678–689.

Carpentier, K.S., and Morrison, T.E. (2018). Innate immune control of alphavirus infection. Curr Opin Virol *28*, 53–60.

Chang, L.-J., Dowd, K.A., Mendoza, F.H., Saunders, J.G., Sitar, S., Plummer, S.H., Yamshchikov, G., Sarwar, U.N., Hu, Z., Enama, M.E., et al. (2014). Safety and tolerability of chikungunya virus-like particle vaccine in healthy adults: a phase 1 dose-escalation trial. Lancet *384*, 2046–2052.

Chen, W., Foo, S.-S., Rulli, N.E., Taylor, A., Sheng, K.-C., Herrero, L.J., Herring, B.L., Lidbury, B.A., Li, R.W., Walsh, N.C., et al. (2014). Arthritogenic alphaviral infection perturbs osteoblast function and triggers pathologic bone loss. Proc Natl Acad Sci U S A *111*, 6040–6045.

Cheng, R.H., Kuhn, R.J., Olson, N.H., Rossmann, M.G., Choi, H.K., Smith, T.J., and Baker, T.S. (1995). Nucleocapsid and glycoprotein organization in an enveloped virus. Cell *80*, 621–630.

Chua, C.L., Chan, Y.F., and Sam, I.-C. (2014). Characterisation of mouse monoclonal antibodies targeting linear epitopes on Chikungunya virus E2 glycoprotein. J Virol Methods *195*, 126–133.

Claflin, S.B., and Webb, C.E. (2015). Ross River Virus: Many vectors and unusual hosts make for an unpredictable pathogen. PLoS Pathog *11*, e1005070.

Correia, B.E., Ban, Y.-E.A., Friend, D.J., Ellingson, K., Xu, H., Boni, E., Bradley-Hewitt, T., Bruhn-Johannsen, J.F., Stamatatos, L., Strong, R.K., et al. (2011). Computational protein design using flexible backbone remodeling and resurfacing: case studies in structure-based antigen design. J Mol Biol *405*, 284–297.

Correia, B.E., Bates, J.T., Loomis, R.J., Baneyx, G., Carrico, C., Jardine, J.G., Rupert, P., Correnti, C., Kalyuzhniy, O., Vittal, V., et al. (2014). Proof of principle for epitope-focused vaccine design. Nature *507*, 201–206.

Danillo Lucas Alves, E., and Benedito Antonio Lopes da, F. (2018). Characterization of the immune response following in vitro Mayaro and Chikungunya viruses (Alphavirus, Togaviridae) infection of mononuclear cells. Virus Res *256*, 166–173.

Davies, J.M., Cai, Y.P., Weir, R.C., and Rowley, M.J. (2000). Characterization of epitopes for virus-neutralizing monoclonal antibodies to Ross River virus E2 using phage-displayed random peptide libraries. Virology *275*, 67–76.

Davis, L.E., Beckham, J.D., and Tyler, K.L. (2008). North American encephalitic arboviruses. Neurol Clin *26*, 727–57–ix.

Doherty, R.L., Carley, J.G., and Best, J.C. (1972). Isolation of Ross River virus from man. Med J Aust *1*, 1083–1084.

Duffus, W.A., Levy-Mintz, P., Klimjack, M.R., and Kielian, M. (1995). Mutations in the putative fusion peptide of Semliki Forest virus affect spike protein oligomerization and virus assembly. J Virol *69*, 2471–2479.

Earnest, J.T., Basore, K., Roy, V., Bailey, A.L., Wang, D., Alter, G., Fremont, D.H., and Diamond, M.S. (2019). Neutralizing antibodies against Mayaro virus require Fc effector functions for protective activity. J Exp Med *71*, jem.20190736–jem.20192301.

Edwards, T., Del Carmen Castillo Signor, L., Williams, C., Larcher, C., Espinel, M., Theaker, J., Donis, E., Cuevas, L.E., and Adams, E.R. (2017). Analytical and clinical performance of a Chikungunya qRT-PCR for Central and South America. Diagn Microbiol Infect Dis *89*, 35–39.

Farmer, J.F., and Suhrbier, A. (2019). Interpreting paired serology for Ross River virus and Barmah Forest virus diseases. Aust J Gen Pract *48*, 645–649.

Fields, W., and Kielian, M. (2013). A key interaction between the alphavirus envelope proteins responsible for initial dimer dissociation during fusion. J Virol *87*, 3774–3781.

Firth, A.E., Chung, B.Y., Fleeton, M.N., and Atkins, J.F. (2008). Discovery of frameshifting in Alphavirus 6K resolves a 20-year enigma. Virol J *5*, 108.

Fischer, M., Staples, J.E., Arboviral Diseases Branch, National Center for Emerging and Zoonotic Infectious Diseases, CDC (2014). Notes from the field: chikungunya virus spreads in the Americas - Caribbean and South America, 2013-2014. MMWR Morb. Mortal. Wkly. Rep. *63*, 500–501.

Fleishman, S.J., Whitehead, T.A., Ekiert, D.C., Dreyfus, C., Corn, J.E., Strauch, E.-M., Wilson, I.A., and Baker, D. (2011). Computational design of proteins targeting the conserved stem region of influenza hemagglutinin. Science *332*, 816–821.

Fox, J.M., Long, F., Edeling, M.A., Lin, H., van Duijl-Richter, M.K.S., Fong, R.H., Kahle, K.M., Smit, J.M., Jin, J., Simmons, G., et al. (2015). Broadly neutralizing alphavirus antibodies bind an epitope on E2 and inhibit entry and egress. Cell *163*, 1095–1107.

Fox, J.M., Roy, V., Gunn, B.M., Huang, L., Edeling, M.A., Mack, M., Fremont, D.H., Doranz, B.J., Johnson, S., Alter, G., et al. (2019). Optimal therapeutic activity of monoclonal antibodies against chikungunya virus requires Fc-FcγR interaction on monocytes. Sci Immunol *4*, eaav5062.

Franklin, R.P., Kinde, H., Jay, M.T., Kramer, L.D., Green, E.-G.N., Chiles, R.E., Ostlund, E., Husted, S., Smith, J., and Parker, M.D. (2002). Eastern equine encephalomyelitis virus infection in a horse from California. Emerging Infect Dis *8*, 283–288.

Garcia, N.K., Guttman, M., Ebner, J.L., and Lee, K.K. (2015). Dynamic changes during acid-induced activation of influenza hemagglutinin. Structure *23*, 665–676.

Garmashova, N., Gorchakov, R., Volkova, E., Paessler, S., Frolova, E., and Frolov, I. (2007). The Old World and New World alphaviruses use different virus-specific proteins for induction of transcriptional shutoff. J Virol *81*, 2472–2484.

Gibbons, D.L., Ahn, A., Liao, M., Hammar, L., Cheng, R.H., and Kielian, M. (2004). Multistep regulation of membrane insertion of the fusion peptide of Semliki Forest virus. J Virol *78*, 3312–3318.

Gould, E.A., Buckley, A., Barrett, A.D., and Cammack, N. (1986). Neutralizing (54K) and non-neutralizing (54K and 48K) monoclonal antibodies against structural and non-structural yellow fever virus proteins confer immunity in mice. J Gen Virol *67 (Pt 3)*, 591–595.

Goyal, M., Chauhan, A., Goyal, V., Jaiswal, N., Singh, S., and Singh, M. (2018). Recent development in the strategies projected for chikungunya vaccine in humans. Drug Des Devel Ther *12*, 4195–4206.

Guo, F., and Jiang, W. (2014). Single particle cryo-electron microscopy and 3-D reconstruction of viruses. Methods Mol Bio *1117*, 401–443.

Guttman, M., and Lee, K.K. (2016). Isotope labeling of biomolecules: structural analysis of

viruses by HDX-MS. Meth Enzymol *566*, 405–426.

Guttman, M., Cupo, A., Julien, J.-P., Sanders, R.W., Wilson, I.A., Moore, J.P., and Lee, K.K. (2015). Antibody potency relates to the ability to recognize the closed, pre-fusion form of HIV Env. Nat Commun *6*, 6144.

Haese, N.N., Broeckel, R.M., Hawman, D.W., Heise, M.T., Morrison, T.E., and Streblow, D.N. (2016). Animal models of chikungunya virus infection and disease. J Infect Dis *214*, S482–S487.

Haist, K.C., Burrack, K.S., Davenport, B.J., and Morrison, T.E. (2017). Inflammatory monocytes mediate control of acute alphavirus infection in mice. PLoS Pathog *13*, e1006748.

Harley, D., Sleigh, A., and Ritchie, S. (2001). Ross River virus transmission, infection, and disease: a cross-disciplinary review. Clin Microbiol Rev *14*, 909–32–tableofcontents.

Hassing, R.-J., Leparc-Goffart, I., Blank, S.N., Thevarayan, S., Tolou, H., van Doornum, G., and van Genderen, P.J. (2010). Imported Mayaro virus infection in the Netherlands. J Infect *61*, 343–345.

Hawman, D.W., Stoermer, K.A., Montgomery, S.A., Pal, P., Oko, L., Diamond, M.S., and Morrison, T.E. (2013). Chronic joint disease caused by persistent Chikungunya virus infection is controlled by the adaptive immune response. J Virol *87*, 13878–13888.

Hazelton, R.A., Hughes, C., and Aaskov, J.G. (1985). The inflammatory response in the synovium of a patient with Ross River arbovirus infection. Aust N Z J Med *15*, 336–339.

He, L., Cheng, Y., Kong, L., Azadnia, P., Giang, E., Kim, J., Wood, M.R., Wilson, I.A., Law, M., and Zhu, J. (2015). Approaching rational epitope vaccine design for hepatitis C virus with meta-server and multivalent scaffolding. Sci Rep *5*, 12501.

Heidner, H.W., Knott, T.A., and Johnston, R.E. (1996). Differential processing of sindbis virus glycoprotein PE2 in cultured vertebrate and arthropod cells. J Virol *70*, 2069–2073.

Heil, M.L., Albee, A., Strauss, J.H., and Kuhn, R.J. (2001). An amino acid substitution in the coding region of the E2 glycoprotein adapts Ross River virus to utilize heparan sulfate as an attachment moiety. J Virol *75*, 6303–6309.

Henry Dunand, C.J., Leon, P.E., Huang, M., Choi, A., Chromikova, V., Ho, I.Y., Tan, G.S., Cruz, J., Hirsh, A., Zheng, N.-Y., et al. (2016). Both neutralizing and non-neutralizing human H7N9 influenza vaccine-induced monoclonal antibodies confer protection. Cell Host Microbe *19*, 800–813.

Her, Z., Malleret, B., Chan, M., Ong, E.K.S., Wong, S.-C., Kwek, D.J.C., Tolou, H., Lin, R.T.P., Tambyah, P.A., Rénia, L., et al. (2010). Active infection of human blood monocytes by Chikungunya virus triggers an innate immune response. J Immunol *184*, 5903–5913.

Hessell, A.J., Hangartner, L., Hunter, M., Havenith, C.E.G., Beurskens, F.J., Bakker, J.M., Lanigan, C.M.S., Landucci, G., Forthal, D.N., Parren, P.W.H.I., et al. (2007). Fc receptor but not complement binding is important in antibody protection against HIV. Nature *449*, 101–104.

Holzer, G.W., Coulibaly, S., Aichinger, G., Savidis-Dacho, H., Mayrhofer, J., Brunner, S., Schmid, K., Kistner, O., Aaskov, J.G., Falkner, F.G., et al. (2011). Evaluation of an inactivated Ross River virus vaccine in active and passive mouse immunization models and establishment of a correlate of protection. Vaccine *29*, 4132–4141.

Izurieta, R.O., Macaluso, M., Watts, D.M., Tesh, R.B., Guerra, B., Cruz, L.M., Galwankar, S., and Vermund, S.H. (2011). Hunting in the rainforest and Mayaro virus infection: an emerging alphavirus in Ecuador. J Glob Infect Dis *3*, 317–323.

Jain, J., Nayak, K., Tanwar, N., Gaind, R., Gupta, B., Shastri, J.S., Bhatnagar, R.K., Kaja, M.K., Chandele, A., and Sunil, S. (2017). Clinical, serological, and virological analysis of 572 chikungunya patients from 2010 to 2013 in India. Clin Infect Dis *65*, 133–140.

Jegaskanda, S., Luke, C., Hickman, H.D., Sangster, M.Y., Wieland-Alter, W.F., McBride, J.M., Yewdell, J.W., Wright, P.F., Treanor, J., Rosenberger, C.M., et al. (2016). Generation and protective ability of influenza virus-specific antibody-dependent cellular cytotoxicity in humans elicited by vaccination, natural infection, and experimental challenge. J Infect Dis *214*, 945–952.

Jin, J., and Simmons, G. (2019). Antiviral functions of monoclonal antibodies against Chikungunya virus. Viruses *11*, 305.

Jin, J., Galaz-Montoya, J.G., Sherman, M.B., Sun, S.Y., Goldsmith, C.S., O'Toole, E.T., Ackerman, L., Carlson, L.-A., Weaver, S.C., Chiu, W., et al. (2018). Neutralizing antibodies inhibit Chikungunya virus budding at the plasma membrane. Cell Host Microbe *24*, 417–428.e5.

Jin, J., Liss, N.M., Chen, D.-H., Liao, M., Fox, J.M., Shimak, R.M., Fong, R.H., Chafets, D., Bakkour, S., Keating, S., et al. (2015). Neutralizing monoclonal antibodies block Chikungunya virus entry and release by targeting an epitope critical to viral pathogenesis. Cell Rep *13*, 2553–2564.

Johansson, M.A. (2015). Chikungunya on the move. Trends Parasitol. *31*, 43–45.

Jose, J., Snyder, J.E., and Kuhn, R.J. (2009). A structural and functional perspective of alphavirus replication and assembly. Future Microbiol *4*, 837–856.

Jöst, H., Bialonski, A., Storch, V., Günther, S., Becker, N., and Schmidt-Chanasit, J. (2010). Isolation and phylogenetic analysis of Sindbis viruses from mosquitoes in Germany. J Clin Microbiol *48*, 1900–1903.

Kajihara, M., Marzi, A., Nakayama, E., Noda, T., Kuroda, M., Manzoor, R., Matsuno, K., Feldmann, H., Yoshida, R., Kawaoka, Y., et al. (2012). Inhibition of Marburg virus budding by nonneutralizing antibodies to the envelope glycoprotein. J Virol *86*, 13467–13474.

Kerr, P.J., Fitzgerald, S., Tregear, G.W., Dalgarno, L., and Weir, R.C. (1992). Characterization of a major neutralization domain of Ross river virus using anti-viral and anti-peptide antibodies. Virology *187*, 338–342.

Khan, A.G., Whidby, J., Miller, M.T., Scarborough, H., Zatorski, A.V., Cygan, A., Price, A.A., Yost, S.A., Bohannon, C.D., Jacob, J., et al. (2014). Structure of the core ectodomain of the hepatitis C virus envelope glycoprotein 2. Nature *509*, 381–384.

Kielian, M. (2010). Structural biology: An alphavirus puzzle solved. Nature *468*, 645–646.

Kielian, M., Chanel-Vos, C., and Liao, M. (2010). Alphavirus entry and membrane fusion. Viruses *2*, 796–825.

Kim, M., Sun, Z.-Y.J., Rand, K.D., Shi, X., Song, L., Cheng, Y., Fahmy, A.F., Majumdar, S., Ofek, G., Yang, Y., et al. (2011). Antibody mechanics on a membrane-bound HIV segment essential for GP41-targeted viral neutralization. Nat Struct Mol Biol *18*, 1235–1243.

Klimstra, W.B., Ryman, K.D., and Johnston, R.E. (1998). Adaptation of Sindbis virus to BHK cells selects for use of heparan sulfate as an attachment receptor. J Virol *72*, 7357–7366.

Klimstra, W.B., Nangle, E.M., Smith, M.S., Yurochko, A.D., and Ryman, K.D. (2003). DC-SIGN and L-SIGN can act as attachment receptors for alphaviruses and distinguish between mosquito cell- and mammalian cell-derived viruses. J Virol *77*, 12022–12032.

Kose, N., Fox, J.M., Sapparapu, G., Bombardi, R., Tennekoon, R.N., de Silva, A.D., Elbashir, S.M., Theisen, M.A., Humphris-Narayanan, E., Ciaramella, G., et al. (2019). A lipid-encapsulated mRNA encoding a potently neutralizing human monoclonal antibody protects against chikungunya infection. Sci Immunol *4*, eaaw6647.

Krutikov, M., and Manson, J. (2016). Chikungunya Virus Infection: An Update on Joint Manifestations and Management. Rambam Maimonides Med J *7*, e0033.

Kulp, D.W., and Schief, W.R. (2013). Advances in structure-based vaccine design. Curr Opin Virol *3*, 322–331.

Kumanomido, T., Kamada, M., Wada, R., Kenemaru, T., Sugiura, T., and Akiyama, Y. (1988). Pathogenicity for horses of original Sagiyama virus, a member of the Getah virus group. Vet Microbiol *17*, 367–373.

La Linn, M., Eble, J.A., Lübken, C., Slade, R.W., Heino, J., Davies, J., and Suhrbier, A. (2005). An arthritogenic alphavirus uses the alpha1beta1 integrin collagen receptor. Virology *336*, 229–239.

Laakkonen, P., Auvinen, P., Kujala, P., and Kääriäinen, L. (1998). Alphavirus replicase protein NSP1 induces filopodia and rearrangement of actin filaments. J Virol *72*, 10265–10269.

Labadie, K., Larcher, T., Joubert, C., Mannioui, A., Delache, B., Brochard, P., Guigand, L., Dubreil, L., Lebon, P., Verrier, B., et al. (2010). Chikungunya disease in nonhuman primates involves long-term viral persistence in macrophages. J Clin Invest *120*, 894–906.

Lau, C., Aubry, M., Musso, D., Teissier, A., Paulous, S., Desprès, P., de-Lamballerie, X., Pastorino, B., Cao-Lormeau, V.-M., and Weinstein, P. (2017). New evidence for endemic circulation of Ross River virus in the Pacific Islands and the potential for emergence. Int J Infect Dis *57*, 73–76.

Lee, C.Y., Kam, Y.-W., Fric, J., Malleret, B., Koh, E.G.L., Prakash, C., Huang, W., Lee, W.W.L., Lin, C., Lin, R.T.P., et al. (2011). Chikungunya virus neutralization antigens and direct cell-to-cell transmission are revealed by human antibody-escape mutants. PLoS Pathog *7*, e1002390.

Lee, S., Owen, K.E., Choi, H.K., Lee, H., Lu, G., Wengler, G., Brown, D.T., Rossmann, M.G., and Kuhn, R.J. (1996). Identification of a protein binding site on the surface of the alphavirus nucleocapsid and its implication in virus assembly. Structure *4*, 531–541.

Leung, J.Y.-S., Ng, M.M.-L., and Chu, J.J.H. (2011). Replication of alphaviruses: a review on the entry process of alphaviruses into cells. Adv Virol *2011*, 249640–249649.

Levi, L.I., and Vignuzzi, M. (2019). Arthritogenic alphaviruses: a worldwide emerging threat? Microorganisms *7*, 133.

Lewis, G.K., Finzi, A., DeVico, A.L., and Pazgier, M. (2015). Conformational masking and receptor-dependent unmasking of highly conserved Env epitopes recognized by non-neutralizing antibodies that mediate potent ADCC against HIV-1. Viruses *7*, 5115–5132.

Li, L., Jose, J., Xiang, Y., Kuhn, R.J., and Rossmann, M.G. (2010). Structural changes of envelope proteins during alphavirus fusion. Nature *468*, 705–708.

Lidbury, B.A., and Mahalingam, S. (2000). Specific ablation of antiviral gene expression in macrophages by antibody-dependent enhancement of Ross River virus infection. J Virol *74*, 8376–8381.

Liebschner, D., Afonine, P.V., Baker, M.L., Bunkóczi, G., Chen, V.B., Croll, T.I., Hintze, B., Hung, L.W., Jain, S., McCoy, A.J., et al. (2019). Macromolecular structure determination using X-rays, neutrons and electrons: recent developments in Phenix. Acta Crystallogr D Struct Biol *75*, 861–877.

Lim, X.-X., Chandramohan, A., Lim, X.Y.E., Bag, N., Sharma, K.K., Wirawan, M., Wohland, T., Lok, S.-M., and Anand, G.S. (2017). Conformational changes in intact dengue virus reveal serotype-specific expansion. Nat Commun *8*, 14339.

Ling, J., Smura, T., Lundström, J.O., Pettersson, J.H.-O., Sironen, T., Vapalahti, O., Lundkvist, Å., and Hesson, J.C. (2019). Introduction and dispersal of Sindbis virus from Central Africa to Europe. J Virol *93*, 58.

Linn, M.L., Aaskov, J.G., and Suhrbier, A. (1996). Antibody-dependent enhancement and persistence in macrophages of an arbovirus associated with arthritis. J Gen Virol *77 (Pt 3)*, 407–411.

Liu, W.J., Rourke, M.F., Holmes, E.C., and Aaskov, J.G. (2011). Persistence of multiple genetic lineages within intrahost populations of Ross River virus. J Virol *85*, 5674–5678.

López-Sagaseta, J., Malito, E., Rappuoli, R., and Bottomley, M.J. (2016). Self-assembling protein nanoparticles in the design of vaccines. Comput Struct Biotechnol J *14*, 58–68.

Lu, G., Ou, J., Ji, J., Ren, Z., Hu, X., Wang, C., and Li, S. (2019). Emergence of Getah Virus infection in horse with fever in China, 2018. Front Microbiol *10*, 1416.

Lundström, J.O., Hesson, J.C., Schäfer, M.L., Östman, Ö., Semmler, T., Bekaert, M., Weidmann, M., Lundkvist, Å., and Pfeffer, M. (2019). Sindbis virus polyarthritis outbreak signalled by virus prevalence in the mosquito vectors. PLoS Neglect Trop Dis *13*, e0007702.

Lwande, O.W., Obanda, V., Bucht, G., Mosomtai, G., Otieno, V., Ahlm, C., and Evander, M. (2015). Global emergence of alphaviruses that cause arthritis in humans. Infect Ecol Epidemiol *5*, 29853.

Mancini, E.J., Clarke, M., Gowen, B.E., Rutten, T., and Fuller, S.D. (2000). Cryo-electron microscopy reveals the functional organization of an enveloped virus, Semliki Forest virus. Mol Cell *5*, 255–266.

Martinez, M.G., and Kielian, M. (2016). Intercellular extensions are induced by the alphavirus structural proteins and mediate virus transmission. PLoS Pathog *12*, e1006061.

Martinez, M.G., Snapp, E.-L., Perumal, G.S., Macaluso, F.P., and Kielian, M. (2014). Imaging the alphavirus exit pathway. J Virol *88*, 6922–6933.

MASON, P.J., and HADDOW, A.J. (1957). An epidemic of virus disease in Southern Province, Tanganyika Territory, in 1952-53; an additional note on Chikungunya virus isolations and serum antibodies. Trans R Soc Trop Med Hyg *51*, 238–240.

McLellan, J.S., Correia, B.E., Chen, M., Yang, Y., Graham, B.S., Schief, W.R., and Kwong, P.D. (2011). Design and characterization of epitope-scaffold immunogens that present the motavizumab epitope from respiratory syncytial virus. J Mol Biol *409*, 853–866.

Mendoza, Q.P., Stanley, J., and Griffin, D.E. (1988). Monoclonal antibodies to the E1 and E2 glycoproteins of Sindbis virus: definition of epitopes and efficiency of protection from fatal encephalitis. J Gen Virol *69 (Pt 12)*, 3015–3022.

Miner, J.J., Aw-Yeang, H.-X., Fox, J.M., Taffner, S., Malkova, O.N., Oh, S.T., Kim, A.H.J., Diamond, M.S., Lenschow, D.J., and Yokoyama, W.M. (2015). Chikungunya viral arthritis in the United States: a mimic of seronegative rheumatoid arthritis. Arthritis Rheumatol *67*, 1214–1220.

Morrison, C.R., Plante, K.S., and Heise, M.T. (2016). Chikungunya virus: current perspectives on a reemerging virus. Microbiol Spectr *4*, 143–161.

Morrison, T.E., Oko, L., Montgomery, S.A., Whitmore, A.C., Lotstein, A.R., Gunn, B.M., Elmore, S.A., and Heise, M.T. (2011). A mouse model of chikungunya virus-induced musculoskeletal inflammatory disease: evidence of arthritis, tenosynovitis, myositis, and persistence. Am J Pathol *178*, 32–40.

Morrison, T.E., Whitmore, A.C., Shabman, R.S., Lidbury, B.A., Mahalingam, S., and Heise, M.T. (2006). Characterization of Ross River virus tropism and virus-induced inflammation in a mouse model of viral arthritis and myositis. J Virol *80*, 737–749.

Mostafavi, H., Abeyratne, E., Zaid, A., and Taylor, A. (2019). Arthritogenic alphavirus-induced immunopathology and targeting host inflammation as a therapeutic strategy for alphaviral disease. Viruses *11*, 290.

Nanfack Minkeu, F., and Vernick, K.D. (2018). A systematic review of the natural virome of anopheles mosquitoes. Viruses *10*, 222.

Nasci, R.S. (2014). Movement of chikungunya virus into the Western hemisphere. Emerging Infect Dis *20*, 1394–1395.

Nelson, M.A., Herrero, L.J., Jeffery, J.A.L., Hoehn, M., Rudd, P.A., Supramaniam, A., Kay, B.H., Ryan, P.A., and Mahalingam, S. (2016). Role of envelope N-linked glycosylation in Ross River virus virulence and transmission. J Gen Virol *97*, 1094–1106.

Ofek, G., Guenaga, F.J., Schief, W.R., Skinner, J., Baker, D., Wyatt, R., and Kwong, P.D. (2010). Elicitation of structure-specific antibodies by epitope scaffolds. Proc Natl Acad Sci USA *107*, 17880–17887.

Owen, K.E., and Kuhn, R.J. (1997). Alphavirus budding is dependent on the interaction between the nucleocapsid and hydrophobic amino acids on the cytoplasmic domain of the E2 envelope glycoprotein. Virology *230*, 187–196.

Pal, P., Dowd, K.A., Brien, J.D., Edeling, M.A., Gorlatov, S., Johnson, S., Lee, I., Akahata, W., Nabel, G.J., Richter, M.K.S., et al. (2013). Development of a highly protective combination monoclonal antibody therapy against Chikungunya virus. PLoS Pathog *9*, e1003312.

Pal, P., Fox, J.M., Hawman, D.W., Huang, Y.-J.S., Messaoudi, I., Kreklywich, C., Denton, M., Legasse, A.W., Smith, P.P., Johnson, S., et al. (2014). Chikungunya viruses that escape monoclonal antibody therapy are clinically attenuated, stable, and not purified in mosquitoes. J Virol *88*, 8213–8226.

Paredes, A., Weaver, S., Watowich, S., and Chiu, W. (2005). Structural biology of old world and new world alphaviruses. Arch Virol Suppl *65*, 179–185.

Pettersen, E.F., Goddard, T.D., Huang, C.C., Couch, G.S., Greenblatt, D.M., Meng, E.C., and Ferrin, T.E. (2004). UCSF Chimera--a visualization system for exploratory research and analysis. J Comput Chem *25*, 1605–1612.

Phelps, A.L., O'Brien, L.M., Eastaugh, L.S., Davies, C., Lever, M.S., Ennis, J., Zeitlin, L., Nunez, A., and Ulaeto, D.O. (2017). Susceptibility and lethality of Western Equine Encephalitis virus in balb/c mice when infected by the aerosol route. Viruses *9*, 163.

Poo, Y.S., Nakaya, H., Gardner, J., Larcher, T., Schroder, W.A., Le, T.T., Major, L.D., and Suhrbier, A. (2014). CCR2 deficiency promotes exacerbated chronic erosive neutrophil-dominated chikungunya virus arthritis. J Virol *88*, 6862–6872.

Porta, J., Jose, J., Roehrig, J.T., Blair, C.D., Kuhn, R.J., and Rossmann, M.G. (2014). Locking and blocking the viral landscape of an alphavirus with neutralizing antibodies. J Virol *88*, 9616–9623.

Porta, J., Mangala Prasad, V., Wang, C.-I., Akahata, W., Ng, L.F.P., and Rossmann, M.G. (2016). Structural studies of Chikungunya virus-like particles complexed with human antibodies: neutralization and cell-to-cell transmission. J Virol *90*, 1169–1177.

Powers, A.M., Brault, A.C., Shirako, Y., Strauss, E.G., Kang, W., Strauss, J.H., and Weaver, S.C. (2001). Evolutionary relationships and systematics of the alphaviruses. J Virol *75*, 10118–10131.

Quiroz, J.A., Malonis, R.J., Thackray, L.B., Cohen, C.A., Pallesen, J., Jangra, R.K., Brown, R.S., Hofmann, D., Holtsberg, F.W., Shulenin, S., et al. (2019). Human monoclonal antibodies against chikungunya virus target multiple distinct epitopes in the E1 and E2 glycoproteins. PLoS

Pathog *15*, e1008061.

Radoshitzky, S.R., Pegoraro, G., Chī, X.O., D Ng, L., Chiang, C.-Y., Jozwick, L., Clester, J.C., Cooper, C.L., Courier, D., Langan, D.P., et al. (2016). siRNA screen identifies trafficking host factors that modulate alphavirus infection. PLoS Pathog *12*, e1005466.

Ramsauer, K., Schwameis, M., Firbas, C., Müllner, M., Putnak, R.J., Thomas, S.J., Desprès, P., Tauber, E., Jilma, B., and Tangy, F. (2015). Immunogenicity, safety, and tolerability of a recombinant measles-virus-based chikungunya vaccine: a randomised, double-blind, placebo-controlled, active-comparator, first-in-man trial. Lancet Infect Dis *15*, 519–527.

Rezza, G., Chen, R., and Weaver, S.C. (2017). O'nyong-nyong fever: a neglected mosquito-borne viral disease. Pathog Glob Health *111*, 271–275.

Rohou, A., and Grigorieff, N. (2015). CTFFIND4: Fast and accurate defocus estimation from electron micrographs. J Struct Biol *192*, 216–221.

Roseman, A.M. (2004). FindEM--a fast, efficient program for automatic selection of particles from electron micrographs. J Struct Biol *145*, 91–99.

Rossmann, M.G., Bernal, R., and Pletnev, S.V. (2001). Combining electron microscopic with x-ray crystallographic structures. J Struct Biol *136*, 190–200.

Roussel, A., Lescar, J., Vaney, M.-C., Wengler, G., Wengler, G., and Rey, F.A. (2006). Structure and interactions at the viral surface of the envelope protein E1 of Semliki Forest virus. Structure *14*, 75–86.

Roy, A., Kucukural, A., and Zhang, Y. (2010). I-TASSER: a unified platform for automated protein structure and function prediction. Nat Protoc *5*, 725–738.

Sane, J., Kurkela, S., Lokki, M.-L., Miettinen, A., Helve, T., Vaheri, A., and Vapalahti, O. (2012). Clinical Sindbis alphavirus infection is associated with HLA-DRB1*01 allele and production of autoantibodies. Clin Infect Dis *55*, 358–363.

Sapparapu, G., Fernandez, E., Kose, N., Bin Cao, Fox, J.M., Bombardi, R.G., Zhao, H., Nelson, C.A., Bryan, A.L., Barnes, T., et al. (2016). Neutralizing human antibodies prevent Zika virus replication and fetal disease in mice. Nature *540*, 443–447.

Saunders, K.O. (2019). Conceptual approaches to modulating antibody effector functions and circulation half-life. Front Immunol *10*, 1296.

Sánchez-San Martín, C., Sosa, H., and Kielian, M. (2008). A stable prefusion intermediate of the alphavirus fusion protein reveals critical features of class II membrane fusion. Cell Host Microbe *4*, 600–608.

Schnierle, B.S. (2019). Cellular attachment and entry factors for Chikungunya virus. Viruses *11*, 1078.

Sheehan, K.C.F., Lai, K.S., Dunn, G.P., Bruce, A.T., Diamond, M.S., Heutel, J.D., Dungo-Arthur, C., Carrero, J.A., White, J.M., Hertzog, P.J., et al. (2006). Blocking monoclonal antibodies specific for mouse IFN-alpha/beta receptor subunit 1 (IFNAR-1) from mice

immunized by in vivo hydrodynamic transfection. J Interf Cytok Res *26*, 804–819.

Sherman, M.B., and Weaver, S.C. (2010). Structure of the recombinant alphavirus Western equine encephalitis virus revealed by cryoelectron microscopy. J Virol *84*, 9775–9782.

Shin, G., Yost, S.A., Miller, M.T., Elrod, E.J., Grakoui, A., and Marcotrigiano, J. (2012). Structural and functional insights into alphavirus polyprotein processing and pathogenesis. Proc Natl Acad Sci USA *109*, 16534–16539.

Shirako, Y., and Yamaguchi, Y. (2000). Genome structure of Sagiyama virus and its relatedness to other alphaviruses. J Gen Virol *81*, 1353–1360.

Silva, L.A., and Dermody, T.S. (2017). Chikungunya virus: epidemiology, replication, disease mechanisms, and prospective intervention strategies. J Clin Invest *127*, 737–749.

Silva, L.A., Khomandiak, S., Ashbrook, A.W., Weller, R., Heise, M.T., Morrison, T.E., and Dermody, T.S. (2014). A single-amino-acid polymorphism in Chikungunya virus E2 glycoprotein influences glycosaminoglycan utilization. J Virol *88*, 2385–2397.

Smatti, M.K., Thani, Al, A.A., and Yassine, H.M. (2018). Viral-induced enhanced disease illness. Front Microbiol *9*, 2991.

Smith, J.L., Pugh, C.L., Cisney, E.D., Keasey, S.L., Guevara, C., Ampuero, J.S., Comach, G., Gomez, D., Ochoa-Diaz, M., Hontz, R.D., et al. (2018). Human antibody responses to emerging Mayaro virus and cocirculating alphavirus infections examined by using structural proteins from nine new and Old World lineages. mSphere *3*, 33.

Smith, S.A., and Crowe, J.E. (2015). Use of human hybridoma technology to isolate human monoclonal antibodies. In Antibodies for Infectious Diseases, D. Boraschi, J.E. Crowe, and R. Rappuoli, eds. (American Society of Microbiology), pp. 141–156.

Smith, S.A., Silva, L.A., Fox, J.M., Flyak, A.I., Kose, N., Sapparapu, G., Khomandiak, S., Khomadiak, S., Ashbrook, A.W., Kahle, K.M., et al. (2015). Isolation and characterization of broad and ultrapotent human monoclonal antibodies with therapeutic activity against Chikungunya virus. Cell Host Microbe *18*, 86–95.

Snyder, A.J., Sokoloski, K.J., and Mukhopadhyay, S. (2012). Mutating conserved cysteines in the alphavirus e2 glycoprotein causes virus-specific assembly defects. J Virol *86*, 3100–3111.

Solignat, M., Gay, B., Higgs, S., Briant, L., and Devaux, C. (2009). Replication cycle of chikungunya: a re-emerging arbovirus. Virology *393*, 183–197.

Song, H., Zhao, Z., Chai, Y., Jin, X., Li, C., Yuan, F., Liu, S., Gao, Z., Wang, H., Song, J., et al. (2019). Molecular basis of arthritogenic alphavirus receptor MXRA8 binding to Chikungunya virus envelope protein. Cell 177, 1714-1724.e12.

Stephenson, E.B., Peel, A.J., Reid, S.A., Jansen, C.C., and McCallum, H. (2018). The non-human reservoirs of Ross River virus: a systematic review of the evidence. Parasit Vectors *11*, 188.

Suloway, C., Pulokas, J., Fellmann, D., Cheng, A., Guerra, F., Quispe, J., Stagg, S., Potter,

C.S., and Carragher, B. (2005). Automated molecular microscopy: the new Leginon system. J Struct Biol *151*, 41–60.

Sun, S., Xiang, Y., Akahata, W., Holdaway, H., Pal, P., Zhang, X., Diamond, M.S., Nabel, G.J., and Rossmann, M.G. (2013). Structural analyses at pseudo atomic resolution of Chikungunya virus and antibodies show mechanisms of neutralization. Elife *2*, e00435.

Tanabe, I.S.B., Tanabe, E.L.L., Santos, E.C., Martins, W.V., Araújo, I.M.T.C., Cavalcante, M.C.A., Lima, A.R.V., Câmara, N.O.S., Anderson, L., Yunusov, D., et al. (2018). Cellular and molecular immune response to Chikungunya virus infection. Front Cell Infect Microbiol *8*, 345.

Tay, M.Z., Wiehe, K., and Pollara, J. (2019). Antibody-dependent cellular phagocytosis in antiviral immune responses. Front Immunol *10*, 332.

Taylor, G.M., Hanson, P.I., and Kielian, M. (2007). Ubiquitin depletion and dominant-negative VPS4 inhibit rhabdovirus budding without affecting alphavirus budding. J Virol *81*, 13631–13639.

Terral, G., Champion, T., Debaene, F., Colas, O., Bourguet, M., Wagner-Rousset, E., Corvaia, N., Beck, A., and Cianferani, S. (2017). Epitope characterization of anti-JAM-A antibodies using orthogonal mass spectrometry and surface plasmon resonance approaches. mAbs *9*, 1317–1326.

Thran, M., Mukherjee, J., Pönisch, M., Fiedler, K., Thess, A., Mui, B.L., Hope, M.J., Tam, Y.K., Horscroft, N., Heidenreich, R., et al. (2017). mRNA mediates passive vaccination against infectious agents, toxins, and tumors. EMBO Mol Med *9*, 1434–1447.

Valentine, M.J., Murdock, C.C., and Kelly, P.J. (2019). Sylvatic cycles of arboviruses in non-human primates. Parasit Vectors *12*, 463–18.

van Erp, E.A., Luytjes, W., Ferwerda, G., and van Kasteren, P.B. (2019). Fc-mediated antibody effector functions during respiratory syncytial virus infection and disease. Front Immunol *10*, 548.

Van Hoecke, L., and Roose, K. (2019). How mRNA therapeutics are entering the monoclonal antibody field. J Transl Med *17*, 54.

Van Lint, S., Goyvaerts, C., Maenhout, S., Goethals, L., Disy, A., Benteyn, D., Pen, J., Bonehill, A., Heirman, C., Breckpot, K., et al. (2012). Preclinical evaluation of TriMix and antigen mRNA-based antitumor therapy. Cancer Res. *72*, 1661–1671.

Voss, J.E., Vaney, M.-C., Duquerroy, S., Vonrhein, C., Girard-Blanc, C., Crublet, E., Thompson, A., Bricogne, G., and Rey, F.A. (2010). Glycoprotein organization of Chikungunya virus particles revealed by X-ray crystallography. Nature *468*, 709–712.

Vrati, S., Fernon, C.A., Dalgarno, L., and Weir, R.C. (1988). Location of a major antigenic site involved in Ross River virus neutralization. Virology *162*, 346–353.

Wahid, B., Ali, A., Rafique, S., and Idrees, M. (2017). Global expansion of chikungunya virus: mapping the 64-year history. Int J Infect Dis *58*, 69–76.

Way, S.J.R., Lidbury, B.A., and Banyer, J.L. (2002). Persistent Ross River virus infection of murine macrophages: an in vitro model for the study of viral relapse and immune modulation during long-term infection. Virology *301*, 281–292.

Weger-Lucarelli, J., Aliota, M.T., Kamlangdee, A., and Osorio, J.E. (2015). Identifying the role of E2 domains on alphavirus neutralization and protective immune responses. PLoS Neglect Trop Dis *9*, e0004163.

Wei, H., Mo, J., Tao, L., Russell, R.J., Tymiak, A.A., Chen, G., Iacob, R.E., and Engen, J.R. (2014). Hydrogen/deuterium exchange mass spectrometry for probing higher order structure of protein therapeutics: methodology and applications. Drug Discov Today *19*, 95–102.

Williams, M.C., Woodall, J.P., Corbet, P.S., and Gillett, J.d. (1965). O'nyong-n'yong fever: an epidemic virus disease in East Africa. 8. Virus Isolations from Anopheles Mosquitoes. Trans R Soc Trop Med Hyg *59*, 300-306

Wong, H.V., Chan, Y.F., Sam, I.-C., Sulaiman, W.Y.W., and Vythilingam, I. (2016). Chikungunya Virus Infection of Aedes Mosquitoes. Methods Mol Biol *1426*, 119–128.

Woodruff, A.W., Bowen, E.T., and Platt, G.S. (1978). Viral infections in travellers from tropical Africa. Br Med J *1*, 956–958.

Wressnigg, N., van der Velden, M.V.W., Portsmouth, D., Draxler, W., O'Rourke, M., Richmond, P., Hall, S., McBride, W.J.H., Redfern, A., Aaskov, J., et al. (2015). An inactivated Ross River virus vaccine is well tolerated and immunogenic in an adult population in a randomized phase 3 trial. Clin Vaccine Immunol *22*, 267–273.

Xiao, C., and Rossmann, M.G. (2007). Interpretation of electron density with stereographic roadmap projections. J Struct Biol *158*, 182–187.

Yamashita, M., Kitano, S., Aikawa, H., Kuchiba, A., Hayashi, M., Yamamoto, N., Tamura, K., and Hamada, A. (2016). A novel method for evaluating antibody-dependent cell-mediated cytotoxicity by flowcytometry using cryopreserved human peripheral blood mononuclear cells. Sci Rep *6*, 19772.

Yang, Y., Huang, Y., Gnanadurai, C.W., Cao, S., Liu, X., Cui, M., and Fu, Z.F. (2015). The inability of wild-type rabies virus to activate dendritic cells is dependent on the glycoprotein and correlates with its low level of the de novo-synthesized leader RNA. J Virol *89*, 2157–2169.

Yap, M.L., Klose, T., Urakami, A., Hasan, S.S., Akahata, W., and Rossmann, M.G. (2017). Structural studies of Chikungunya virus maturation. Proc Natl Acad Sci USA *114*, 13703–13707.

Zacks, M.A., and Paessler, S. (2010). Encephalitic alphaviruses. Vet Microbiol *140*, 281–286.

Zeitlin, L., Pettitt, J., Scully, C., Bohorova, N., Kim, D., Pauly, M., Hiatt, A., Ngo, L., Steinkellner, H., Whaley, K.J., et al. (2011). Enhanced potency of a fucose-free monoclonal antibody being developed as an Ebola virus immunoprotectant. Proc Natl Acad Sci USA *108*, 20690–20694.

Zeller, H., Van Bortel, W., and Sudre, B. (2016). Chikungunya: its history in Africa and Asia and its spread to new regions in 2013-2014. J Infect Dis *214*, S436–S440.

Zhang, R., Kim, A.S., Fox, J.M., Nair, S., Basore, K., Klimstra, W.B., Rimkunas, R., Fong, R.H., Lin, H., Poddar, S., et al. (2018). Mxra8 is a receptor for multiple arthritogenic alphaviruses. Nature *557*, 570–574.

Zhang, R., Hryc, C.F., Cong, Y., Liu, X., Jakana, J., Gorchakov, R., Baker, M.L., Weaver, S.C., and Chiu, W. (2011). 4.4 Å cryo-EM structure of an enveloped alphavirus Venezuelan equine encephalitis virus. Embo J *30*, 3854–3863.

Zhang, W., Fisher, B.R., Olson, N.H., Strauss, J.H., Kuhn, R.J., and Baker, T.S. (2002a). Aura virus structure suggests that the T=4 organization is a fundamental property of viral structural proteins. J Virol *76*, 7239–7246.

Zhang, W., Mukhopadhyay, S., Pletnev, S.V., Baker, T.S., Kuhn, R.J., and Rossmann, M.G. (2002b). Placement of the structural proteins in Sindbis virus. J Virol *76*, 11645–11658.

Zhang, Y. (2008). I-TASSER server for protein 3D structure prediction. BMC Bioinformatics *9*, 40.

Zhao, H., and Garoff, H. (1992). Role of cell surface spikes in alphavirus budding. J Virol *66*, 7089–7095.

Zheng, S.Q., Palovcak, E., Armache, J.-P., Verba, K.A., Cheng, Y., and Agard, D.A. (2017). MotionCor2: anisotropic correction of beam-induced motion for improved cryo-electron microscopy. Nat Methods *14*, 331–332.

Zhou, T., Zhu, J., Yang, Y., Gorman, J., Ofek, G., Srivatsan, S., Druz, A., Lees, C.R., Lu, G., Soto, C., et al. (2014). Transplanting supersites of HIV-1 vulnerability. PLoS One *9*, e99881.